MASTERARBEIT

„Epitope mimics for pathogenic anti-aquaporin 4 autoantibodies in Neuromyelitis optica"

verfasst von

Isabel Julia Bauer, BSc

angestrebter akademischer Grad

Master of Science (MSc)

Wien, 2015

Abstract

Neuromyelitis optica (NMO) is a severe autoimmune astrocytopathy of the central nervous system (CNS) that preferentially affects the optic nerve and the spinal cord leading to paralysis and impaired vision. The disease is hallmarked by specific autoantibodies that target conformational epitopes composed of the extracellular loops of the astrocytic water channel aquaporin 4 (AQP4).

This study addresses the identification of epitope mimics (so-called mimotopes) for these AQP4-specific autoantibodies (NMO-IgG) For this purpose, we used a random phage-displayed 12-mer peptide library for biopanning with purified polyclonal immunoglobulin G (IgG) of an NMO-IgG-seropositive patient as target. After increasing target specificity within three rounds of panning, single phage clones were picked and their reactivity with NMO-IgG was evaluated via ELISA. For further characterization, mimotope-based prediction softwares were employed to map the peptides obtained by DNA sequencing of the single phage clones on human AQP4 *in silico*. Eight promising candidates were selected and tested for their potential to block the binding of NMO-IgG to its target, AQP4, in a FACS-based analysis using AQP4-transfected HEK293A cells. The FACS measurements revealed four peptides to be capable of reducing the binding of NMO-IgG to the extracellular loops of AQP4, indicating that these peptides successfully mimic epitopes of the autoantibody. Due to its polyclonal origin, the IgG fraction used in this study probably contains not one but several subpopulations of NMO-IgG. Here, we identified mimotopes for at least two subtypes of NMO-IgG: one loop A independent and one loop A dependent subpopulation.

The identification of these four mimotopes provides a solid basis from which the development of several applications is conceivable in the long term. Mimotopes could enable the characterization and classification of patients' antibody pools according to their reactivity with different mimotopes or could be used for active immunization strategies, e.g. to raise antibodies in valid animal models to investigate the effect of distinct NMO-IgG subpopulations.

Zusammenfassung

Neuromyelitis optica (NMO) ist eine gegen Astrozyten gerichtete Autoimmunerkrankung des zentralen Nervensystems, die vor allem den optischen Nerv und das Rückenmark betrifft und zu Lähmungen und eingeschränkter Sehkraft führt. Die Krankheit ist gekennzeichnet durch spezifische Autoantikörper, die sich gegen konformationelle Epitope auf den extrazellulären Schleifen des astrozytären Wasserkanals Aquaporin 4 (AQP4) richten.

Die vorliegende Arbeit behandelt die Identifizierung von Epitop-Imitatoren für diese AQP4-spezifischen Antikörper (NMO-IgG). Hierfür wurde eine Phagen-präsentierte 12-Mer-Peptid-Bibliothek für ein Biopanning mit aufgereinigten polyklonalen Immunglobulinen eines NMO-IgG-seropositiven Patienten verwendet. Nach einer Spezifitätszunahme in drei Biopanning-Runden wurden einzelne Phagen-Klone isoliert und ihre Reaktivität mit NMO-IgG in ELISA-Versuchen evaluiert. Weiters wurden die Peptide, die durch DNA-Sequenzierung der einzelnen Phagen-Klone ermittelt wurden, mit Hilfe Mimotop-basierter Computerprogramme auf humanes AQP4 abgebildet. Basierend auf den ELISA-Ergebnissen und der errechneten Lage der Mimotope wurden acht vielversprechende Kandidaten ausgewählt und in einer FACS-basierten Analyse auf ihr Potential, die Bindung von NMO-IgG an sein Antigen, AQP4, zu blockieren, untersucht. Die FACS-Experimente ergaben, dass vier Peptide dazu fähig sind, die Interaktion von NMO-IgG mit AQP4 zu reduzieren, was darauf hindeutet, dass diese Peptide in der Tat Epitope von NMO-IgG imitieren. Aufgrund seines polyklonalen Ursprungs enthält der in dieser Arbeit verwendete Antikörper-Pool nicht nur eine, sondern mehrere Subpopulationen von NMO-IgG. Hier wurden Mimotope für mindestens zwei Untergruppen von NMO-IgG gefunden: eine A-Schleifen-unabhängige und eine A-Schleifen-abhängige.

Die Identifizierung der vier Mimotope stellt eine solide Grundlage dar, von der ausgehend langfristig einige Anwendungen vorstellbar sind. Die Mimotope könnten die Klassifizierung der Antikörper-Pools verschiedener Patienten nach ihrer Reaktivität mit unterschiedlichen Mimotopen ermöglichen, oder für aktive Immunisierungsstrategien verwendet werden, z. B. um im Tiermodell den Effekt bestimmter NMO-IgG-Subpopulationen zu untersuchen.

List of abbreviations

7-AAD	7-aminoactinomycin D
ADCC	Antibody-dependent cellular cytotoxicity
APS	Ammonium persulfate
AQP4	Aquaporin
BBB	Blood-brain barrier
BN-PAGE	Blue native polyacrylamide gel electrophoresis
BSA	Bovine serum albumin
CBB	Coomassie Brilliant Blue
CDC	Complement-dependent cytotoxicity
CDCC	Complement-dependent cellular cytotoxicity
CNS	Central nervous system
CSF	Cerebrospinal fluid
DAPI	4', 6-diamidino-2-phenylindole
ddH$_2$O	Double-distilled water
DMEM	Dulbecco's modified Eagle medium
DMF	N,N-Dimethylformamide
DMSO	Dimethyl sulfoxide
EAE	Experimental autoimmune encephalomyelitis
EDTA	Ethylendiaminetetraacetic acid
ELISA	Enzyme-linked immunosorbent assay
emGFP	Emerald green fluorescent protein
FACS	Fluorescence-activated cell sorting
FBS	Fetal bovine serum
FCS	Fetal calf serum
FFEM	Freeze fracture electron microscopy
GFAP	Glial fibrillary acidic protein
HRP	Horseradish peroxidase
IVMP	Intravenous methylprednisolone
MAC	Membrane attack complex
MBP	Myelin basic protein
MOG	Myelin oligodendrocyte protein
MRI	Magnetic resonance imaging

MS	Multiple sclerosis
NMO	Neuromyelitis optica
NPSLE	Neuropsychiatric systemic lupus erythematosus
OAP	Orthogonal array of particles
ON	Optic neuritis
PBS	Phosphate-buffered saline
PEG	Polyethylene glycol
PLL	Poly-L-lysine
Pfu	Plaque forming units
RT	Room temperature
ssDNA	Single-stranded DNA
TBS	Tris-buffered saline
TBST	Tris-buffered saline with Tween -20
TEMED	Tetramethylethylenediamine
TIS	Translation initiation site
TMB	3,3',5,5'-tetramethylbenzidine

Table of Contents

1. Introduction

Neuromyelitis optica (NMO), also known as Devic's disease or Devic's syndrome, is a severe inflammatory astrocytopathic disease of the central nervous system (CNS) characterized by recurrent inflammation and demyelination of the optic nerve (optic neuritis, ON) and the spinal cord (transverse myelitis) (Wingerchuk et al., 1999). It may cause eye pain and blindness, paralysis and at worst may lead to death. It has firstly been described by Devic and Gault in 1894 (Devic, 1894; Gault, 1894). Thenceforth, due to similar clinical manifestations (optic neuritis, myelitis and inflammatory demyelination), NMO has been widely considered a severe variant of multiple sclerosis (MS) for many years. Only in 2004, when Lennon and her coworkers discovered a serum autoantibody to be present in NMO but not in MS, NMO was recognized as a distinct pathological entity (Lennon et al., 2004). One year later, the water channel aquaporin-4 (AQP4) was identified as target of the NMO-specific antibody (NMO-IgG) (Lennon et al., 2005).

1.1. Epidemiology of NMO

NMO occurs worldwide among diverse races and cultures with differing incidence and prevalence. The prevalence of NMO is up to nine times higher in women than it is in men (de Seze et al., 2003; Ghezzi et al., 2004). With a median age of onset of 39 years (Wingerchuk et al., 1999), NMO develops on average ten years later than MS (Kantarci and Weinshenker, 2005). However, there is no age where NMO may not break out. Pediatric cases have been reported (Arabshahi et al., 2006) as well as disease onset occurring in elderly patients (Barbieri and Buscaino, 1989). Most NMO cases occur sporadic but rarely existing reports of familial NMO-IgG seropositive NMO support a genetic component to NMO susceptibility (Braley and Mikol, 2007; Matiello et al., 2010). The life expectancy for untreated patients suffering from NMO is approximately eight years after disease onset (Papais-Alvarenga et al., 2008). With treatment, the course of the disease rarely has a fast and fatal outcome; however, NMO is a severe disease and medical complaints accumulate with relapsing attacks (Bichuetti et al., 2013)

1.2.   Clinical characteristics and diagnosis

The key features of NMO are severe attacks of unilateral or bilateral ON leading to eye pain and impairments of vision, and transverse acute myelitis coming along with bilateral motor deficits and bladder and bowel dysfunction as well as pain and neurological deficits. At least 85 % of patients suffer from relapsing disease defined by recurrent attacks of ON or/and myelitis. However, NMO may also follow a monophasic course characterized by permanent clinical remission after the index events. (Wingerchuk et al., 1999; Wingerchuk and Weinshenker, 2003). Acute myelitis episodes are typically linked to spinal cord lesions extending over three or more vertebral segments on T2 weighted images (figure 1.1A). Magnetic resonance imaging (MRI) is used to diagnose ON (figure 1.1B) and transverse myelitis as indicated by gadolinium enhancement. In addition, approximately half of the patients develop brain lesions within the course of the disease. For example, some patients suffer from brainstem encephalitis leading to nausea, vomiting and hiccups (Misu et al., 2005). Occasionally, the lesions also extend to brain tissue surrounding the third and fourth ventricle (Pittock et al., 2006). These brain lesions are atypical for MS and hence serve as distinction criterion. The distribution of the characteristic NMO brain lesions mirrors the periventricular and hypothalamic localization of AQP4, a water channel expressed on astrocytes. This is in line with the fact that more than 75 % of all NMO patients produce autoantibodies against AQP4 (Waters et al., 2008) which serve as highly specific diagnostic biomarkers (Pittock et al., 2006). Binding of NMO-IgG to AQP4 leads to antibody-dependent cellular cytotoxicity (ADCC) as well as complement-dependent cytotoxicity (CDC) and complement-dependent cellular cytotoxicity (CDCC) which cause the destruction of astrocytes and resulting secondary loss of myelin in these lesions. The immunopathological features will be further discussed in chapter 1.4. These pathologic processes lead to accumulation of disability in recurrent attacks: long-term follow-up studies showed that 22 % of patients had permanent visual loss in at least one eye and 31 % suffered from permanent monoplegia or paraplegia (Wingerchuk et al., 1999; Wingerchuk and Weinshenker, 2003). The high mortality rate (23.3 % among the white population and up to 58.3 % among Afro-Brazilian patients) is mostly explained by cervical myelitis leading to respiratory failure (Papais-Alvarenga et al., 2008).
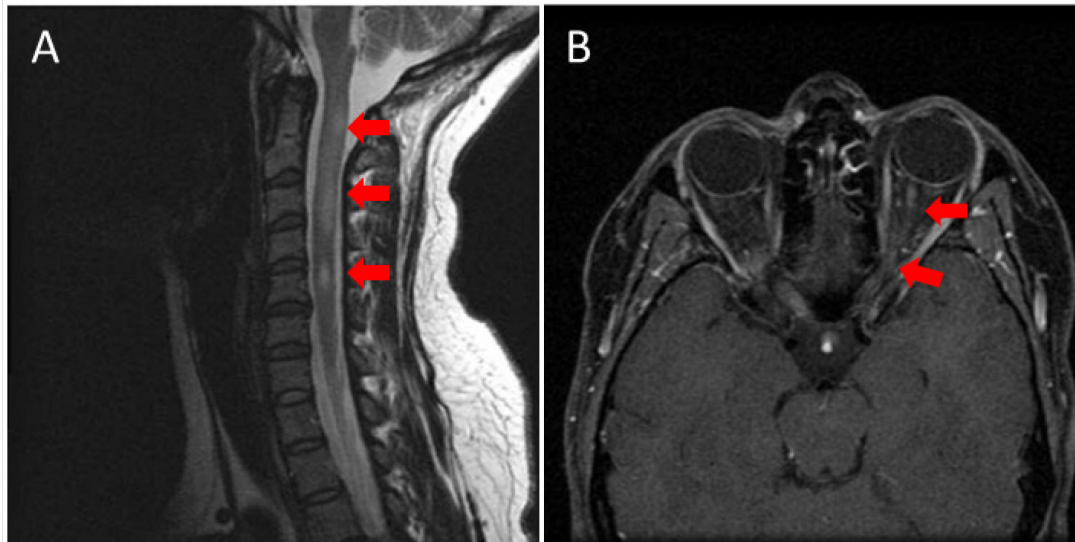
Figure 1.1: MRI of an NMO patient

(A) Sagittal T2-weighted cervical spine MRI demonstrates a lesion extending from the cervicomedullary junction to the superior border of the C4 vertebral body. (B) Axial T1-weighted magnetic resonance imaging with orbital views demonstrating gadolinium enhancement of the left optic nerve. This ON attack occurred simultaneously with the myelitis event shown in (A). Figures adapted and modified from Wingerchuk, 2006

These above mentioned signs and symptoms are nowadays commonly used to diagnose NMO and are summarized in the 2006 revised NMO diagnostic criteria (Wingerchuk et al., 2006). According to those, diagnosis of NMO needs the presence of optic neuritis and acute myelitis as well as at least two of the three supportive criteria: a spinal cord lesion extending over three or more vertebral segments as determined by MRI, a brain MRI lacking the diagnostic criteria for MS and the presence of NMO-IgG (table 1.1)

Table 1.1: 2006 revised NMO diagnostic criteria.

Table adapted from Wingerchuk et al., 2006

Definite NMO
Optic neuritis
Acute myelitis
At least 2 of 3 supportive criteria
1.   Contiguous spinal cord MRI lesion extending over ≥ 3 vertebral segments
2.   Brain MRI not meeting diagnostic criteria for multiple sclerosis
3.   NMO-IgG seropositive status

1.3.   Involvement of AQP4-specific autoantibodies

As mentioned above, Lennon and coworkers discovered an AQP4-specific autoantibody to be present in NMO (Lennon et al., 2005; Lennon et al., 2004). The pathogenicity of NMO-IgG has been proven in several studies (Bradl et al., 2009; Waters et al., 2008). Later on, NMO-IgG has been shown to be of polyclonal origin by isolating several clones with different AQP4-binding characteristics from the cerebrospinal fluid (CSF) of an NMO patient (Bennett et al., 2009), whereby the antibodies mainly belong to the IgG_1 subclass (Hinson et al., 2007; Waters et al., 2008). The autoantigen of NMO-IgG constitutes a conformational epitope which is formed by the extracellular loops of AQP4. This is supported by two observations: firstly, altering the structural rearrangements of these loops resulted in decreased binding between NMO-IgG and AQP4 (Pisani et al., 2014), and secondly, the induction of several point mutations and the resulting impaired binding of different NMO-IgG clones (Owens et al., 2015). The binding of NMO-IgG to these epitopes initiates the complement system and thus a cascade of immunological reactions (Lucchinetti et al., 2014). Studies correlating serum NMO-IgG titers with disease activity, severity, outcome and response to therapy have yielded inconsistent results (Takahashi et al., 2007; Waters et al., 2008). Some studies suggest a correlation between the presence of NMO-IgG and the probability of relapsing disease (Ketelslegers et al., 2011; Weinshenker et al., 2006b) or the severity of the disease course, respectively (Matiello et al., 2008). The situation in AQP4-antibody negative NMO patients is even more complicated. Recent studies suggest that some of these patients produce antibodies against other proteins, e.g. against the myelin oligodendrocyte glycoprotein (MOG) (Mader et al., 2011; Ramanathan et al., 2014) which resides at the outer surface of oligodendrocytes and the myelin sheath (Brunner et al., 1989). Other patients which appear NMO-IgG negative were under immunosuppressive therapies at the time point of testing, leading to NMO-IgG titers below the detection threshold and thus causing false-negative results when the antibody status is only determined from the serum (McKeon and Pittock, 2009). Moreover, the testing procedures for NMO-IgG titers vary among different studies and so does their sensitivity.

Despite rapid advances in the understanding of NMO pathogenesis, unanswered questions remain, particularly with regards to individual susceptibility and antigenic triggers for NMO-IgG production, respectively.

1.4.   Immunopathology

The current idea of NMO's pathogenesis states that NMO-IgG which gain access to the CNS to AQP4 on perivascular astrocyte endfeet, elicits the activation of the classical complement cascade with an inflammatory response. These processes lead to granulocyte and macrophage infiltration and secondary oligodendrocyte damage as well as demyelination and neuronal death (Papadopoulos et al., 2014; Wingerchuk et al., 2007).
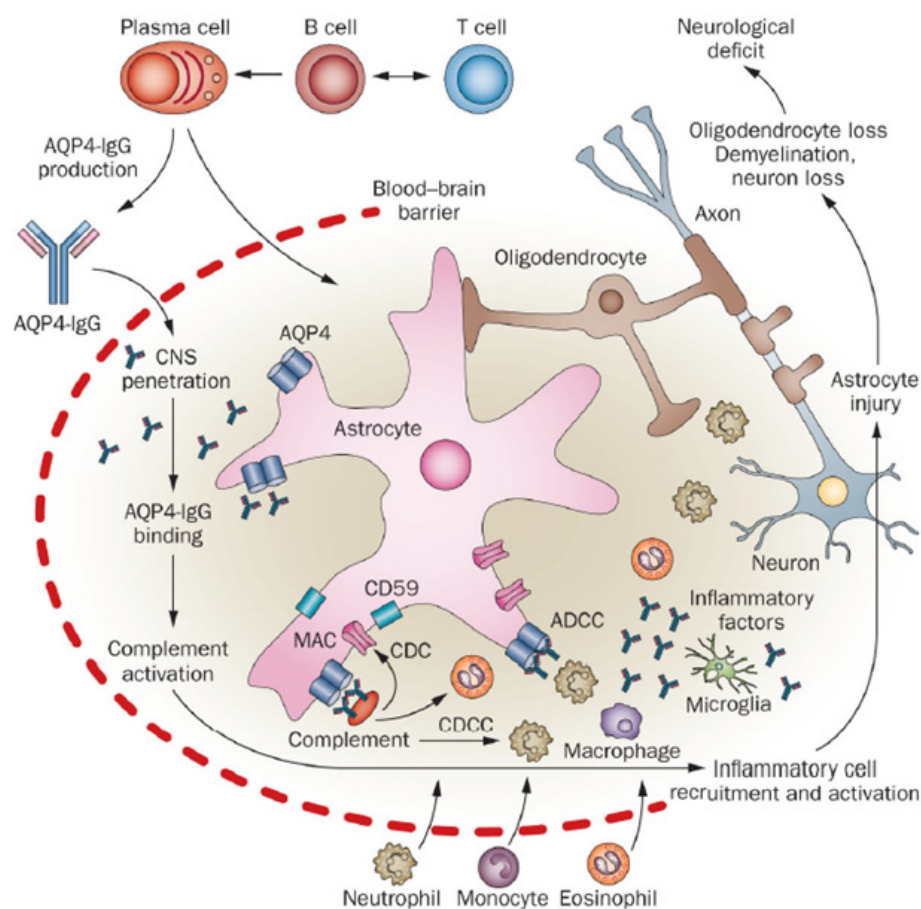
Figure 1.2: Immunopathological processes in NMO

Within the CNS, NMO-IgG recognize their antigen AQP4, which is strongly expressed on astrocyte foot processes at the glia limitans. Complement activation leads to complement-dependent cytotoxicity (CDC) and to deposition of membrane attack complexes causing the disruption of targeted cell membranes. Activated complement also recruits inflammatory cells (mainly neutrophils and eosinophils). Complement-dependent cellular cytotoxicity (CDCC) together with the inflammatory milieu causes further injury to oligodendrocytes and neurons, resulting in neurological deficits characteristic for NMO. Figure adapted by permission from Macmillan Publishers Ltd. from Papadopoulos et al., 2014 (Copyright 2014).

Under physiological conditions, the blood-brain barrier (BBB) shields the CNS from the infiltration of immune cells and antibodies, hence NMO-IgG has only limited access to the

5

CNS parenchyma. For this reason, patients have been described who were NMO-IgG positive for up to 16 years prior to the onset of inflammatory CNS disease and clinical diagnosis of NMO (Leite et al., 2012; Nishiyama et al., 2009). When NMO-IgG gains access to the CNS, e.g. when the BBB is opened by CNS inflammation, the antibodies bind to AQP4, the target of NMO-IgG, which is densely expressed on ependymal cells and astrocytic endfeet forming the perivascular and subpial glia limitans. During CNS inflammation, NMO-IgG and T cells, but also eosinophils and neutrophils enter the CNS (Lucchinetti et al., 2002; Weinshenker et al., 2006a). This combination of complement- and cell-mediated injury causes astrocyte loss and subsequent loss of oligodendrocytes leading to demyelination and neuronal necrosis. (Papadopoulos et al., 2014; Wingerchuk et al., 2007). (Figure 1.2)

These immunopathological processes lead to lesions coming along with an impaired neurological function which accounts for the various symptoms and characteristics of NMO.

1.5.   Current treatment options

The fundamental principle of NMO therapy constitutes in diminishing neurological disability by mitigating acute attacks, accelerating recovery and preventing future aggravations. The first-line therapy to alleviate the symptoms of NMO during acute disease exacerbations constitutes the administration of intravenous methylprednisolone (IVMP), a synthetic corticosteroid drug. Corticosteroids are known to have myriads of anti-inflammatory and immunosuppressive effects, such as reduction of circulating lymphocytes and monocytes and altered transcription of proinflammatory cytokines (Barnes, 2006). A second very common treatment during acute disease exacerbations constitutes plasmapheresis to deplete pathogenic NMO-IgG, especially for patients who occur to be resistant against IVMP treatment or who suffer from very severe attacks (Bonnan et al., 2009; Watanabe et al., 2007; Weinshenker et al., 1999). Furthermore, a combination of both plasma exchange and the administration of corticosteroids is more likely to improve the patients' condition than IVMP alone (Abboud et al., 2015). Both treatments are not only applied during acute attacks but have also been demonstrated to reduce relapse activity when used regularly (Miyamoto and Kusunoki, 2009).

Another currently applied therapeutic approach is the use of monoclonal antibodies. Great success was obtained with the administration of rituximab, a humanized anti-CD-20 monoclonal antibody that depletes B cells. Rituximab achieved a reduction of the annual relapse rates by at least 87 % and patients were relapse-free for years. (Collongues et al., 2015; Radaelli et al., 2015; Zephir et al., 2015). Furthermore, there are anti-complement therapies via monoclonal antibodies, e.g. eculizumab, which neutralizes the C5 complement protein. Upon treatment with eculizumab, most of the patients were relapse-free for at least one year (Pittock et al., 2013).

Since scientists still try hard to elucidate and understand the etiology of NMO, the currently available therapies clearly cannot offer a cure but aim to reduce the suffering of the patients. This objective is achieved better since the discovery of NMO-IgG leading to a better disease outcome due to earlier diagnosis and therapies lowering IgG levels (Zekeridou and Lennon, 2015).

1.6.   Aquaporin 4 – the target of NMO-IgG

Aquaporins constitute the main class of channels facilitating passive transepithelial water transport along osmotic gradients. The family of mammalian AQP comprises 13 different types (AQP0–AQP12) whose principal function is water transport across membranes, whereby a subset of the AQP family, the aquaglyceroporins, also function as channels for glycerol (AQPs 3, 7, 9 and 10). Besides water and glycerol, AQPs are suggested to regulate the passage of other solutes such as, for example, ammonia (Musa-Aziz et al., 2009) and urea (Ishibashi et al., 1994), its metabolite across cell membranes. (Kitchen et al., 2015)

AQP4 transports only water and is the principal water channel of the CNS. It is expressed in astrocytes throughout the CNS, particularly on astrocyte endfeet of the glia limitans at interfaces between brain parenchyma and cerebrospinal fluid in the ventricular and subarachnoid compartments (figure 1.3) (Nielsen et al., 1997; Rash et al., 1998). AQP4-deficient mice exhibit reduced accumulation of water in the brain than wild-type mice in models of brain edema (Manley et al., 2000).
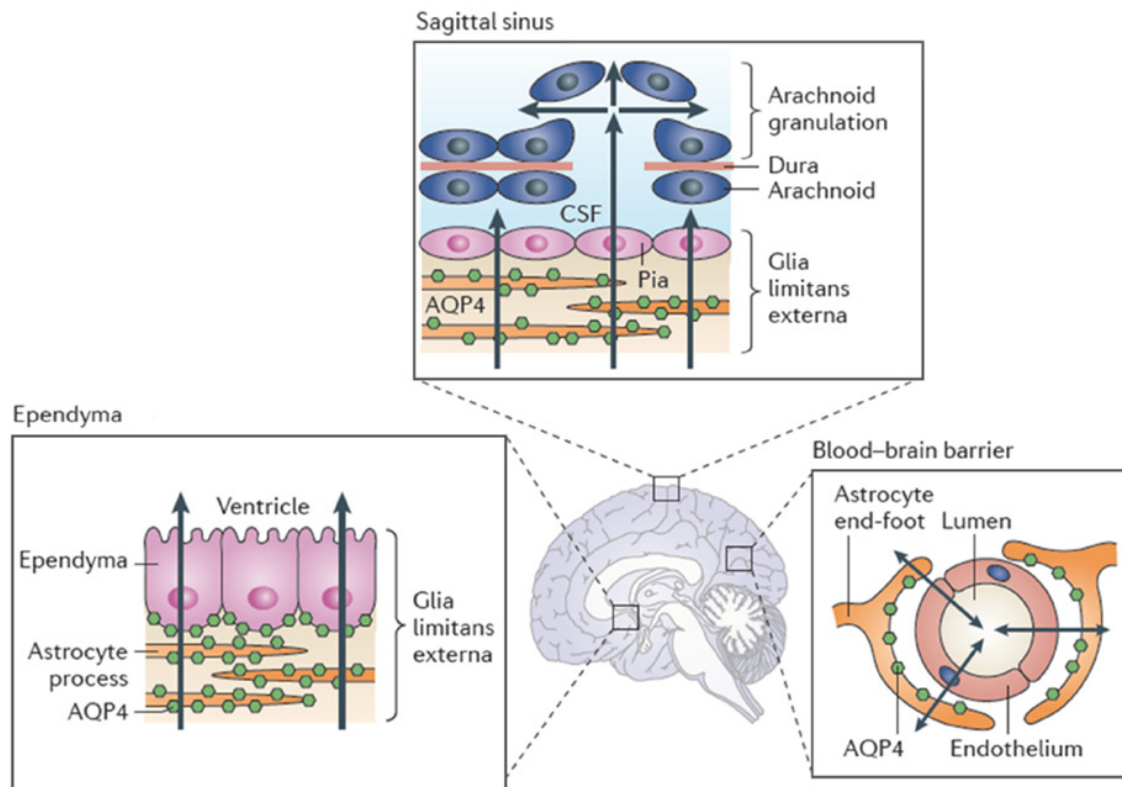
Figure 1.3: Expression of AQP4 on astrocytic foot processes

AQP4 facilitates water movements across blood-brain and blood-CSF barriers. Figure adapted by permission from Macmillan Publishers Ltd and modified from Verkman et al., 2014 (Copyright 2014)

Besides the CNS, AQP4 is also expressed in a variety of peripheral tissues such as the lacrimal gland, the duct cells of the salivary glands, the inner ear, olfactory epithelial cells, gastric parietal cells, tracheal epithelial cells, airway epithelium, kidney collecting ducts (Verkman, 2008), and on the fast twitch fibers of skeletal muscles. (Kitchen et al., 2015; Verkman, 2012; Verkman et al., 2014)

1.6.1.   Structural properties of AQP4

The size of AQP monomers accounts to approximately 30 kDa and the family members share several common features: the monomer comprises six membrane-spanning α-helical segments (M1, M2, M4-M7 and M8) that surround a central cavity containing two shorter helical segments (M3 and M7) that do not span the entire membrane but enter and exit from the same side of the membrane. Both the N- and C-terminal domains are located in the cytoplasm. In total, one monomer is equipped with five extra-membrane loops: three on the extracellular surface (loops A, C and E) and two intracellular loops (B and D) (figures 1.4 and 1.5).
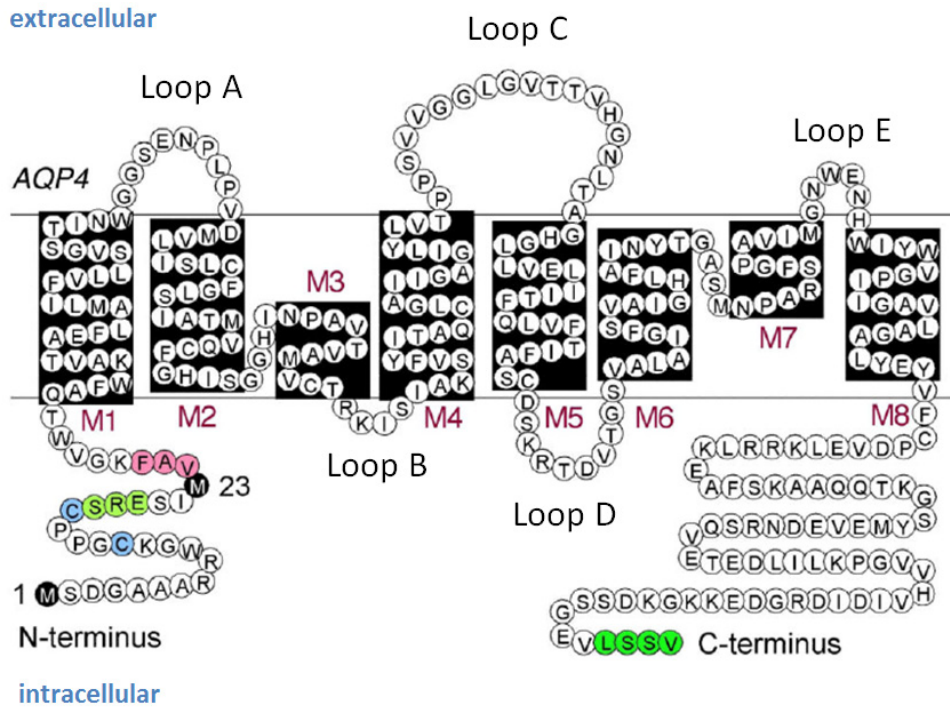
Figure 1.4: Schematic of AQP membrane topography

Aquaporins comprise six transmembrane domains and two shorter α-helices that do not span the entire membrane. Figure adapted by permission from John Wiley and Sons and modified from Verkman et al., 2013 (Copyright 2013).
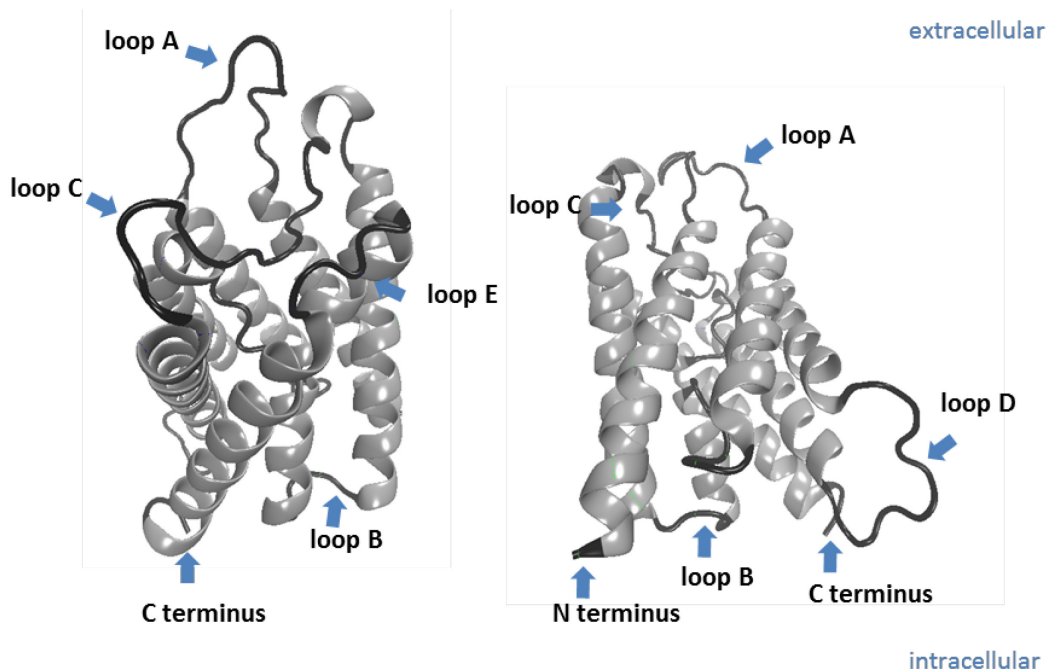
Figure 1.5: Arrangement of human AQP4 in the plasma membrane

The schematic depicts the structural features of AQP4 with loops A, C and E on the extracellular surface and loops B and D as well as the C and N termini in the cytoplasm. The images were created using VMD 1.9.2

The monomers arrange in a way that the helical domains form a narrow aqueous pore (20-25 Å) with a cytoplasmic and an extracellular vestibule. (Fujiyoshi et al., 2002; Walz et al., 2009). Through this pore, water transport and selectivity is conferred by electrostatic and steric factors (Khalili-Araghi et al., 2009). Four of these monomers each assemble to tetramers in cell membranes.

1.6.2. Two isoforms of AQP4

The human *AQP4* gene is located on chromosome 18 q11-q12 and encodes two different isoforms. The two major isoforms are a longer (M1, 32 kDa) and a shorter (M23, 30 kDa) isoform, termed according to the methionine position of their translation initiation, i.e. translation of the M23 isoform starts at Met-23 of the AQP4 mRNA. Thus, the M1 and M23 isoforms differ by 22 amino acids in the N terminus. (Lu et al., 1996) Both isoforms can assemble as homotetramers and as heterotetramers in plasma membranes (Neely et al., 1999).
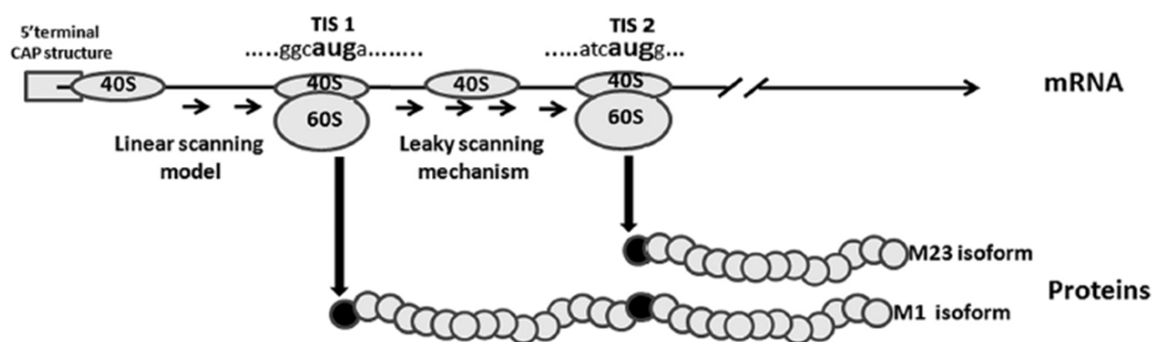
Figure 1.6: Translational regulation of AQP4-M1 and AQP4-M23

The image shows a part of the M1 mRNA with the two translation initiation sites (TIS) for both isoforms and outlines the leaky scanning mechanism, in which the 40s ribosome fails to initiate translation in the suboptimal context of the M1 start codon and hence, continues scanning up to the TIS2 (M23). Figure adapted from Rossi et al., 2010

So far, there is limited knowledge about the mechanisms defining the expression ratios of the two isoforms. Interestingly, even though a much higher relative abundance of M1 mRNA in comparison to M23 mRNA in human brain has been shown (Umenishi and Verkman, 1998), this ratio is inverted when it comes to AQP4 protein expression levels. Lu and colleagues have shown that AQP4-M23 is more abundant in human brain tissue (Lu et al., 1996) which might be explained by a leaky scanning mechanism meaning that some

ribosomes fail to initiate the translation at the Met-1 position and continue scanning until the next methionine, namely Met-23 (Kozak, 1999). The Kozak consensus sequence, which was found upon examining 699 vertebrate mRNAs, states that the optimal context of the AUG[start] codon for translation initiation is 'GCC[A/G]CCaugG' (Kozak, 1987). Most importance is attached to the guanine directly downstream of the start codon, and for the third base upstream of AUG, adenine is better than guanine. According to these findings, the initiation site for AQP4-M1, which is 'GGCaugA' is less favorable than the one for AQP4-M23 ('ATCaugG') since it is more similar to the Kozak consensus sequence. Since ribosomes scan the M1 position first and encounter a non-optimal context, some of them might fail to initiate translation and continue scanning and then start translation at the Met-23 position (Kozak, 2002) (figure 1.6). (Rossi et al., 2010)

1.6.3. Assembly in higher order structures

In plasma membranes, AQP4 forms tetramers which in turn may assemble to orthogonal arrays of particles (OAPs) constituting square arrays of (up to more than hundred) intramembrane particles (Nicchia et al., 2010). Freeze fracture electron microscopy (FFEM) further revealed that M23 assembles into large OAPs, whereas M1 tetramers alone are widely dispersed. When co-expressed as under physiological conditions, AQP4 forms OAPs of intermediate size suggesting that the ratio of the two isoforms determines the OAP size (Furman et al., 2003). However, the M1 isoform alone is not capable of forming OAPs. Crane and Verkman provided evidence that the N-terminal residues upstream of Met-23 (which are not present in AQP4-M23) block the inter-tetrameric interactions that facilitate OAP formation in the M1 isoform (Crane and Verkman, 2009a). Due to these differential properties of M1 and M23, their relative abundance *in vivo* is the primary determinant for the formation of OAPs of different sizes. The major role of OAP formation in NMO has been shown by Nicchia and colleagues in 2009, when they provided evidence that NMO-IgG binds to OAPs but not to AQP4 tetramers in immunofluorescence experiments using M23- and M1-transfected HeLa-cells. The cells transfected with M23 formed OAPs whereas the M1-transfected cells did not; thus, the impact of OAPs on epitope-recognition of NMO-IgG could be examined and the results revealed that NMO-IgG did not bind to non-OAP-forming AQP4 (figure 1.7) (Nicchia et al., 2009).
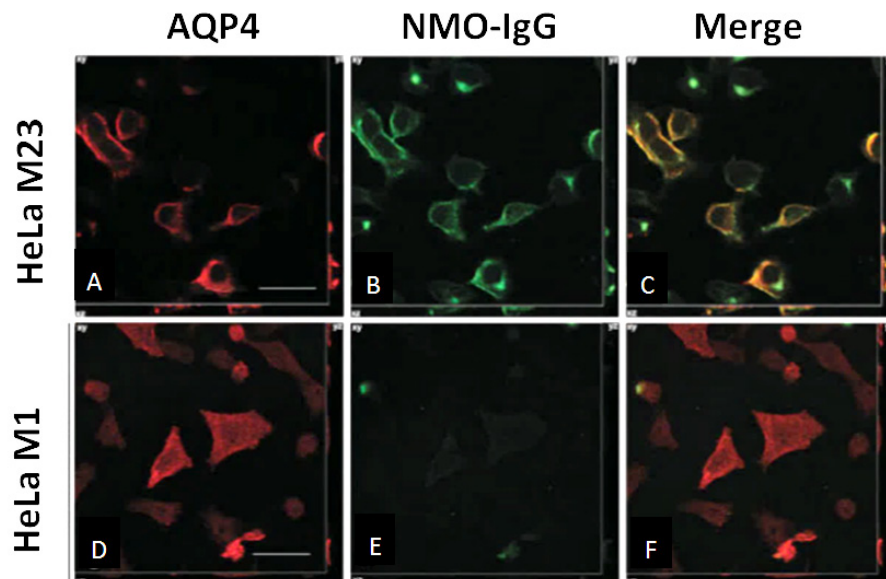
Figure 1.7: Double immunofluorescence experiments with AQP4 antibodies and NMO serum (NMO-IgG)

Merging NMO and AQP4 images shows a complete colocalization in HeLa M23. Note the absence of staining with NMO serum in HeLa cells transfected with AQP4 M1 isoform. Scale bars: 20 μm. Figure and legend adapted by permission from John Wiley and Sons and modified from Nicchia et al., 2009 (Copyright 2009).

However, there are contradicting studies indicating that NMO-IgG also binds to tetramers of AQP4-M1 that do not form OAPs, even though in a decreased amount as compared to AQP4-M23 which is organized in OAPs (Crane et al., 2009; Crane et al., 2011). To sum up, the binding epitope for many NMO-IgG may be located at inter-tetrameric interfaces which are present in OAPs (figure 1.8), whereby at least some subpopulations may bind to intra-tetrameric epitopes as found in M1 tetramers.

Figure 1.8: Schematic model on how NMO epitopes could be associated to OAP formation

Side (left panel) and top views (central panel) of an AQP4 OAP are shown. Upon OAP formation, the extracellular loops of each tetramer rearrange and create at least two different NMO-IgG epitopes. Figure and legend adapted and modified from Pisani et al., 2011

Current studies suggest that the preferential binding of NMO-IgG to OAPs is rather based on structural changes upon array assembly than on bivalent NMO-IgG binding (Pisani et al., 2011; Verkman et al., 2013). It has been shown that efficient CDC requires AQP4 assembly in OAPs (Phuan et al., 2012) and was mostly absent in AQP4-M1-expressing cells.
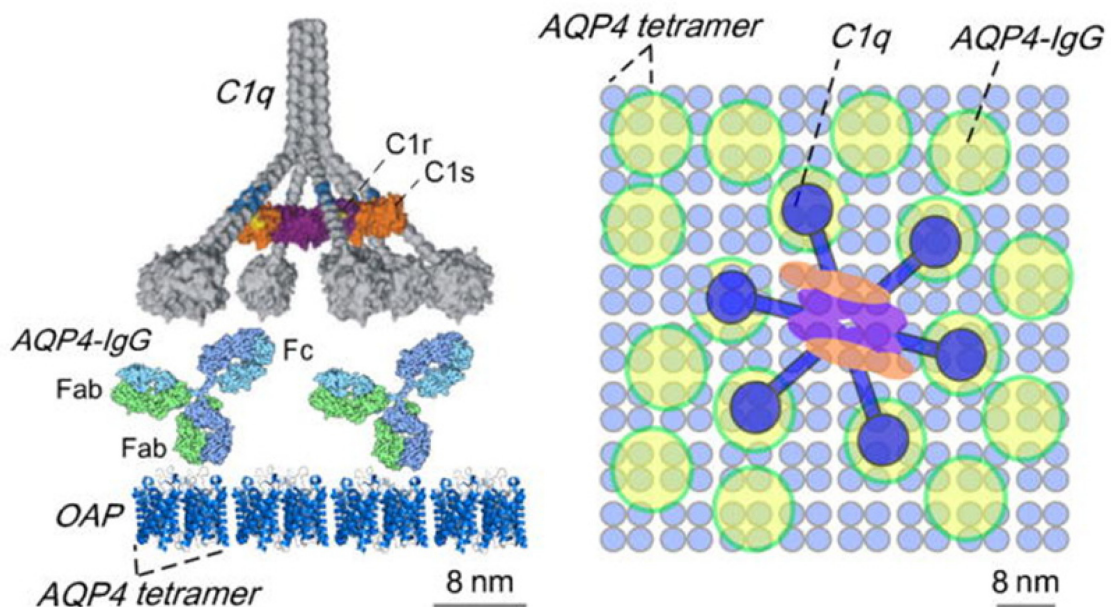
Figure 1.9: Multivalent binding of C1q to Fc regions of NMO-IgG bound to OAP-assembled AQP4
Schematic is shown in side (left) and top view (right). Figure adapted and modified from Phuan et al., 2012

Measurements of complement protein binding revealed that the binding affinity of C1q, a large, multivalent protein, is enhanced with increased binding valence of antibodies; i.e. OAPs constitute assemblies of NMO-IgG-epitopes leading to clustered binding of NMO-IgG and thus enhance binding of C1q to clustered NMO-IgG (figure 1.9). This leads to an increased complement activation (Hinson et al., 2012). Moreover, it has been demonstrated that the binding of NMO-IgG itself does not alter the cellular distribution or OAP assembly of AQP4 nor does it impair the function of AQP4 (Nicchia et al., 2009; Rossi et al., 2012). This indicates that the pathogenic effect of the autoantibodies is not even partially explicable by a direct impairment of astrocyte water transport, but, according to current knowledge by activated immunoresponse (see chapter 1.4) (Hinson et al., 2007).

1.7.   Epitope mimics

Epitope mimics are, as their name suggests, defined as mimics of an epitope and have firstly been mentioned under the term "mimotopes" in 1986 (Geysen et al., 1986). Mimotopes imitate a part of the original epitope whereby amino acid sequence homology does not necessarily exist between the sequences of the mimotope and the epitope of the native antigen. However, both are recognized by the same antibody paratope (so-called cross-reactivity), which is expected to rely on similar physicochemical properties and spatial organization. Hence, the epitope and its mimic exhibit similar structural properties. However, the interaction with such a mimotope (usually, a synthetic peptide) is often decreased in comparison to the reactivity with the native protein because its conformation is not identical to that of the protein or because other elements of the discontinuous epitope are energetically missing. (Moreau et al., 2006)

Mimotopes can be obtained via biopanning using phage-displayed peptide libraries presented to a given antibody (Smith and Petrenko, 1997). There is a broad variety of research areas benefitting from mimotopes, such as the identification of anti-tumor antibodies (Hardy and Raiter, 2005) or the development of vaccines to raise antibodies against a specific epitope (Knittelfelder et al., 2009; Li et al., 2006). Mimotopes can also be analyzed using bioinformatics tools, e.g. for mapping the epitope of the antigen recognized by an antibody using mimotope-based prediction software. In this way, they can also help in protein engineering, drug design and identification of protein function (Moreau et al., 2006).

1.8.   Aim of the thesis

One of the pathological key features of NMO is the presence of AQP4-specific antibodies in the majority of patients and yet, we do not know the exact epitope(s) recognized by these antibodies, or whether the epitopes recognized in a given patient predict better or worse prognosis or response to therapy. Unfortunately, however, conformational epitopes are extremely hard to handle. Therefore, I was searching for linear peptides mimicking these conformational epitopes in a phage display library. Finding such mimotopes might enable the identification of several subpopulations of the polyclonal NMO-IgG and to characterize different patients' antibody pools and thus potential reasons for differences in disease outcome and severity. Moreover, mimotopes can be used for active immunization strategies, e.g. to raise antibodies in valid animal models to investigate the effect of distinct NMO-IgG subpopulations.

2. Materials and Methods

2.1. NMO-IgG

For the present work, purified IgG obtained by plasmapheresis of an NMO-IgG-seropositive patient were used. The 21 years old female patient was found to suffer from neuropsychiatric systemic lupus erythematosus (NPSLE) with stroke and developed a mild NMO at a later time point. One of the characteristic features of NPSLE is the presence of anti-DNA-antibodies (Ceppellini et al., 1957). Hence, the IgG fraction of this patient with a total protein concentration of 9.7 mg/ml contains elevated amounts of anti-DNA-antibodies in addition to AQP4-reactive IgG. The titer of AQP4-specific antibodies within this polyclonal fraction was determined as 1:10240 comprising IgG1 and IgM isotypes. The *in vivo* pathogenicity of these NMO-IgG has been proven by Dr. Satoru Oji (Department of Neuroimmunology, Center for Brain Research, Vienna) by injecting the patient's plasmapheresis product into the periphery Lewis rats after induction of myelin basic protein (MBP)-specific T-cell mediated experimental autoimmune encephalomyelitis (EAE). NMO-typical lesions were formed in the spinal cord and were characterized by perivascular loss of AQP4 reactivity (figure 2.1A), by loss of astrocytes in these areas (as determined by loss of the astrocytic marker, i.e. the glial fibrillary acidic protein (GFAP)) (figure 2.1B), and by leakage of human IgG in these regions (figure 2.1C).

The plasmapheresis product was kindly provided by Zsolt Illes from the Department of Neurology of the University of Southern Denmark in Odense, and its use for the mimotope search was approved by the Regional and National Ethical Committee of Hungary (3893.316-12464/KK4/2010 and 42341-2/2013/EKU). Hereinafter, the patient's plasmapheresis product will be referred to as NMO-IgG Pt1.
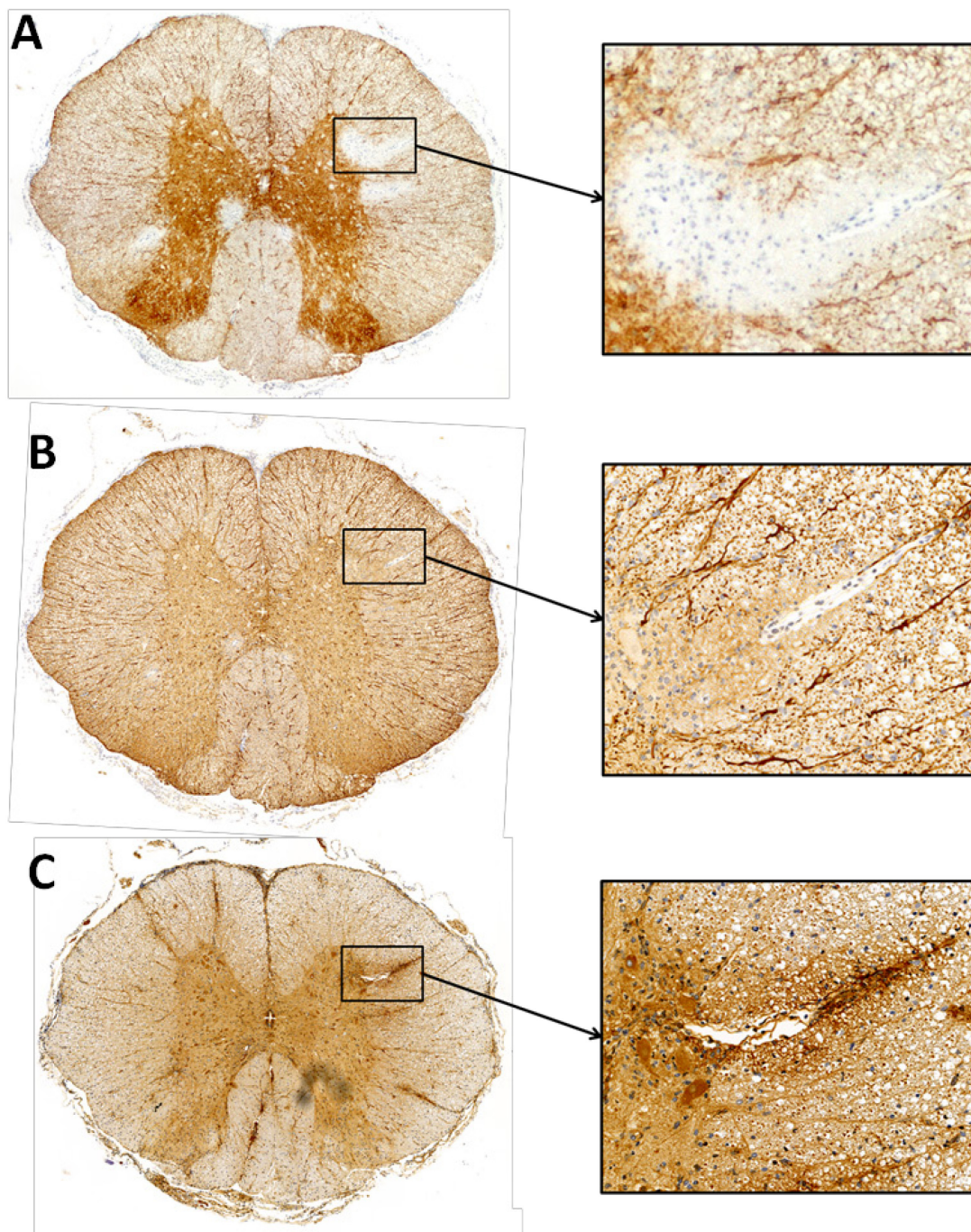
Figure 2.1: Immunohistochemical staining of the spinal cord of a rat injected with NMO-IgG Pt1 after EAE-induction

Consecutive sections were stained for AQP4 (A), GFAP (B) and human IgG (C). Stainings are provided by Satoru Oji (unpublished data)

2.2.   Immunocytochemistry of rat astrocytes

In order to confirm and visualize the binding of NMO-IgG Pt1 to AQP4 *in vitro*, rat astrocytes expressing AQP4 were stained with NMO-IgG Pt1 to show colocalization of the antibody and its target, AQP4.

2.2.1. Antibodies and media

- **Freezing medium**
    - RPMI (Bio Whittaker®, Lonza)
    - 45% fetal calf serum (FCS) (Lonza)
    - 10% DMSO (Dimethyl Sulfoxide, Sigma-Aldrich, St. Louis, MO, USA)

- **Mixed glia medium**
    - RPMI (Bio Whittaker®, Lonza)
    - 10 % FCS (Lonza)
    - 1 % Glutamate (L-Glu 200 mM in 85% NaCl Solution, Invitrogen, Carlsbad, CA, USA)
    - 1 % Penicillin/Streptomycin (10 000 U/ml + 10 000 U/ml, Lonza)

- **Primary antibodies**
    - Rabbit-anti-AQP4 (#A5971, Sigma, St. Louis, MO, USA)
    - Goat-anti-GFAP (#SC-6170, Santa Cruz Biotechnologies Inc., Paso Robles, CA, USA)

- **Secondary antibodies**
    - Donkey-anti-rabbit-Cy2 (#711-225-152, Jackson ImmunoResearch Laboratories, Inc., West Grove, PA, USA)
    - Donkey-anti-goat-Cy5 (#705-175-147, Jackson ImmunoResearch Laboratories, Inc.)
    - Donkey-anti-human-Cy3 (#709-165-149, Jackson ImmunoResearch Laboratories, Inc.)

2.2.2. Staining of live astrocytes

Paraffin dots (Paraffin wax, Sigma-Aldrich) serving as spacers were applied to glass cover slips (Ø 12 mm, Carl Roth, Karlsruhe, Germany). The cover slips were subsequently coated with 5 ml Poly-L-Lysine (5 µg/ml in 1x PBS (Bio Whittaker®, Lonza) for 2 hours at 37 °C. Then, the cover slips were exposed to UV light for 15 min in a 6 cm Petri dish for sterilization. In the meantime, mixed glia cells from Lewis rats (frozen after 8 days in culture) were thawed from liquid N_2 storage in a water bath (37 °C). In order to get rid of the freezing medium in which the cells had been stored, the cell suspension (corresponding to approximately 10^5 cells) was added to 10 ml RPMI (Bio Whittaker®, Lonza) and centrifuged at 270 g and 4 °C for 10 min (1 min/ml). The supernatant was discarded and the cells were resuspended in 5 ml mixed glia medium. Glass cover slips were washed two times with 1X PBS (Lonza) before the

cells were seeded in the dish containing the cover slips and incubated overnight at 37 °C and 5 % CO_2.

On the next day, the cells were washed three times with ice-cold RPMI and cover slips were transferred to 100 µl drops of NMO-IgG Pt1 (1:1000 in mixed glia medium) each in one well of a 12-well plate (Greiner Bio-One, Kremsmünster, Austria) and incubated for 30 min at 4 °C in a humidity chamber on a shaking platform (3 rpm). After washing three times with ice-cold RPMI, the secondary antibody for NMO-IgG (Donkey-anti-human-Cy3, 1:100 in mixed glia medium) was applied for 45 min at 4°C in a humidity chamber in the dark. Cells were washed three times with 1x PBS and then fixed with 4 % PFA (Merck KGaA, Darmstadt, Germany) for 15 min at room temperature (RT) protected from light. After another three times of washing with 1x PBS, the cells were permeabilized with 0.1 % Triton-X-100 (t-Octylphenoxypoly-ethoxyethanol, Sigma-Aldrich) in RPMI/10% FCS for 5 min at RT in the dark and again washed with 1x PBS. Incubation with primary antibodies (rabbit-anti-AQP4 and goat-anti-GFAP, 1:100 in PBS/10% DAKO Diluent (DAKO Real™ Antibody Diluent, Agilent Technologies Inc., Santa Carla, CA, USA) was conducted overnight at 4 °C in a humidity chamber and under protection from light on a shaking platform (3 rpm). Afterwards, the cells were washed three times with 1x PBS and secondary antibodies (donkey-anti-rabbit-Cy 2, 1:150, donkey-anti-goat-Cy5, 1:100 in DAKO buffer (DAKO Wash buffer, Agilent Technologies Inc.)/10% FCS) were applied for 1h at RT and under protection from light. Having washed the cells three times with 1x PBS, 4', 6-diamidino-2-phenylindole (DAPI) (Carl Roth GmbH und Co KG) (1:10000 in double-distilled water (ddH$_2$O)) was applied for 5 min at RT and under protection from light. After washing with 1x PBS and with ddH$_2$O, cover slips were left in ddH$_2$O until mounting. Finally, the cover slips were mounted in one drop of Gallate/Geltol (Sigma-Aldrich) on glass slides and stored at 4 °C under protection from light.

2.2.3. Single staining controls

Single staining controls served as validation of the staining and to check for bleed-through of emission of fluorophores into the detection channels of other fluorophores. The procedure was the same as described above, whereby each cover slip was only stained with one fluorophore, i.e. in the end, there were four differentially stained cover slips: AQP4-Cy2 (primary antibody: rabbit-anti-AQP4, secondary antibody: donkey-anti-rabbit-Cy 2), GFAP-

Cy5 (primary antibody: goat-anti-GFAP, secondary antibody: donkey-anti-goat-Cy5), DAPI and NMO-IgG-Cy3 (secondary antibody: donkey-anti-human-Cy3). In all steps where no antibody was applied to a cover slip, it was exclusively incubated with mixed glia medium and DAKO buffer, respectively.

2.2.4. Confocal microscopy

The stainings were analyzed using a Leica TCS SP5 setup (Leica Microsystems, CMS-GmbH, Germany). Cy2 signals were detected with an argon laser (488nm excitation), detection of Cy3 was carried out using a DPSS561 laser and DAPI staining was detected with a 405 Diode laser. Images were edited and auto-adapted for contrast and brightness with ImageJ (Schneider et al., 2012). Supplementary figure S1 gives detailed information about the spectral properties of the used fluorophores.

2.3.   Phage display

Phage display constitutes a powerful tool to isolate specific ligands for a variety of protein targets and for the analysis and manipulation of their binding properties. In principle, this is facilitated by insertion of the nucleotide sequence encoding the peptide to be displayed into a phage genome fused to a gene encoding a phage coat protein. This fusion ascertains that the protein is displayed on the surface. The corresponding DNA sequence is contained within the same phage particle and can be easily replicated with the phage, which are fundamental features for the phage display technique. These features facilitate rapid distinction of binding affinities to a given target molecule (e.g. an antibody) by panning, an *in vitro* selection process. Biopanning is carried out by incubating a library of phage-displayed peptides on a plate coated with the target, washing away the non-binding phage, and eluting the specifically bound phage. (Rodi and Makowski, 1999; Smith, 1985; Willats, 2002). The technique offers several benefits such as providing high diversity of peptides despite its simplicity and relatively low costs since no special equipment is required. Hence, phage display constitutes an appropriate method to search for mimotopes of NMO-IgG.

In the present study, the Ph.D.[TM]-12 Peptide Library (New England BioLabs, Ipswich, MA, USA) was used. It is based on the M13 phage vector presenting random 12-mer peptides on the N-terminus of the minor coat protein pIII linked by the short sequence Gly-Gly-Gly-

Ser (GGGS) (M13KE). The random sequence is designed according to an NNK library, i.e. the first and second codon positions are either A, C, G, or T with equal probability and the third codon position is chosen only from G or T, again with equal probabilities. The protein is present in five copies on one end of the mature phage engendering the presence of five copies of the random peptide (figure 2.2). The peptide is sufficiently short to not impair the ability of the phages to infect bacteria.
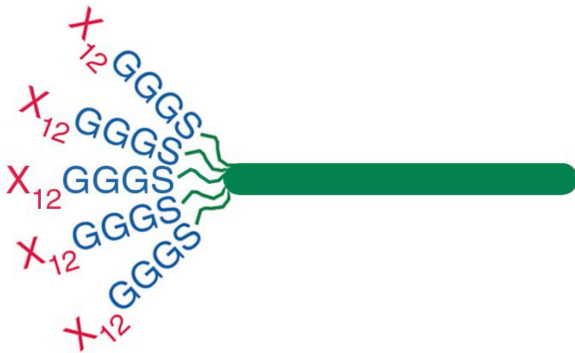
Figure 2.2: Structure of the phage particles contained in the pentavalent library

Five copies of a single randomized 12-mer peptide are displayed each at one of the five copies of the pIII protein, connected by the short linker sequence Gly-Gly-Gly-Ser. Image adapted and modified from New England BioLabs Ph.D.[TM] Phage Display Libraries Instruction Manual.

M13 is a non-lytic phage and forms turbid plaques which are caused by diminished bacterial growth upon plating. Another feature of the M13 phage virion is its male-specificity, i.e. these phages only infect bacteria harboring the F-factor and thus developing an F-pilus. The F-factor of the used E.coli2738 contains a transposon conferring tetracycline-resistance, hence using tetracycline-containing medium for plating and propagating of E.coli facilitates selection of bacteria. Furthermore, the recommended ER2738 host strain is an alpha-complementing strain resulting in blue plaques on plates with IPTG and XGal when infected with phages containing the *laczα* gene like the M13KE. Thus, blue, turbid plaques indicated the presence of M13KE. Since the library contains about 10^9 distinct 12-mer sequences and 10^{10} phages per µl, approximately ten copies of each peptide are found in 1 µl.

To validate experiments conducted using the Ph.D.[TM]-12 Phage Display Peptide Library Kit, the manufacturer suggests a positive control panning experiment with streptavidin as target. Since streptavidin has been shown to bind to peptides containing the motif His-Pro-Gln (HPQ), this sequence should be present in single phage clones after three rounds of panning

and amplification. This panning control experiment has been conducted previously in the lab. Four valid sequences were revealed of which three were positive for the HPQ motif (supplementary table S1), i.e. the validity of biopanning experiments with other targets is ensured.

2.3.1. Media and solutions

- **Ph.D.™-12 Phage Display Peptide Library Kit (New England BioLabs) components**
    - Phage Display Peptide Library 100 µl, ~ 1 x 10^{13} plaque forming units (pfu)/ml. Supplied in TBS with 50% glycerol. Stored at -20 °C
    - 96 gIII sequencing primer 5´- ^{HO}CCC TCA TAG TTA GCG TAA CG -3´, 100 µl, 1 pmol/µl. Stored at -20 °C
    - 28 gIII sequencing primer 5´-^{HO}GTA TGG GAT TTT GCT AAA CAA C-3´, 100 µl, 1 pmol/µl. Stored at -20 °C
    - *E. coli* ER2738 host strain F´ *proA+B+ lacIq Δ(lacZ)M15 zzf::Tn10(TetR)/fhuA2 glnV Δ(lac-proAB) thi-1 Δ(hsdS-mcrB)5*.Host strain supplied as 50% glycerol culture; not competent. Stored at -80 °C

- **20% PEG/ 2.5 M NaCl**
    - 20% /(w/v) polyethylene glycol-8000 (PEG)
    - 2.5 M NaCl
      Stored at 4 °C
- **Elution buffer**
    - 0.2 M Glycine-HCl (pH 2.2)
    - 1 mg/ml bovine serum albumin (BSA) (PAA Laboratories GmbH, Pasching, Austria)
      Filter sterilized, stored at 4 °C
- **General blocking buffer**
    - 0.1 M NaHCO$_3$ (pH 8.6) (Merck)
    - 5 mg/ml BSA
      Filter sterilized, stored at 4 °C
- **IPTG/XGal stock**
    - 0.5 g IPTG (Isopropyl β-D-1-thiogalactopyranoside, AppliChem GmbH, Darmstadt, Germany)
    - 0.4 g XGal (5-bromo-4-chloro-3-indolyl-β-D-galactopyranoside, Sigma-Aldrich)
    - 10 ml DMF (N,N- Dimethylformamide; Alfa Aesar GmbH & Co KG, Darmstadt, Germany)
      Stored at -20 °C

- **LB medium**
    - 10 g tryptone (Sigma-Aldrich)
    - 5 g granulated yeast extract (Merck KGaA)
    - 5 g NaCl (Sigma-Aldrich)
    - 1 l ddH$_2$O
- **LB+Tet medium**
    - 1 l LB medium

    Autoclaved, cooled to < 70 °C, added 1 ml Tetracycline stock, stored at RT
- **LB+Tet plates**
    - 1 l LB medium
    - 15 g agar (Select agar, Invitrogen)

    Autoclaved, cooled to < 70 °C, added 1 ml Tetracycline stock, poured into 6 cm
    Petri dishes while hot, stored wrapped with parafilm® at 4 °C in the dark
- **LB/IPTG/XGal plates**
    - 1 l LB medium
    - 15 g/l agar (Select agar, Invitrogen)

    Autoclaved, cooled to < 70 °C, added 1 ml IPTG/XGal stock. Poured into 6 cm Petri
    dishes while hot, stored wrapped with parafilm® at 4 °C in the dark
- **Neutralization buffer**
    - 1 M Tris-HCl (pH 9.1) (AppliChem GmbH)

    Stored at 4 °C
- **Subcuvia** 160 g/l (Baxter AG, Deerfield, Illinois, United States)
- **Tris-buffered saline (TBS)**
    - 50 mM Tris-HCl (pH 7.5)
    - 150 mM NaCl

    Autoclaved, stored at RT
- **TBST 0.1 %**
    - TBS
    - 0.1 % [v/v] Tween-20 (TWEEN®, Sigma-Aldrich)

    Stored at 4 °C
- **TBST 0.5%**
    - TBS
    - 0.5 % [v/v] Tween-20 (TWEEN®, Sigma-Aldrich)

    Stored at 4 °C
- **Tetracycline stock solution**
    - 20 mg/ml Tetracycline
    - 15 ml ddH$_2$O
    - 15 ml ethanol (96%)

    Stored at -20 °C

- **Top Agar**
    - 1 l LB medium
    - 7 g electrophoresis grade agarose (Biozym Scientific GmbH, Hessisch Oldendorf, Germany)
      Autoclaved, dispensed into 150 ml aliquots, stored at RT

2.3.2. Experimental procedure

The experiment was performed using the Ph.D.[TM]-12 Phage Display Peptide Library Kit (New England BioLabs) following manufacturer's protocol with some adaptations. To minimize the risk of contamination, all steps were conducted under sterile conditions on an ethanol-cleaned bench next to a Bunsen burner flame using sterile solutions and equipment as well as clotted pipette tips.

2.3.2.1.   Streaking of E.coli ER2738

After vortexing briefly, approximately 10 µl of the E.coli stock were put onto a pre-warmed LB+Tet plate and gently distributed using a sterile plastic loop. Streaking was performed by wiping some of the already spread bacteria onto a fresh area to subsequently reduce the number of streaked bacteria. This technique allowed growth of single colonies in the last streaks. The plate was inverted and incubated at 37 °C overnight and afterwards stored at 4 °C and wrapped in parafilm[®] (Bemis NA, Neenah, WI, USA) in the dark for a maximum of one week.

2.3.2.2.   Panning with NMO-IgG Pt1

Panning with NMO-IgG Pt1 and pre-incubation with Subcuvia to exclude unspecific phages were conducted in two separate sterile 24-well plates (Greiner Bio-One). Solutions of 10 µg/ml of the target, NMO-IgG Pt1, and Subcuvia, respectively, in 0.1 M NaHCO$_3$ (pH8.6) were prepared and 900 µl were added each to one well for coating overnight at 4 °C in a humidity chamber. Since the titer of the phage library is 1×10^{13} pfu per ml, the input volume of 10 µl corresponds to an amount of 1×10^{11} phages.

On the next day, coating solutions were poured off from 24-well plates and the plates were firmly slapped down onto a clean paper towel to remove residual liquid. Subsequently, both wells were filled with 2 ml general blocking buffer and incubated for 2 hours at 4°C on a

rotating platform (3 rpm). After removing the blocking solution, the Subcuvia-coated well was washed six times with TBST 0.1% and 500 µl of the diluted 100-fold representation of the library (1:50 in TBST 0.1%) were added. Duration of incubation was 20 min at RT on a rotating platform. Simultaneously, the Pt1-coated well was washed six times with TBST 0.1% and after 20 min, the non-binding phages from the Subcuvia-coated well were transferred to the NMO-IgG Pt1-coated well. After 40 min incubation at RT on a rotating platform (3 rpm), the solution containing non-binding phages was discarded and the plate was slapped onto a clean paper towel. The well was washed ten times with TBST 0.1% in order to remove the remaining phages. Bound phages were eluted in 500 µl elution buffer for 10 min at RT on a rotating platform (3 rpm) to compete the phages away from the immobilized target on the plate. The solution was transferred to a microcentrifuge tube in which the pH was immediately neutralized with 75 µl of neutralization buffer. This 1st round unamplified eluate was stored at 4 °C overnight. For the amplification on the following day, 20 ml of LB+Tet medium were inoculated with one well-defined colony of ER2738 picked from a LB plate with a sterile 10 µl pipette tip in a 250 ml Erlenmeyer flask. The same amount of LB+Tet medium with a sterile 10 µl pipette tip without E.coli served as negative control. Both flasks were incubated overnight at 37 °C with shaking (180 rpm).

2.3.2.3. Phage titering

Titering was conducted after each round of panning and amplification in order to evaluate the number of phages contained in the eluate.

Three times 5 ml of LB+Tet medium were dispensed into 14 ml sterile culture tubes (Greiner Bio-One) and two of them were inoculated with one well-defined colony of ER2738 from the previously prepared plate (compare chapter 2.3.2.1) using 10 µl sterile pipette tips. The third culture tube served as a negative control. The tubes were incubated at 37 °C with vigorous shaking (180 rpm) (Unitron Incubation shaker, Infors HT, Basel, Switzerland) for approximately 2.5 hours, until the culture reaches mid-log phase (OD_{600nm} ~0.5) as measured by a spectrophotometer (Hitachi U2001 UV VIS Spectrophotometer, Hitachi Ltd. Corporation, Chiyoda, Japan). While bacteria were growing, Top Agar was melted in a microwave and 3 ml each were added to sterile culture tubes, one per phage dilution, and then kept at 46 °C in a water bath. Additionally, for each dilution, one LB/IPTG/XGal plate

was pre-warmed to 37 °C in an incubator (Heraeus, Thermo Scientific, Waltham, MA, USA). Serial dilutions with 5 µl input volume of the phage eluate in LB medium were prepared and different dilutions were titered according to different sample types (table 2.1).

Table 2.1: Dilutions for phage titering of different sample types

Sample type	Dilutions for titering
1st round unamplified eluate	10^1-10^4, no duplicates
2nd and 3rd round unamplified eluates	10^3-10^6, no duplicates
Amplified eluates	10^6,10^9,10^{10}, 10^{11}, duplicates
1st, 2nd and 3rd round phage stocks and single phage clone stocks for ELISA	10^8-10^{10}, duplicates

When one of the two ER2738 cultures reached mid-log phase, 190 µl each were dispensed into microcentrifuge tubes, one for each phage dilution plus one for the negative control. 10 µl each of the prepared phage dilutions were added to one tube, vortexed briefly and incubated for 1-5 min at RT. Subsequently, the infected cells were transferred one at a time to a culture tube containing Top Agar, vortexed briefly and immediately poured onto a pre-warmed LB/IPTG/XGal plate. The plate was tilted and rotated gently to spread Top Agar evenly. After 5 min of cooling down, plates were inverted and incubated overnight at 37 °C in the incubator. On the next day, the blue plaques on the plates were counted and multiplied by the dilution factor and divided by ten (due to the input volume of 10 µl) to calculate the phage titer as pfu/µl. If plaques were present in proportional density on different dilution plates, i.e. approximately 10-fold reductions with 10-fold increasing dilutions, the experiment was carried on.

2.3.2.4. First round of Amplification

On the next day, the shaking speed of the overnight culture was reduced to 100 rpm for 15 min to allow the bacterial cells to regenerate their F-pilus. Afterwards, the overnight culture was diluted 1:100 in 20 ml LB+Tet medium in a 250 ml Erlenmeyer flask, the total volume of the 1st round unamplified eluate was added and subsequently incubated with vigorous shaking (225 rpm) for 5 hours at 37 °C. After transferring the culture to a centrifuge tube, it was spun for 10 min at 12 000 g at 4 °C. The phage containing supernatant was then

transferred to a fresh tube and re-span for 10 min at 12 000 g at 4 °C. The upper 80 % of the supernatant (approximately 16 ml) were added to a fresh tube with 20 % PEG/2.5 M NaCl (1/6 of the supernatant's volume, i.e. approximately 2.6 ml) and incubated overnight at 4 °C to allow phage precipitation. On the following day, the precipitate was spun at 12 000 g for 15 min at 4 °C and supernatant was discarded subsequently. After a re-spin of 3 min, residual supernatant was removed with a pipette and the pellet was resuspended in 1 ml TBS. The suspension was transferred to a micro-centrifuge tube and, wrapped with parafilm®, placed horizontally on ice for 1 hour at 4 °C and 3 rpm to give the phages time to resuspend after precipitation. Thereafter, the suspension was centrifuged at 14 500 g for 5 min at 4 °C to pellet residual bacterial cells. The supernatant (approximately 1 ml) was transferred to a fresh microcentrifuge tube and 20% PEG/2.5 M NaCl (1/6 of the supernatant's volume, i.e. approximately 165 µl) was added before incubating on ice for 1 hour and subsequent centrifugation at 14 500 g for 10 min at 4 °C. Supernatant was discarded and the precipitate was re-spun for 2 min to facilitate removal of residual supernatant. The pellet was resuspended in 200 µl TBS and the parafilm®-wrapped microcentrifuge tube was again placed horizontally on ice for 60 min with agitation (10 rpm) to enable complete resuspension. After another centrifugation step for 1 min at 14 500 g for pelleting remaining insoluble material, the supernatant was transferred to a fresh tube.

This was the 1st round amplified eluate which was stored at 4 °C and, after taking out the input volume for the second round of panning, 1:1 diluted in glycerol and stored at -20 °C. To evaluate the amount of phages, titering was conducted with 1st round amplified eluate as described in 2.3.2.3 but this time with dilutions of 10^6, 10^9, 10^{10} and 10^{11} (compare table 2.1).

2.3.2.5. Second round of panning and amplification

Since the input titer for the second round of panning should be identical to the one for the first round of panning, the input volume of the 1st round amplified eluate was calculated to achieve a concentration of 1 x10^{11} pfu/µl. The second round of panning and amplification was conducted as described in chapters 2.3.2.2 – 2.3.2.4. Besides using the 1st round amplified eluate as input phage, the only modification consisted of raising the Tween® concentration in TBST from 0.1 % to 0.5% [v/v] to increase the stringency of interaction between antibody and phage.

The 2nd round amplified eluate was also diluted 1:1 in glycerol and stored at -20 °C after taking out the input volume for the third round of panning.

2.3.2.6.   Third round of panning

The input volume of the 2nd round amplified eluate for the third round of panning was adjusted to achieve the desired input titer of 1 x10^{11} pfu/µl. The third panning procedure was conducted identically to the second round of panning until titering the unamplified eluate (see chapters 2.3.2.2 and 2.3.2.3). In parallel to the titering of the 3rd round unamplified eluate, the plaque assay was conducted with the phage library in order to get single phage clones with random peptides.

2.3.2.7.   Amplification of single phage clones and 3rd round eluate

From the titering of the 3rd round unamplified eluate, 20 plaques, i.e. single phage clones, were isolated and used for sequencing and further experiments. As a control, five additional plaques were picked from the titering plates of the phage library. These 25 phage clones were amplified for DNA sequencing and, as well as the 3rd round unamplified eluate, for phage ELISA (enzyme-linked immunosorbent assay), respectively. An overnight culture of ER2738 was diluted 1:100 in 30 ml LB+Tet medium. 1 ml of the diluted culture each was dispensed to 26 sterile 14-ml culture tubes. 10 µl of the 3rd round unamplified eluate were added to one culture tube. The remaining 25 tubes were inoculated with the plaques that were stabbed from the titering plates using a sterile pipette tip for each plaque. All 26 tubes were incubated with shaking (180 rpm) for 5 h at 37 °C. Afterwards, the cultures were transferred to microcentrifuge tubes and were centrifuged at 14 000 rpm for 30 seconds, before supernatant was transferred to a fresh tube and re-spun. The upper 80 % of the supernatant (800µl) were again transferred to a new microcentrifuge tube. These are the 3rd round amplified eluate and the amplified phage stock, respectively, which were stored at 4 °C. From each of them, 20 µl were transferred to new microcentrifuge tubes and 1:1 diluted in glycerol and stored at -20 °C until further use for the ELISA experiments.

2.3.3. ssDNA isolation of single phage clones

Isolation of single-stranded DNA (ssDNA) from the single phage clones was conducted using the QIAprep Spin M13 Kit (Qiagen, Hilden, Germany) according to manufacturer's protocol which is especially designed for preparation of M13 ssDNA from E.coli grown in LB medium.

QIAprep Spin M13 Kit components

- QIAprep spin columns
- Buffer MP (M13 precipitation)
- Buffer PB (M13 lysis and binding)
- Buffer PE (concentrate), added 24 ml ethanol (96 %) before use
- Buffer EB (10 mM Tris·Cl, pH 8.5)
- Collection tubes (2 ml)

First, 8 µl of Buffer MP were added to each of the 25 phage stocks, vortexed well and incubated for 15 min at RT facilitating precipitation of bacteriophage particles. Samples were then transferred to a QIAprep spin column, which was placed in a 2 ml microcentrifuge tube. Since the maximum capacity of the columns amounts to 700 µl, samples were loaded in two successive fractions of 400 µl each. Phage supernatant was centrifuged for 15 s at 8 000 rpm and flow-through was discarded from the collection tube whereby intact phages were retained on the QIAprep silica membrane. Loading and centrifugation was repeated once for each sample to load the entire volume onto the spin column. Subsequently, 700 µl of Buffer MLB for M13 lysis and binding of the M13 DNA to the silica membrane were applied to the spin columns and centrifuged for 15 s at 8 000 rpm. Another 700 µl pf Buffer MLB were added to the spin column and incubated for 1 min at RT to complete lysis of bacteriophages, followed by a centrifugation step for 15 s at 8 000 rpm. In order to remove residual salt, 700 µl Buffer PE were added and centrifuged for 15 s at 8 000 rpm. Preventing residual ethanol from being transferred into subsequent reactions, the spin column was dried by centrifuging for 15 s at 8 000 rpm. For elution of the ssDNA, the spin column was placed in a microcentrifuge tube and 50 µl of RNAse free water were applied to the center of the column membrane, incubated for 10 min and centrifuged for 30 s at 8 000 rpm. In the end, additional 50 µl of RNAse free water were added to the center of the column and the

samples were centrifuged again for 30 s at 8 000 rpm. The final ssDNA concentration was determined as measured by absorption at 260 nm using a NanoDrop 2000 spectrophotometer (Thermo Scientific). The phage stocks of a total volume of 100 µl were stored at -20 °C.

2.3.4. Sequencing and identification of single phage clones

20 µl of the isolated ssDNA of the 25 single phage stocks were sent to VBC Biotech GmbH, Vienna, Austria, for sequencing. Sanger sequencing was conducted using the 96 gIII sequencing primer contained in the Ph.D.[TM]-12 Phage Display Peptide Library Kit. The identified sequences were checked for their completeness and quality.
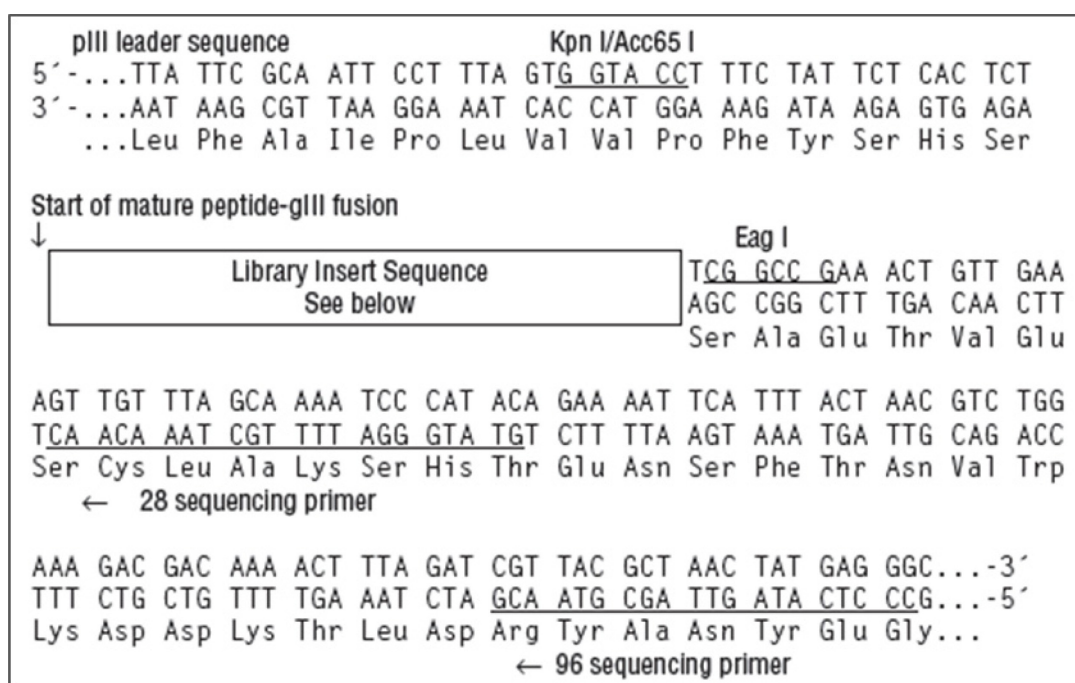
```
pIII leader sequence                          Kpn I/Acc65 I
5´-...TTA TTC GCA ATT CCT TTA GTG GTA CCT TTC TAT TCT CAC TCT
3´-...AAT AAG CGT TAA GGA AAT CAC CAT GGA AAG ATA AGA GTG AGA
   ...Leu Phe Ala Ile Pro Leu Val Val Pro Phe Tyr Ser His Ser

Start of mature peptide-gIII fusion
↓
                                              Eag I
┌─────────────────────────────────┐   TCG GCC GAA ACT GTT GAA
│   Library Insert Sequence        │   AGC CGG CTT TGA CAA CTT
│   See below                      │   Ser Ala Glu Thr Val Glu
└─────────────────────────────────┘

AGT TGT TTA GCA AAA TCC CAT ACA GAA AAT TCA TTT ACT AAC GTC TGG
TCA ACA AAT CGT TTT AGG GTA TGT CTT TTA AGT AAA TGA TTG CAG ACC
Ser Cys Leu Ala Lys Ser His Thr Glu Asn Ser Phe Thr Asn Val Trp
   ←   28 sequencing primer

AAA GAC GAC AAA ACT TTA GAT CGT TAC GCT AAC TAT GAG GGC...-3´
TTT CTG CTG TTT TGA AAT CTA GCA ATG CGA TTG ATA CTC CCG...-5´
Lys Asp Asp Lys Thr Leu Asp Arg Tyr Ala Asn Tyr Glu Gly...
                         ←   96 sequencing primer
```

Figure 2.3: Sequence of random peptide library-gIII fusions

Figure adapted from New England Biolabs Ph.D.[TM] Phage Display Libraries Instruction Manual

If inserted correctly, the peptide sequence should be bordered by specific marker sequences: N-terminally of the mimotope, the leader sequence "**LFAIPLVVPFYSHS"**, containing 5´-GGTACC-3´, the restriction site for inserting the randomized sequence (Kpn I/Acc65 I) in the phage genome, was displayed. This N-terminal leader sequence was removed upon secretion leading to the randomized peptide being displayed directly at the N-terminus of the mature pIII protein connected by the short linker sequence Gly-Gly-Gly-

Ser. Thus, the C-terminal amino acid sequence of the peptide sequences was "**GGGSAETVESCLAK**" which contains the restriction site of EagI (5'-CGGCCG-3'), the other restriction enzyme for the insertion of the library sequence into the phage genome (figure 2.3). Using the ExPASy Translate tool (available online at http://web.expasy.org/translate/), the obtained sequences were translated into the corresponding amino acid sequence. The sequencing data constitute the (-)ssDNA in 5' → 3' direction since (+)ssDNA served as template and the synthesized DNA is elongated at the 3' end of the primer. Given that in the course of translation, the mRNA (which corresponds to the (+)ssDNA) is read starting from 5' to 3', the (-)ssDNA has to be read in 3'→ 5' constituting the reverse complement. Fortunately, the ExPASy Translate tool provides the reverse complement and the corresponding amino acid sequence. Furthermore, the ExPASy Translate tool displays all three possible reading frames.

2.3.5. Characterization of obtained mimotope sequences

The obtained mimotope sequences were translated using the ExPASy translate tool (SIB Swiss Institute of Bioinformatics, available online at http://web.expasy.org/translate/).

The mimotope sequences were examined using the free web tool SAROTUP (available online at http://immunet.cn/sarotup/) that compares the obtained sequences with MimoDB, a mimotope database consisting of sequences revealed in multiple previously published biopanning studies in order to rule out target-unrelated peptides (Huang et al., 2010). SAROTUP includes several tools to address this issue: TUPScan was used to check the sequences for all known target-unrelated motifs and MimoScan detects patterns within the submitted mimotope sequences that correspond to previously uploaded peptides. Furthermore, the MimoSearch tool was used to assess whether one of the obtained peptides has been found before in different biopanning experiments since the occurrence of one mimotope in two different setups would strongly indicate a lack of specificity. To find out an eventual consensus sequence of the obtained mimotope sequences, the online tool MIMOX was used (Huang et al., 2006).

2.4. Phage ELISA binding assay with direct target coating

To examine the target specificity of the eluates and the single phage clones, ELISAs were performed. Thereby, the reactivity of each sample with NMO-IgG Pt1, Subcuvia and BSA was tested.

2.4.1. Media and solutions

- **General blocking buffer**
  - 0.1 M NaHCO$_3$ (pH 8.6) (Merck)
  - 5 mg/ml BSA
    Filter sterilized, stored at 4 °C

- **Mouse anti-M13 Monoclonal antibody conjugated with Horseradish Peroxidase (HRP)**, GE Healthcare #27-9421-01 (Little Chalfont, Buckinghamshire, United Kingdom).

- **IPTG/XGal stock**
  - 0.5 g IPTG (Isopropyl β-D-1-thiogalactopyranoside, AppliChem GmbH)
  - 0.4 g XGal (5-bromo-4-chloro-3-indolyl-β-D-galactopyranoside, Sigma-Aldrich)
  - 10 ml DMF (N,N- Dimethylformamide; Alfa Aesar GmbH & Co KG, Darmstadt, Germany)
    Stored at -20 °C

- **LB+Tet medium**
  - 10 g tryptone (Sigma-Aldrich)
  - 5 g granulated yeast extract (Merck)
  - 5 g NaCl (Sigma-Aldrich)
  - 1 l ddH$_2$O
    Autoclaved, cooled to < 70 °C, added 1 ml Tetracycline stock, stored at RT

- **LB+Tet plates**
  - 1 l LB medium
  - 15 g agar (Select agar, Invitrogen)
    Autoclaved, cooled to < 70 °C, added 1 ml Tetracycline stock, poured into 6 cm Petri dishes while hot, stored wrapped with parafilm® at 4 °C in the dark

- **LB/IPTG/XGal plates**
  - 1 l LB medium
  - 15 g/l agar (Select agar, Invitrogen)
    Autoclaved, cooled to < 70 °C, added 1 ml IPTG/XGal stock. Poured into 6 cm Petri dishes while hot, stored wrapped with parafilm® at 4 °C in the dark

- **PEG/ NaCl**
  - 20% /(w/v) polyethylene glycol-8000
  - 2.5 M NaCl

- **Subcuvia** 10 mg/ml (Baxter AG, Deerfield, Illinois, United States)

- **Stop reagent** for TMB Substrate (Sigma-Aldrich)
- **TBS**
    - 50 mM Tris-HCl (pH 7.5)
    - 150 mM NaCl

- **0.1 % TBST**
    - TBS
    - 0.1 % [v/v] Tween-20 (TWEEN®, Sigma-Aldrich)
    Stored at 4 °C
- **0.5% TBST**
    - TBS
    - 0.5 % [v/v] Tween-20 (TWEEN®, Sigma-Aldrich)
    Stored at 4 °C
- **Tetracycline stock**
    - 20 mg/ml Tetracycline
    - 15 ml ddH$_2$O
    - 15 ml ethanol (96%)
    Stored at -20 °C
- **TMB** (3,3',5,5'-Tetramethyl-benzidine liquid substrate) Liquid Substrate System for ELISA (Sigma-Aldrich)
- **Top Agar**
    - 1 l LB medium
    - 7 g electrophoresis grade agarose (Biozym Scientific GmbH, Hessisch Oldendorf, Germany)
    Autoclaved, dispensed into 150 ml aliquots, stored at RT

2.4.2. Experimental procedure

For ELISA, the three amplified eluates and 20 phage stocks were amplified once more as described in chapter 2.3.2.4. The modifications consisted of the input volume of 10 µl of each eluate/phage stock instead of the entire volume and the pellet was resuspended in only 50 µl TBS instead of 200 µl. Furthermore, the last centrifugation step of 1 min after resuspension was cut out. For the titering, dilutions of 1:10^8, 1:10^9 and 1:10^{10} were used (compare chapter 2.3.2.3). For each pool to be characterized, six wells of a 96-well plate (Greiner Bio-One) were coated with a target: two wells with 200 µl Pt1 and Subcuvia, respectively, each with a concentration of 100 µg/ml in 0.1 M NaHCO$_3$, and two only with 0.1 M NaHCO$_3$ that would serve as a control for the blocking reagent BSA later on. The plates were incubated overnight at 4 °C with gentle agitation in a humidity chamber.

On the next day, the target solutions were shaken out and the plate was slapped face-down onto a paper towel. Each well was filled with 300 µl general blocking buffer, including one additional row that served as a blank control. Blocking was carried out for 2 hours at 4 °C on a rotating platform (3 rpm) in a humidity chamber. According to the titering results, input volumes needed to achieve a final concentration of 10^6 pfu/µl were calculated. General blocking buffer was discarded and the plate was washed six times with 0.5 % TBST, before 100 µl of the diluted amplified eluates and the phage stocks (in 0.1 % TBST), respectively, were added to their corresponding wells (six wells each). The wells for the blank control were filled with 0.1 % TBST. After incubation for 1 hour at 4 °C on a rotating platform (3rpm) in a humidity chamber, the unbound phages were shaken out and the plate was washed six times with 0.5 % TBST. HRP-conjugated anti-M13 monoclonal antibody was diluted 1: 5 000 in general blocking buffer and 200 µl were added to each well and incubated for 1 hour at RT with gentle agitation (3 rpm). After another washing step (six times with 0.5 % TBST), 100 µl of TMB substrate were applied to each well and incubated for 15 min at RT under protection from light. Afterwards, 100 µl of stop reagent for TMB substrate were added to each well and the plate was read with a microplate reader (GloMax®-Multi Detection System, Promega, Madison, WI, USA) at 450 nm.

2.5.   Mapping mimotopes on AQP4 with EpiSearch and *PepSurf*

Another feature to characterize the peptides in terms of their capability to mimic binding sites of NMO-IgG Pt1 on AQP4 is to map them on the structure of human AQP4 (PDB accession number 3GD8). Mapping was conducted using two programs, EpiSearch (Negi and Braun, 2009) (available online at http://curie.utmb.edu/episearch.html) and *PepSurf* (Mayrose et al., 2007)(available online at http://pepitope.tau.ac.il/).

For EpiSearch, parameters were set as follows: Patch Size (A) was set to 12 for 12mers. The Area cutoff (A^2) indicates the minimum accessible surface area which is required for protein residues to be considered as solvent exposed and thus to be taken into account for the mapping. If using the default value of A^2=10 (i.e., only residues with a surface area greater than 10 Å are considered as solvent exposed) did not reveal any results, the cut off was lowered to increase the number of accessible residues. The accuracy cutoff value was set to the default value of 3.0. The settings for *PepSurf* were not changed from the default settings.

BLOSUM62 was chosen as substitution matrix, gap penalty was set to -0.5 and the phage-display settings were adapted to the Ph.D.[TM]-12 Phage Display Peptide Library: the library type "NNK" as well as replacing the stop codon UAG by glutamine were chosen. The predicted residues of both mapping algorithms of one mimotope were then remapped on one molecule of human AQP4 using the software VMD 1.9.2 (Humphrey et al., 1996) to facilitate better visualization and a direct comparison between EpiSearch and *PepSurf*.

2.6. Peptide synthesis of promising mimotopes

Peptides for mimotopes with promising results in ELISA (i.e. better binding to NMO-IgG Pt1 than to BSA or Subcuvia) and/or convenient prediction of localization on AQP4, i.e. on the extracellular surface, according to the mapping tools were synthesized by Centic Biotec (Berolfweg 35; 69123 Heidelberg; Germany). In addition, the random peptide L8 was synthesized. This peptide resulted from one of the randomly selected phage clones without positive or negative selection on NMO-IgG P1 and Subcuvia. All peptides except for L8, Pt1-13 and Pt1-19 were ordered comprising an amidated Serine in the linker sequence Gly-Gly-Gly-Ser to abolish the negative charge at the carboxyl group. This creates the same charge conditions as given during biopanning where the linker sequence is directly connected to the N-terminus of the pIII protein and thus is not charged negatively. Water solubility of the peptides was calculated using the Innovagen peptide property calculator (available online at http://pepcalc.com/peptide-solubility-calculator.php). For most of the peptides, the program predicted poor water solubility (except for the random peptide L8 and Pt1-19). However, all peptides could be dissolved in 1 ml ddH$_2$O. Table 2.2 shows the amino acid sequences of the ordered peptides.

Table 2.2: Amino acid sequence of synthesized peptides

ID	Peptide sequence	ID	Peptide sequence
Pt1-04	WRYHVHPTPFKSGGGS	Pt1-13	GPFHFLHHHWSQGGGS
Pt1-05	WHRTHILQYGKPGGGS	Pt1-18	WSSHAHRHNHFRGGGS
Pt1-07	WPWHAHGNTRGIGGGS	Pt1-19	WGMHRHAPVYDRGGGS
Pt1-08	WHWKPYMSSRAQGGGS	L8 (random)	FPTDSLRGDVGMGGGS
Pt1-11	VPSNSLLQSSRVGGGS		

2.7.   HEK293A – cell culture

2.7.1. Media and solutions

- **Counting solution**
    - ϒ 60 µl Trypan Blue Solution, 0.4% (Gibco®, Life Technologies, Carlsbad, CA, USA)
    - ϒ 30 µl 1X PBS
- **DMEM** (Dulbecco's Modified Eagle's Medium) - high glucose (Sigma-Aldrich)
  Stored at 4 °C
- **DNA constructs for transfection of HEK293A cells**; plasmids encoding human AQP4-M23 and AQP4-M1 C-terminally fused to emGFP. Provided by the group of Markus Reindl (Medical University of Innsbruck, Austria; Research Unit Neuroimmunology). A plasmid map is provided in supplementary figure S 16. Plasmids were stored at 4 °C
- **Freezing medium**
    - ϒ HEK293A-complete medium
    - ϒ 10 % DMSO (Dimethyl Sulfoxide, Sigma-Aldrich)
      Stored at 4 °C
- **HEK293A-complete medium**
    - ϒ DMEM (Dulbecco's Modified Eagle's Medium) - high glucose (4500 mg glucose/l, 110 ml sodium pyruvate and L-glutamine) (Sigma-Aldrich)
    - ϒ 10 % fetal bovine serum (FBS), heat-inactivated at 56 °C for 30 min (Gibco®, Life Technologies)
    - ϒ 1 % NEAA (non-essential amino acids; Gibco®, Life Technologies)
    - ϒ 1 % penicillin/streptomycin (10,000 U/ml; Lonza)
      Stored at 4 °C
- **Trypsin- Ethylendiaminetetraacetic acid** (EDTA) (Trypsin-Versene (EDTA) Mixture (1X) 100ml; Lonza)
      Stored at 4 °C

2.7.2. Maintenance of the cell line

The cells were kept in 15 ml HEK293A-complete medium in 250 ml-culture flasks (CELLSTAR®, TC-treated, growth area: 75 cm^2; Greiner Bio-One) in an incubator with culture conditions of 37 °C and 5 % CO_2. They were passaged approximately every fourth day, at the time point cells form a confluent layer. For splitting the cells, the old medium was discarded and cells were washed with 10 ml 1x PBS. By adding 3 ml Trypsin-EDTA and incubating for 2 min at RT, cells were detached from the surface. Trypsin was stopped with 10 ml HEK293A-complete medium (prewarmed to RT) and the suspension was transferred to a 50 ml Falcon and centrifuged at 500 g for 5 min at RT. After discarding the supernatant, the cell pellet was

resuspended in 10 ml HEK293A-complete medium. 10 µl of the cell suspension were added to 90 µl counting solution and concentration of viable cells as indicated by absence of internal trypan blue was determined using a counting chamber (Neubauer improved; Paul Marienfeld GmbH & Co. KG, Lauda-Königshofen, Germany) and a phase contrast microscope (Axiovert 40C, Zeiss, Oberkochen, Germany). According to the counting results, the volume of suspension containing 1 million cells was added to HEK293A-complete medium resulting in a final volume of 15 ml in a new culture flask.

2.7.2.1.   Freezing of cells

In order to generate a cell stock as an eventual backup, aliquots of the cell suspension which was left over during passaging, were frozen. The concentration was adjusted to 1 million cells/ml in freezing medium. Aliquots of 1 ml were then dispensed into Cryo.S^{TM} microtubes (Greiner Bio-One) and placed in a freezing container (Mr. Frosty™ Freezing Container; Thermo Scientific) for storage at -80 °C. After 4 h, the tubes were transferred to liquid N$_2$.

2.7.2.2.   Thawing of cells

Cells were thawed quickly at 37 °C in a water bath and immediately added to 10 ml prewarmed HEK293A-complete medium before centrifugation at 500 g for 5 min at RT to remove DMSO. Afterwards, the cells were resuspended in 15 ml HEK293A-complete medium, dispensed into a culture flask and maintained as described in chapter 2.6.2.

2.7.3. Transfection

Transfection of cells was performed in 75 cm^2 culture flasks, 24-well plates, or 6-well plates when a confluence level of approximately 80 % was reached (but at least one day after passaging) to facilitate previous attachment and further cell growth. Freshly thawed cells were passaged at least three times prior to transfection. For transfection, HEK293A-complete medium was replaced by medium without penicillin/streptomycin in order to ensure highest possible transfection efficiency. The cells were transfected using the transfection reagent Fugene® (Fugene® HD Transfection Reagent, Promega, Madison, WI, USA) either with AQP4-M23-emGFP or AQP4-M11-emGFP constructs. The reaction mix for the transfection consisted of 0.02 µg plasmid per µl and 3.5 µl Fugene® HD per µg plasmid.

For example, for a reaction mix with a total volume of 500 µl, this results in 10 µg DNA and 35 µl Fugene®. Depending on the volume of the culture dish and thus, the amount of cells to be transfected, the volume of the reaction mix was adapted as described in table 2.3. The nucleic acid concentrations of the AQP4-M1-emGFP and the AQP4-M23-emGFP plasmids were determined as 0.6582 µg/µl and 1.1131 µg/µl, respectively.

Table 2.3: Composition of reaction mix for transfection of different types of culture dishes
M1 and M23 represent the plasmids AQP4-M1-emGFP and AQP4-M23-emGFP, respectively.

Type of culture dish	Vol. of medium in dish	Vol. of reaction mix	Amount of plasmid	Vol. of Fugene®	Construct	Vol. of plasmid	Vol. of DMEM
75cm² flask	15 ml	500 µl	10 µg	35 µl	M1	15.2 µl	449.8 µl
					M23	9 µl	449.8 µl
6-well	2 ml	150 µl	3 µg	10.5 µl	M1	4.6 µl	134.9 µl
					M23	2.7 µl	136.8 µl
12-well	1 ml	50 µl	1 µg	3.5 µl	M1	1.5 µl	45 µl
					M23	0.9 µl	45.6µl
24-well	0.5 ml	25 µl	0.5 µg	1.8 µl	M1	0.8 µl	22.4 µl
					M23	0.5 µl	22.7 µl

Both Fugene® and DMEM were pre-warmed to RT before usage. At first, the required volume of plasmid was added to the required amount of DMEM and vortexed briefly before adding the required volume of Fugene®. After exactly 5 min, the reaction mix was transferred into the culture dish. Cells were given 24 h to allow sufficient expression of AQP4 and further growth.

2.8.   Staining of HEK293A cells

HEK293A cells were transfected with AQP4-M1-emGFP and AQP4-M23-emGFP, respectively, and subsequently stained with NMO-IgG Pt1 in order to confirm binding of NMO-IgG Pt1 to human AQP4 expressed by transfected HEK293A cells. Furthermore, this experiment served to evaluate eventual differences in binding to HEK293A cells when transfected with either the AQP4-M1-emGFP or the AQP4-M23-emGFP construct.

2.8.1. Antibodies and media

- **DAPI** (Carl Roth)
- **HEK293A-complete medium**
    - Y DMEM (Dulbecco's Modified Eagle's Medium) - high glucose (4500 mg glucose/l, 110 ml sodium pyruvate and L-glutamine) (Sigma-Aldrich)
    - Y 10 % FBS, heat-inactivated at 56 °C for 30 min (Gibco®, Life Technologies)
    - Y 1 % NEAA (non-essential amino acids; Gibco®, Life Technologies)
    - Y 1 % penicillin/streptomycin (10,000 U/ml; Lonza)
      Stored at 4 °C
- **Secondary antibody**
    - Y Donkey-anti-human-Cy3 (#709-165-149, Jackson ImmunoResearch Laboratories, Inc.)

2.8.2. Experimental procedure

Glass cover slips with a diameter of 12 mm were equipped with paraffin dots and coated with 5 ml Poly-L-Lysine as described in chapter 2.2.2. The cover slips were then distributed among six wells of a 12-well plate (Greiner Bio-One) with one cover slip per well. Cultured HEK293A cells were washed with 10 ml 1x PBS and were detached from the surface of the flask where they were maintained before using 3 ml Trypsin. After incubation for 1 min at RT, Trypsin was stopped with 10 ml HEK293A-complete medium and centrifuged for 5 min at 500 g and RT. Supernatant was discarded and the pellet was resuspended in 10 ml HEK293A-complete medium. For counting, 10 µl of the cell suspension were added to 90 µl counting solution. The suspension was diluted to a final concentration of 150000 cells/ml and 1 ml was dispensed into each well containing a cover slip. Cells were incubated at 37 °C and 5 % CO_2 overnight to allow further growth and attachment to the surface. On the next day, cells were transfected as described in chapter 2.7.3 with a reaction mix volume of 50 µl (as described in table 2.3). Two wells were transfected with the AQP4-M23-emGFP construct, two with the AQP4-M1-emGFP construct. After transfection, cells were again incubated overnight to allow sufficient expression of AQP4. On the next day, cells were washed three times with ice-cold HEK293A-complete medium and cover slips were transferred to new wells containing 100 µl of NMO-IgG Pt1 (diluted 1:200 in HEK293A-complete medium). After incubation for 30 min at 4 °C on a rotating platform (3 rpm), the wells were washed three times with ice-cold DMEM and the secondary antibody was applied (donkey anti-human conj. Cy3, diluted 1:100 in HEK293A-complete medium). The secondary antibody was

incubated for 45 min at 4 °C under protection from light. Before and after fixation with 500 µl of 4 % PFA (Merck KGaA) for 15 min at RT under in the dark, cells were washed three times with ice-cold PBS. Afterwards, the cells were permeabilized with 500 µl of 0.1 % Triton X-100 (diluted in HEK293A-complete medium; t-Octylphenoxypoly-ethoxyethanol, Sigma-Aldrich) for 5 min at RT under protection from light. After washing three times with PBS, nuclei were stained with DAPI (diluted 1:10000 in ddH$_2$O) for 5 min at RT in the dark. The cover slips were washed three times with PBS and once with ddH$_2$O and then left in fresh ddH$_2$O until mounting on glass slides using Gallate/Geltol (Sigma-Aldrich). The slides were stored at 4 °C under protection from light until usage.

The stainings were analyzed using a confocal microscope (Leica TCS SP5 setup; Leica Microsystems, CMS-GmbH, Germany). EmGFP signals were detected with an argon laser (488nm excitation), detection of Cy3 was carried out using a DPSS561 laser and DAPI staining was detected with a 405 Diode laser. Images were edited and auto-adapted for contrast and brightness with ImageJ. Supplementary figure S2 gives detailed information about the spectral properties of the used fluorophores.

2.9.   Blue native polyacrylamide gel electrophoresis

Blue native polyacrylamide gel electrophoresis (BN-PAGE) is a technique that facilitates the separation of multiprotein complexes under native conditions and can be used to determine their size and relative amount. In this study, BN-PAGE was used to determine the size and amount of orthogonal arrays of particles (OAPs) expressed by HEK293A cells transfected with the AQP4-M1-emGFP and the AQP4-M23-emGFP construct, respectively. The experiment was performed according to the protocol published by Wittig and co-workers (Wittig et al., 2006).

2.9.1. Antibodies, buffers and solutions

All buffers and solutions were dissolved in ddH$_2$O.

- **3 x BN-PAGE gel buffer**
    - 75 mM imidazole
    - 1.5 M 6-aminocaproic acid
      pH was adjusted to 7 with HCl. Stored at 4 °C

- **5 % Coomassie brilliant blue (CBB) G-250 solution**
  - 5 % (w/v) CBB-G250
  - 500 mM 6-aminocaproic acid
    Mixed thoroughly before usage. Stored at 4 °C
- **10 % ammonium persulfate (APS)**
  - 10 % (w/v) APS were dissolved in ddH$_2$O
    Stored at 4 °C
- **Anode buffer**
  - 25 mM imidazole
    pH was adjusted to 7. Stored at 4 °C
- **BN-lysis buffer**
  - 500 mM 6-aminocaproic acid
  - 50 mM imidazole
  - 12 mM NaCl
  - 10 % glycerol
  - 1 % (v/v) Triton X-100
    pH was adjusted to 7 with HCl. 1 protease inhibitor cocktail tablet (cOmplete mini; Roche,) was dissolved in 10 ml buffer before usage. Stored at 4 °C
- **Dark blue cathode buffer (pH 7)**
  - 50 mM Tricine
  - 7.5 mM imidazole
  - 0.02 % (w/v) CBB G-250
    Stored at 4 °C
- **Homogenization Buffer**
  - 0.25 M sucrose
  - 10 mM Hepes
    pH was adjusted to 7.4 with NaOH. 1 protease inhibitor cocktail tablet (cOmplete mini; Roche, Basel, Switzerland) was dissolved in 10 ml buffer before usage; stored at 4°C
- **Light blue cathode buffer**
  - 50 mM Tricine
  - 7.5 mM imidazole
  - 0.002 % (w/v) CBB G-250
    Stored at 4 °C
- **Molecular weight marker**
  - 50 mM imidazole
  - 12 mM NaCl
  - 10 % (v/v) glycerol
  - 5 mg/ml ferritin (440 kDa; Ferritin from equine spleen, Sigma)

- **Native transfer buffer (pH 7)**
    - 50 mM tricine
    - 7.5 mM imidazole
- **Primary antibody**: rabbit anti-AQP4 (Sigma); diluted 1:800 in TBST 0.1 % with 5 % (w/v) BSA and 0.1 % NaN$_3$
- **Secondary antibody**: donkey anti-rabbit conjugated with HRP (#711-035-152, Jackson ImmunoResearch Laboratories, Inc.); diluted 1:5000 in TBST 0.1 % with 5 % (w/v) milk
- **TBST 0.1 %**
    - 50 mM Tris
    - 150 mM NaCl
    - 0.1 % (v/v) Tween-20
      pH adjusted to 7.5 with HCl

2.9.2. Experimental procedure

2.9.2.1.   Sample preparation

150000 HEK293A cells each were seeded in four wells of a 6-well plate. After 24 h, two wells each were transfected with AQP4-M1-emGFP and AQP4-M23-emGFP, respectively, as described in chapter 2.7.3. Cells were incubated for 48 h to allow sufficient expression of AQP4 and then harvested. Therefore, 500 µl ice-cold homogenization buffer were applied to each well and the cells were mechanically detached using a cell scraper. The suspensions of two wells each transfected with the same construct were pooled and homogenized in a dounce homogenizer as well as by aspirating and expelling the suspension through a 21 G needle. After that, the samples were centrifuged for 15 min at 4000 g and 4 °C to get rid of the cell debris. The supernatants were transferred to fresh microcentrifuge tubes and after resuspension of the pellets in 500 µl homogenization buffer, those were centrifuged again at 4000 g for 15 min at 4 °C. The supernatants from both runs were pooled and centrifuged for 1 h at 4 °C and 200 000 g using an ultracentrifuge to pellet membrane fractions containing AQP4. Afterwards, the pellets were resuspended in 50 µl ice-cold BN-lysis buffer, vortexed and incubated on ice for 30 min to ensure solubilization of membrane proteins. Another centrifugation step for 30 min at 20000 g and 4 °C served to pellet insoluble material. The supernatants were then transferred to fresh microcentrifuge tubes and stored at -20 °C until further usage. 10 µl of each sample were diluted 1:10 in ddH$_2$O to determine their protein concentration with the Bio-Rad Protein Assay (Bio-Rad, Hercules, CA, USA) according to manufacturer's protocol. The assay was conducted in 96-well plates

with 10 μl sample and 200 μl reagent using Subcuvia in 1:10 diluted BN-lysis buffer as standard. Subsequently, absorbance was measured in a microplate reader (GloMax®-Multi Detection System, Promega).

2.9.2.2. Gradient gel preparation

Both low and high percentage acrylamide solutions (table 2.4) were prepared and polymerization was started by adding APS and tetramethylethylenediamine (TEMED). 2.7 ml of the low percentage solution and subsequently 2.7 ml of the high percentage solution were aspirated using a 5 ml serological pipette.

Table 2.4: Composition of gels for BN-PAGE

Acrylamide percentage	3 % (stacking)	3.5 % (low)	9 % (high)
Total volume	**6 ml**	**6 ml**	**6ml**
3 x BN-PAGE Gel buffer	2 ml	2 ml	2 ml
$_{dd}H_2O$	3.55 ml	3.475 ml	-
$_{dd}H_2O$ with 45 % (v/v) glycerol	-	-	2.65 ml
40 % acrylamide mix (37.5:1)	0.45 ml	0.525 ml	1.35 ml
Polymerization initiators are added immediately before gel casting			
10 % APS	60 μl	40 μl	40 μl
TEMED	5 μl	5 μl	5 μl

The solutions don't intermingle immediately due to the high content of glycerol (20 %) in the high percentage solution constituting the lower half of the liquid column. Aspiration of two air bobbles slowly running through the liquid results in mixing and creating an acrylamide gradient from 3.5 to 9 % from top to bottom. The liquid is then slowly poured into the gel cassette (Xcell Surelock® mini system; Thermo Scientific) and covered by a thin layer of additional low percentage solution. The whole gel was then overlaid with isopropanol to assure an even surface after polymerization. When the gel hardened, isopropanol was removed and the cassette was filled with stacking gel before inserting a 10 slot comb.

2.9.2.3. Electrophoretic separation

After thawing, the samples incubated with 5 % CBB G-250 for 30 min on ice to facilitate the binding of CBB g-250 to proteins and induce the required shift in charge. 35 µg of protein were added to dry slots of the freshly prepared gradient gel. Furthermore, 10 µl of a molecular weight marker (ferritin, 400 kDa) were loaded. The iron-containing ferritin facilitates direct visibility of the marker band on the gel. After loading, all slots were carefully filled with dark blue cathode buffer. The cathode compartment of the electrophoresis chamber (Xcell Surelock® mini system; Thermo Scientific) was completely filled with dark blue cathode buffer whereas the anode compartment was filled with anode buffer. 100 V were applied to the gel at 4 °C until complete entering of the samples. Then, voltage was raised to 200 V and the run was stopped when the dye front reached the end of the gel. To improve efficiency of protein transfer to the membrane during blotting, the CBB G-250 concentration was lowered by exchanging dark blue cathode buffer with light blue cathode buffer when the samples reached the middle of the gel.

2.9.2.4. Blotting of gels after BN-PAGE

After the electrophoretic separation, the proteins were transferred onto 0.2 µm polyvinylidene fluoride (PVDF) membranes. Prior to transfer, the membranes were drowned in pure methanol for 1 min and rehydrated in native transfer buffer. Tank blotting was conducted in native transfer buffer at 4 °C with an additional cooling insert and under constant stirring. Transfer conditions constituted 160 mA for 1.5 h.

2.9.2.5. Probing membranes for AQP4

To remove CBB G-250, the PVDF membranes were briefly destained in pure methanol. The membranes were then rinsed with TBST 0.1 % and blocked with 5 % (w/v) milk (in TBST 0.1 %) for 1.5 h at RT on a rotating platform. Afterwards, membranes were washed three times with TBST 0.1 % for 5 min each and incubated with 15 ml of the primary antibody solution overnight at 4 °C on a rotating platform. On the next day, the membranes were again washed three times with TBST 0.1 % for 5 min each and 15 ml of the diluted secondary antibody was added for 1.5 h at RT on a rotating platform. The membranes were again washed three times, rinsed with ddH$_2$O and incubated with a luminol/H$_2$O$_2$-based

chemiluminescence substrate (SignalFireTM ECL reagent; Cell Signaling, Cambridge, UK) for 1 min. Afterwards, the membranes were wrapped in transparent film for image acquisition.

2.10. Peptide blocking experiments using Fluorescence-activated cell sorting (FACS)

To determine whether the mimotopes are capable of blocking the binding of NMO-IgG Pt1 to AQP4, AQP4-transfected HEK293A cells were stained with NMO-IgG Pt1 which was previously incubated with the respective mimotopes in order to facilitate eventual binding of the mimotopes to NMO-IgG Pt1 and thus to block the antibody's binding site. This capability to mimic the epitopes of NMO-IgG Pt1 was analyzed via FACS.

2.10.1. Media and solutions

- **7-AAD Viability Staining Solution** (7-amino-actinomycin D) (eBioscience Inc., San Diego, CA, USA)
- **Blocking solution**
    - Y 0.02 mg/ml goat IgG
    - Y FACS buffer
- **Counting solution**
    - Y 60 µl Trypan Blue Solution, 0.4% (Gibco®, Life Technologies)
    - Y 30 µl 1X PBS
- **FACS Buffer**
    - Y 1X PBS
    - Y 10 % goat serum; heat-inactivated at 56 °C for 30 min
    - Y 1 mM EDTA
- **HEK293A-complete medium**
    - Y DMEM (Dulbecco's Modified Eagle's Medium) - high glucose (4500 mg glucose/l, 110 ml sodium pyruvate and L-glutamine) (Sigma-Aldrich)
    - Y 10 % FBS, heat-inactivated at 56 °C for 30 min (Gibco®, Life Technologies)
    - Y 1 % NEAA (non-essential amino acids; Gibco®, Life Technologies)
    - Y 1 % penicillin/streptomycin (10,000 U/ml; Lonza)
      Stored at 4 °C
- **Secondary antibody**: Goat anti-human conjugated with Cy3 (#109-165-003, Jackson ImmunoResearch Laboratories, Inc.)

2.10.2. Experimental procedure

Four million cells in 15 ml HEK293A-complete medium were seeded in a 75 cm^2 culture flask one day before transfection, constituting a sufficient amount to ensure a confluence level of approximately 80 % at the time point of transfection.

On the next day, cells were transfected with AQP4-M23-emGFP as described in chapter 2.7.3 and incubated at 37 °C for one more day to ensure sufficient expression of AQP4 and further growth of the cells. One day later, transfection efficiency was examined using an epifluorescence microscope (Olympus IX71, Olympus KK, Tokyo, Japan). If cells were present and transfected in a sufficient amount, FACS staining was conducted. At first, preincubation of NMO-IgG Pt1 with the peptides was carried out. For all samples, NMO-IgG Pt1 was diluted 1:200 in FACS buffer and the peptides were added in a 500-fold excess. The molar mass of NMO-IgG Pt1 was determined as 64.7 µmol/l, since NMO-IgG Pt1 has a protein concentration of 9.7 mg/ml and the standard weight of IgG constitutes 150 kDA, resulting in 0.347 mol/l for the required dilution of 1:200. Information about purity, concentration and molecular weight of each synthesized peptide were provided by Centic Biotec, the company that synthesized the ordered peptides. Based on this, the molar masses of all peptides and the required input volumes to achieve a 500-fold amount of peptide compared to NMO-IgG Pt1 were calculated (table 2.5). NMO-IgG Pt1 and the respective peptides were diluted in FACS buffer and incubated in microcentrifuge tubes for 1 h at RT placed horizontally on a rotating platform (10 rpm). Furthermore, a 1:200 dilution of NMO-IgG Pt1 in FACS buffer without peptide and a 1:200 dilution of Subcuvia in FACS buffer were prepared and incubated under equal conditions. Within the preincubation time, the transfected HEK293A cells were washed, trypsinized and centrifuged as described in chapter 2.7, and were afterwards resuspended in 5 ml blocking solution. For determining the cell number, 10 µl of the cell suspension were added to 90 µl counting solution and the cells were counted using a counting chamber (Neubauer improved; Paul Marienfeld GmbH & Co. KG, Lauda-Königshofen, Germany). The remaining part was incubated for 30 min at 4 °C on a rotating platform (10 rpm).

Table 2.5: : Properties and dilutions of peptides for preincubation with NMO-IgG Pt1

ID	MW (g/mol)	Purity (%)	Conc. (mg/ml)	Purity-corrected conc. (mg/ml)	µM	Required µM	Required dilution
Pt1-04	1812.0	87.2	5.0	4.4	2405.9	161.7	1: 14.9
Pt1-05	1793.0	90.5	5.0	4.5	2523.9	161.7	1: 15.6
Pt1-07	1688.8	84.9	5.0	4.2	2512.7	161.7	1: 15.5
Pt1-08	1834.1	89.4	5.0	4.5	2436.4	161.7	1: 15.1
Pt1-11	1543.7	86.7	5.0	4.3	2807.2	161.7	1: 17.4
Pt1-13	1787.9	85.4	4.7	4.0	2245.0	161.7	1: 13.9
Pt1-18	1829.0	89.3	5.0	4.5	2440.2	161.7	1: 15.1
Pt1-19	1783.0	85.2	4.7	4.0	2246.4	161.7	1: 13.9
L8	1552.7	99.0	4.8	4.8	3060.5	161.7	1: 18.9

After blocking, the cell suspension was centrifuged for 10 min at 300 g and RT and resuspended in FACS buffer. Based on the counting results, the required volume of FACS buffer to achieve a cell concentration of 400 000- 500 000 cells/ml (depending on the available amount of cells) was calculated. 200 µl of the cell suspension each were added to the wells of a 96-well plate (Greiner Bio-One) and centrifuged for 5 min at 400 g and 4 °C. The supernatant was discarded by inverting the plate over the sink and cells were resuspended in 100 µl of the respective solutions of NMO-IgG Pt1 with pept ide which were preincubated for 1 h. For the unstained control and the control with secondary antibody only, one well each was resuspended in FACS buffer. The 96-well plates were then incubated for 30 min at 4 °C on a rotating platform (10 rpm) followed by a centrifugation step of 5 min at 400 g at 4°C to pellet the cells. The supernatant was discarded by inverting the plate over the sink and cells were washed with 150 µl FACS buffer. The centrifugation and washing steps were repeated once more to remove all non-binding primary antibodies (i.e. NMO-IgG Pt1). After another centrifugation step, the cells were resuspended in the secondary antibody. The secondary antibody goat anti-human Cy3 was diluted 1:200 in FACS buffer and 100 µl were applied to each well except for the unstained control. After incubation of 30 min at 4 °C on a rotating platform (10 rpm), the plates were centrifuged for 5 min at 400 g and at 4 °C before removing the supernatant and adding 150 µl FACS buffer to each well. Centrifugation, removal of supernatant and resuspension in FACS buffer were repeated and after a third centrifugation step under the same conditions, cells were resuspended in 100 µl

7-AAD diluted in FACS buffer (5 µl 7-AAD per 1 mio cells). The cells were incubated for 10 min at 4 °C on a rotating platform (10 rpm) and afterwards transferred to FACS tubes which contained 200 µl FACS buffer to achieve a final volume of 300 µl. The samples were kept on ice and in the dark until FACS measurements. The stainings were conducted in triplicates.

2.10.3.   Flow cytometric analysis

FACS measurements were conducted at the Core Facility Flow Cytometry of the Medical University of Vienna (Lazarettgasse 14, 1090 Vienna, Austria) using a BD LSRFortessa™ cell analyzer. Data were acquired and analyzed with the software BD FACSDiva 6.1.3. According to forward and sideward scatter, the main cell population was chosen and based on this population sorted by the absence of the 7-AAD signal since 7-AAD-positive cells are considered to be dead. Living cells among the main population were further sorted according to their positivity for both emGFP and Cy3. Median fluorescence intensities from these two channels were taken into account for the analysis, and the ratio (Cy3/GFP) was calculated to evaluate the reactivity of NMO-IgG Pt1 with AQP4 when preincubated with mimotopes. Figure 2.4 provides an example for the gating strategy applied in the analysis of all FACS experiments. Data shows the analysis of HEK293A cells transfected with the AQP4-M23-emGFP construct that were incubated with NMO-IgG Pt1 (stained with a Cy3-conjugated secondary antibody). Based on forward scatter (FSC-A) and sideward scatter (SSC-A), a cell population was chosen in gate P1 (2.4a). This population was further sorted by its 7-AAD signal intensity to exclude 7-AAD positive cells which are considered to be dead. These P2-gated cells were sorted according to their emGFP and Cy3 signals. Hence, gate P3 comprises double positive cells that were taken into account for the quantification of NMO-IgG Pt1 staining intensity as measured by the ratio of the median Cy3 fluorescence intensity and the median emGFP fluorescence intensity.
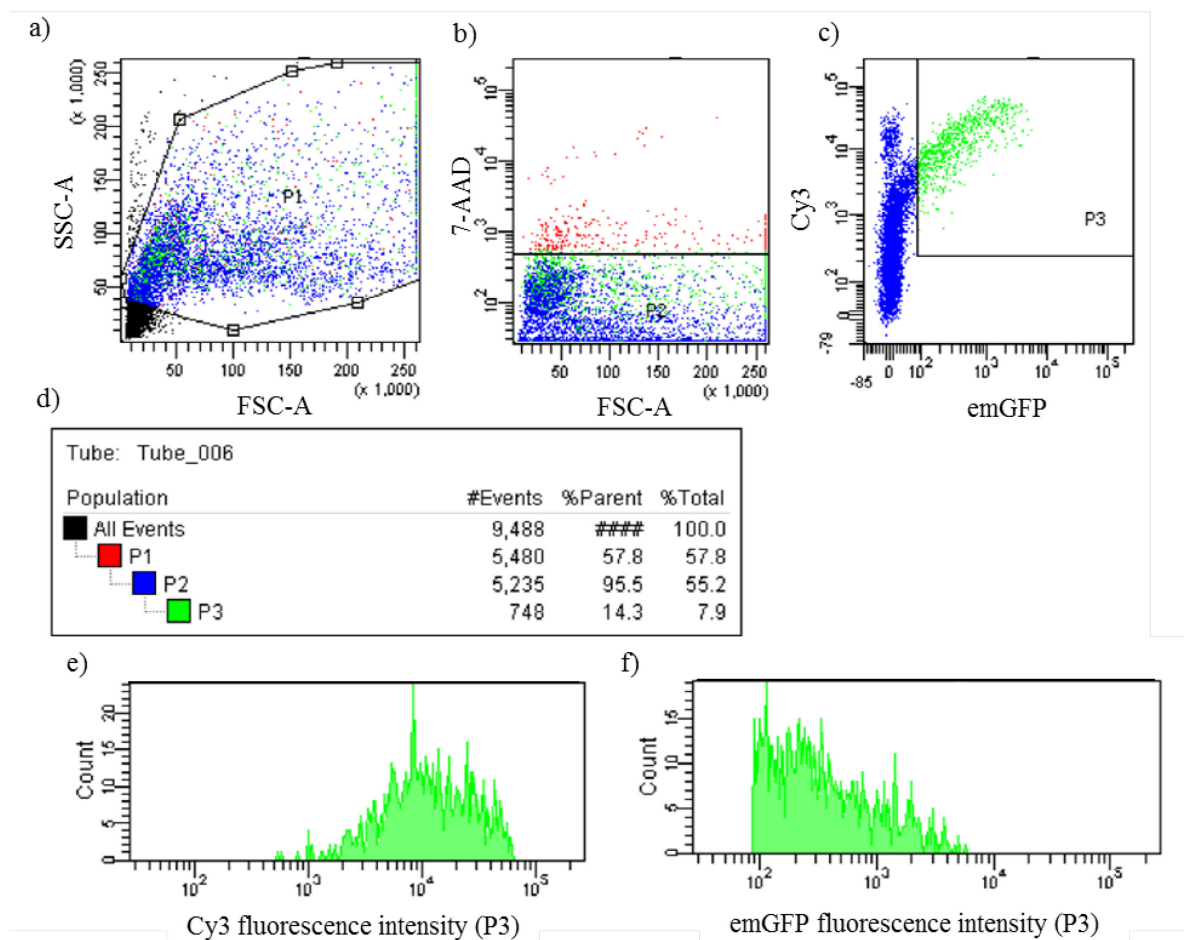
Figure 2.4: Gating strategy for all FACS experiments

Panel a) shows gate P1, where a cell population was chosen according to forward (FSC-A) and sideward scatter (SSC-A). This cell population was further gated for 7-AAD signal (gate P2, panel b)). Among this population, double positive cells (emGFP and Cy3) cells were chosen (gate P3, panel c)) and included in further analysis. Panel d) shows the percentage values of chosen cells in all three gates. Panels e) and f) depict fluorescence intensity histograms for both Cy3 and emGFP of P3 gated cells.

2.11. Statistical analysis

Data analysis was conducted using the statistics program GraphPad Prism 6 (GraphPad Software, Inc., La Jolla, CA, USA) and all graphs were generated with Microsoft Excel 2010. Elisa experiments were statistically analyzed using one-way ANOVA followed by Sidak's multiple comparisons tests. Four significance levels were used: $*p<0.05$, $**p<0.01$, $***p<0.001$ and $****p<0.0001$.

3. Results

3.1. NMO-IgG Pt1 binds to rat AQP4 *in vitro*

For confirmation and visualization of NMO-IgG Pt1-binding to AQP4, rat astrocytes were incubated with the patient's plasmapheresis product containing NMO-IgG to check for colocalization of the antibody and AQP4, its target. NMO-IgG Pt1 was expected to bind to surface epitopes of AQP4 which was stained with a commercial anti-AQP4-antibody recognizing intracellular AQP4 epitopes after permeabilization. Indeed, the staining of astrocytes from new born Lewis rats incubated with NMO-IgG Pt1 (diluted 1:1000) displays a colocalization of the signals for AQP4 (Cy2) and NMO-IgG Pt1 (Cy3) which is most prominent at the end of the astrocytic processes as indicated in yellow (figure 3.1 E). Both AQP4 (figure 3.1A) and NMO-IgG Pt1 (figure 3.1B) stainings show a speckled distribution pattern. This colocalization provides proof that NMO-IgG Pt1 is capable of recognizing extracellular epitopes on rat AQP4.
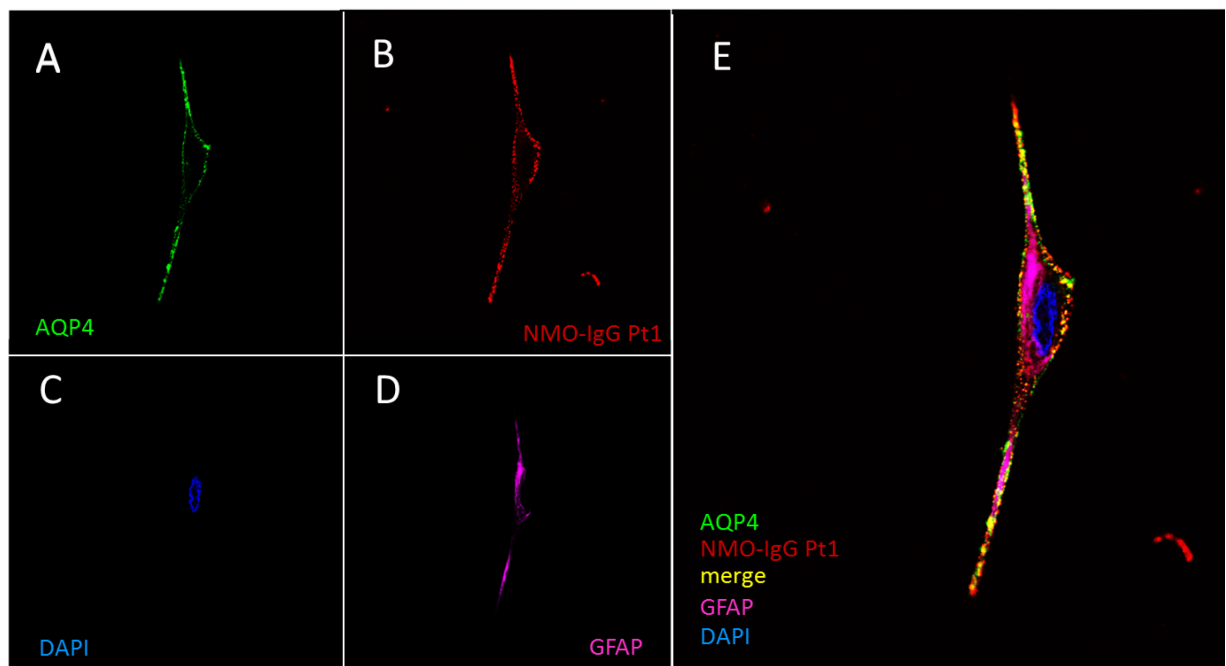
Figure 3.1: Staining of a rat astrocyte incubated with NMO-IgG Pt1

Astrocytes were stained for AQP4 (A), NMO-IgG Pt1 (B), DAPI (C) to render nuclei visible and GFAP (D) which stains astrocytes. The merge of all channels (E) clearly shows colocalization of AQP4 and NMO-IgG Pt1, particularly at the end of astrocytic processes.

To confirm cell identity and integrity, astrocytes were furthermore stained with DAPI (figure 3.1C) which served as a nuclear marker and with the astrocyte marker GFAP (figure 3.1D). To

control for bleed-through of signal in other channels, single stainings of rat astrocytes were performed and are shown in supplementary figures S3-S7. To avoid any bleed-through and spill-over among the different acquisition channels, a sequential scan was performed.

3.2. Target specificity increases after three rounds of biopanning with NMO-IgG Pt1 as compared to Subcuvia

ELISA experiments were conducted with the 1st, 2nd and 3rd round eluates obtained during the biopanning process in order to evaluate target specificity and its increase in the course of the biopanning procedure.
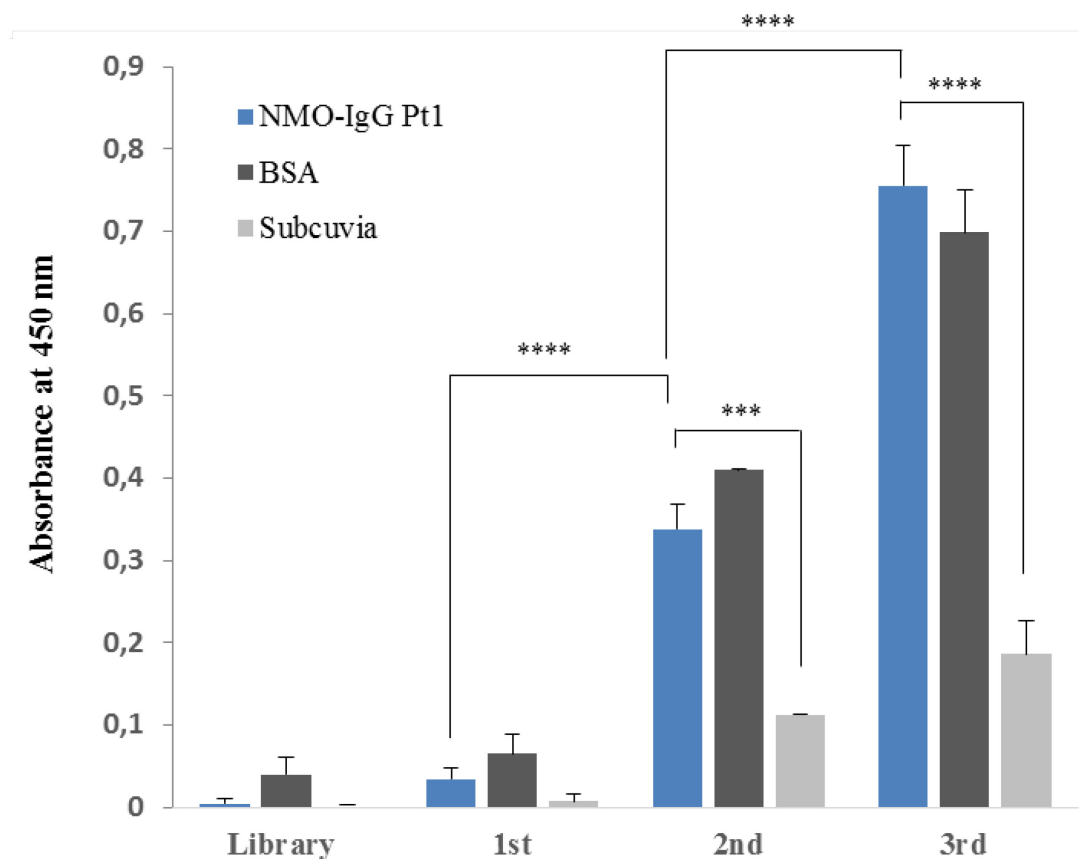
Figure 3.2: ELISA with random phages from the PhD 12TM library and the phage pools from three rounds of biopanning

The phage pools from all three rounds of panning (1st, 2nd and 3rd) and phages from the PhD 12TM library as a control were tested for their reactivity with the actual target NMO-IgG Pt1 as well as with BSA and Subcuvia.. ELISA shows that binding specificity to NMO-IgG Pt1 but also to BSA increases during the three rounds of panning. Reactivity of the phage pools from the 2nd and 3rd round of panning to Subcuvia is significantly decreased as compared to the reactivity to NMO-IgG Pt1. Reactivity of the phage pool to NMO-IgG Pt1 increases significantly in the course of biopanning. Absorbance values have been substracted by blank. Data represent two experiments (n=2) and are shown as mean + SEM (****p<0.0001, ***p<0.001, detected with one-way ANOVA followed by Sidak's multiple comparisons test).

The eluates were tested for their reactivity with the actual target, i.e. NMO-IgG Pt1, as well as BSA since it served as blocking reagent during biopanning Subcuvia which had been used to pick out phages binding randomly to human IgG in the biopanning procedure. Starting from the 2nd round eluate, reactivity of the phage pool with NMO-IgG Pt1 is significantly higher than reactivity with Subcuvia (human control IgG) ($F_{(11,12)=}109.8$, $p<0.0001$, post-hoc: 2nd/NMO-IgG Pt1 *vs.* 2nd/Subcuvia: $p=0.0004$; 3rd/NMO-IgG Pt1 vs. 3rd/Subcuvia: $p<0.0001$), but there is no significant difference between reactivity with NMO-IgG Pt1 and the blocking agent BSA in all three rounds of biopanning indicating high background ($F_{(11,12)=}109.8$, $p<0.0001$, post-hoc: 1st/NMO-IgG Pt1 *vs.* 1st/BSA: $p=0.9877$; 2nd/NMO-IgG Pt1 *vs.* 2nd/BSA: $p=0.4549$; 3rd/NMO-IgG Pt1 *vs.* 3rd/BSA: $p=0.7231$). However, data indicate that there is a continuous increase in reactivity of the phages with NMO-IgG Pt1 ($F_{(11,12)=}109.8$, $p<0.0001$, post-hoc:: 1st/NMO-IgG Pt1 *vs.* 2nd/NMO-IgG Pt1: $p<0.0001$; 2nd/NMO-IgG Pt1 *vs.* 3rd/NMO-IgG Pt1: $p<0.0001$) (figure 3.2). As a negative control, random phages were taken from the Ph.D.^{TM}-12 Phage Display Peptide Library since they have never been in contact with any of the reagents and thus constitute a random mixture representing the variety of phages the biopanning procedure had been started with. Their specificity for NMO-IgG Pt1 does not differ significantly to their reactivity with BSA and Subcuvia ($F_{(11,12)=}109.8$, $p<0.0001$, post-hoc*:* library/NMO-IgG Pt1 *vs.* library/BSA: $p=0.9699$; library/NMO-IgG Pt1 *vs.* library/Subcuvia: $p>0.999$) (figure 3.2).

3.3.   Discovery of 15 single phage clones

From the eluate of the third round of panning, 20 single phage clones were picked and their DNA was sequenced in order to identify mimotopes for NMO-IgG. The analysis of the sequencing data obtained from Centic Biotec from the 20 phage clones revealed 15 correctly inserted peptides. Peptides were considered as inserted correctly when the 12-mer peptide was bordered by the flanking sequences ("LFAIPLVVPFYSHS" and "AETVESCLAK") as well as the linker sequence "GGGS". Furthermore, the restriction enzyme recognition sites "ggtacc" and "cggccg" had to be present (figure 3.3). The flanking sequences of Pt1-09 and Pt1-20 were incorrect so that these phage clones were excluded. The sequencing data of single phage stock Pt1-17 did not contain any of flanking sequences. The phage clones lacking correct inserts were excluded from further analysis (table 3.1).

```
aaattattattcgcaattcctttagtggtacctttctattctcactctcagatgatgaag
 K  L  L  F  A  I  P  L  V  V  P  F  Y  S  H  S  Q  M  M  K

gcttcttcggagtatacgggttttggtggaggttcggccgaaactgttgaaagttgttta
 A  S  S  E  Y  T  G  F  G  G  G  S  A  E  T  V  E  S  C  L

gcaaatcccatacagaaaattcattacta
 A  K  S  H  T  E  N  S  L  L
```

Figure 3.3: Base and amino acid sequence of the region of interest given by the ExPASy Translate tool

All sequencing data were checked for the presence of the mimotope flanking sequences (marked in grey); the restriction enzyme recognition sites (in yellow and green) and the mimotope sequence (12 amino acids) in dark blue with the linker sequence in light blue. The figure shows the sequencing data of mimotope Pt1-01 as an example for correct insertion of the randomized region within correct flanking sequences.

Table 3.1: Validity and peptide sequence of single phage clones Pt1-01 to Pt1-20

ID	Valid?	Peptide sequence
Pt1-01	Yes	QMMKASSEYTGF-GGGS
Pt1-02	Yes	GPFHWHQKVTGK-GGGS
Pt1-03	Yes	NSPWAHDVPPTY- GGGS
Pt1-04	Yes	WRYHVHPTPFKS-GGGS
Pt1-05	Yes	WHRTHILQYGKP-GGGS
Pt1-06	No, DNA concentration too low for sequencing	
Pt1-07	Yes	WPWHAHGNTRGI-GGGS
Pt1-08	Yes	WHWKPYMSSRAQ-GGGS
Pt1-09	No, flanking sequence incorrect	
Pt1-10	Yes	VHKDHHRWHFLK-GGGS
Pt1-11	Yes	VPSNSLLQSSRV-GGGS
Pt1-12	Yes	GLVHHKHWRGNQ-GGGS
Pt1-13	Yes	GPFHFLHHHWSQ-GGGS
Pt1-14	Yes	YRNDSRDAINMM-GGGS
Pt1-15	Yes	IPLGRDGGSYQR-GGGS
Pt1-16	No, DNA concentration too low for sequencing	
Pt1-17	No, flanking sequences not found	
Pt1-18	Yes	WSSHAHRHNHFR-GGGS
Pt1-19	Yes	WGMHRHAPVYDR-GGGS
Pt1-20	No, flanking sequence incorrect	

The random phage clones picked from the Ph.D.12™ Library were sequenced and analyzed in the same manner. All five random single phage stocks contained the correct flanking sequences and the peptides were identified (table 3.2).

Using the web tools MimoSearch and MimoScan to compare the obtained peptides with previously published mimotopes or patterns did not reveal any hits. TUPScan, an online tool to scan mimotopes for known target-unrelated motifs, identified the sequence "HFLHHH" in Pt1-13 as matching pattern to "H-x(2)-H(3)", a confirmed or suspected bivalent metal ion binder. But since no metal ions were used for target immobilization in the phage display experiment, Pt1-13 was not excluded. Furthermore, the online tool MIMOX was used to find an eventual consensus sequence. However, this tool is supposed to find consensus sequences for mimotopes obtained in a biopanning experiment with monoclonal antibodies and since the antibodies used in this study are polyclonal, no meaningful consensus sequence was revealed.

Table 3.2: Validity and peptide sequence of the random phage clones L7 to L11

ID	Valid?	Peptide sequence
L7	Yes	TQPGLIVKRGYF-GGGS
L8	Yes	FPTDSLRGDVGM-GGGS
L9	Yes	GRIHGHPLASSV-GGGS
L10	Yes	VPSLWTSMGRWA-GGGS
L11	Yes	AHGLALDTPYQG-GGGS

3.4. Mimotopes mapped on human AQP4

For further characterization of the 15 obtained mimotopes, the peptide sequences were mapped on the human AQP4 using the online programs EpiSearch and *PepSurf*. The two programs served to examine the mimotopes in terms of their capability to mimic NMO-IgG epitopes on AQP4, i.e. they predict amino acids from the target molecule AQP4 that most probably form an epitope consisting of the amino acids contained in the given peptide sequence. Figures 3.4 and 3.5 show the mapping results of both EpiSearch and *PepSurf* combined in one image to allow a better comparison of the results. Original mapping results

as displayed by the programs themselves are shown in supplementary figures S6-S13. A list of the predicted residues, eventually indicated by both programs, is given in table 3.3. In most cases (Pt1-01, -02, -04, -05, -08, -10, -11, -15, -18), EpiSearch and *PepSurf* reveal contradicting results without any overlapping residue. Mimotope Pt1-04 is mapped on the intracellular surface by both EpiSearch and *PepSurf*. For Pt1-03, -07, -12, -13 and -19, EpiSearch and *PepSurf* reveal mapping on at least one of the extracellular loops and at least two suggested residues overlap (table 3.3).
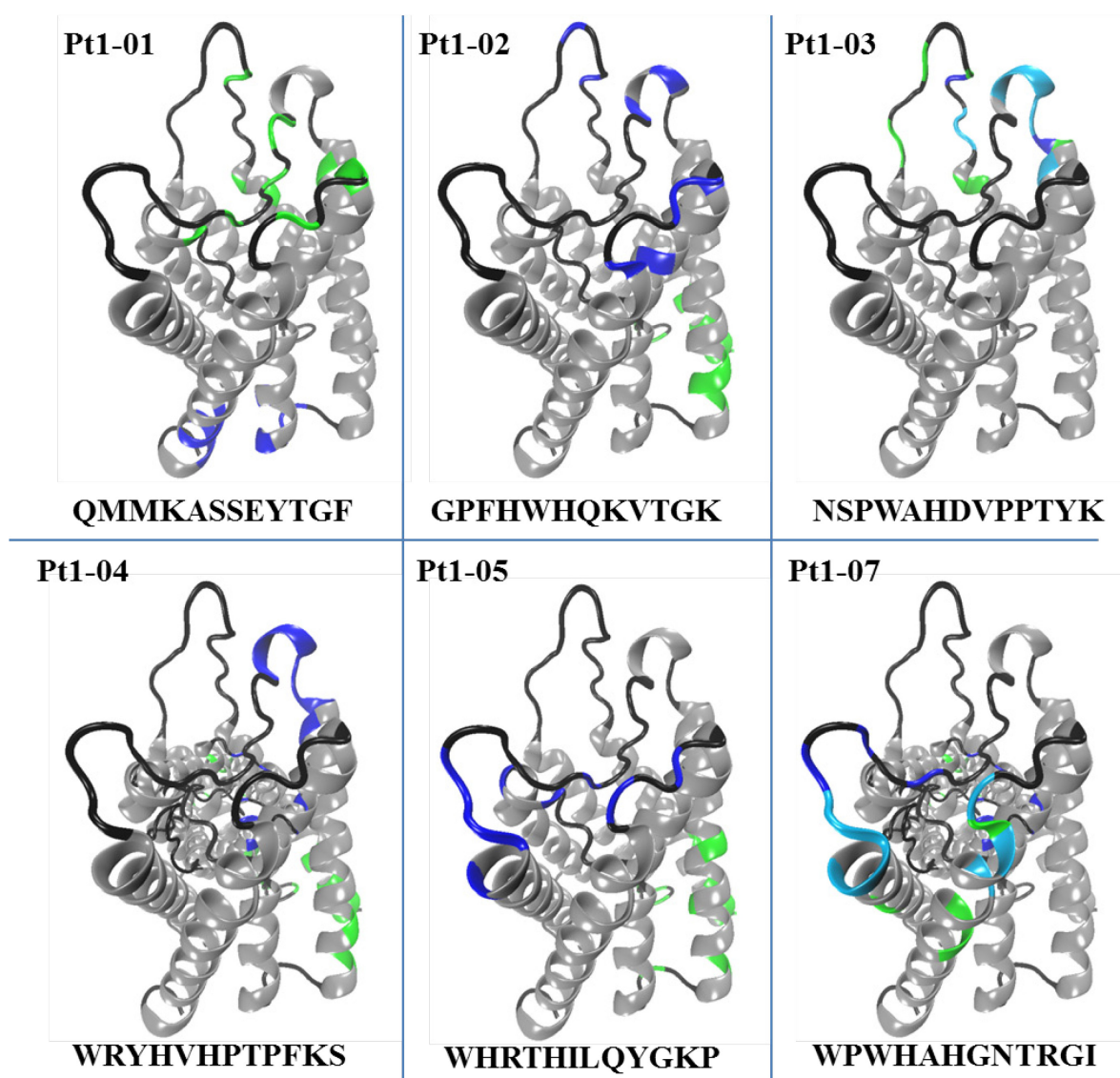
Figure 3.4: Epitope predictions of *PepSurf* and EpiSearch for Pt1-01 to Pt-07 on human AQP4

PepSurf results are shown in blue; predictions of EpiSearch are indicated in green. Cyan indicates overlapping sites. Images were created using the software VMD 1.9.2.
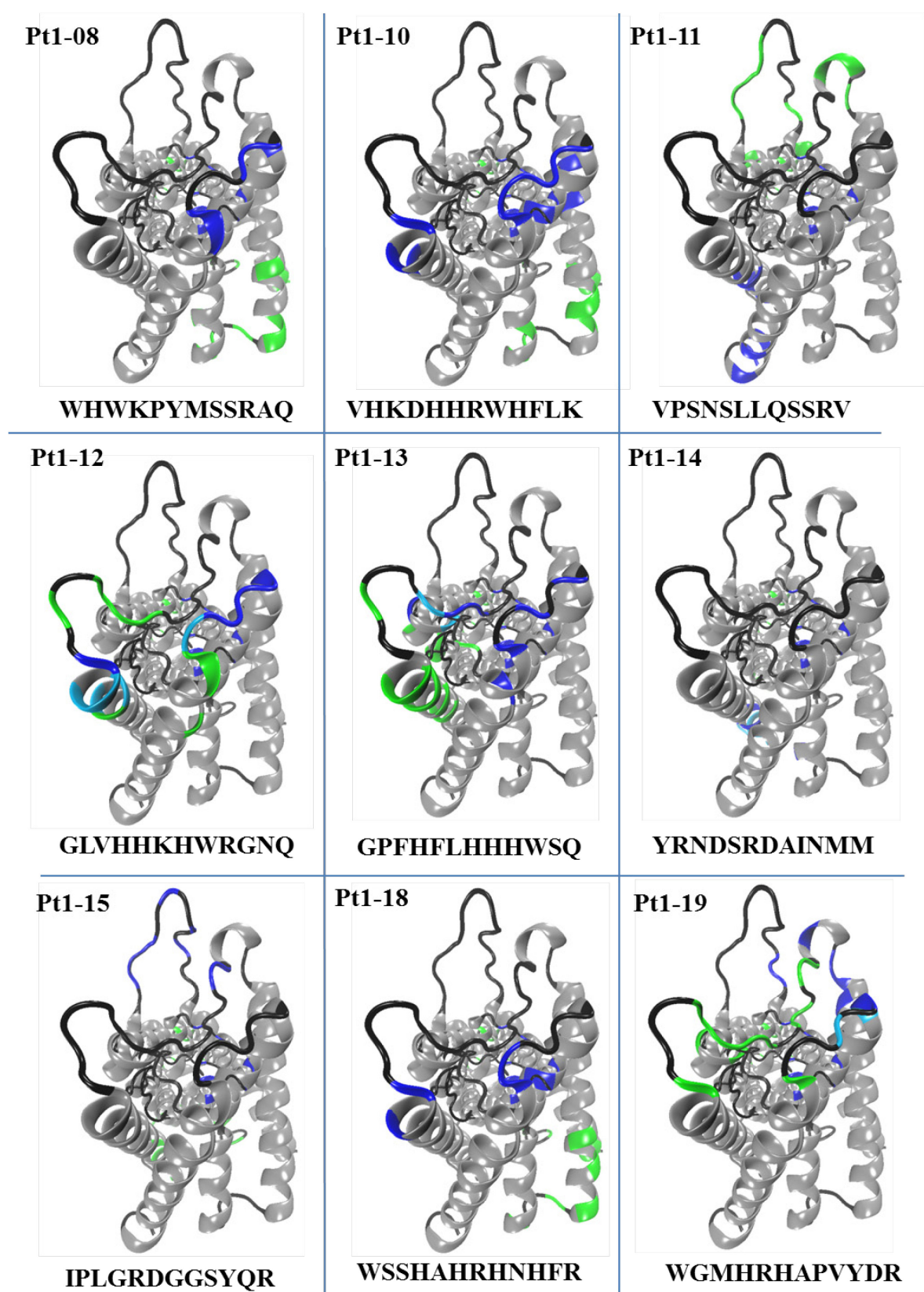
Figure 3.5: Epitope predictions of *PepSurf* and EpiSearch for Pt1-08 to Pt-19 on human AQP4

PepSurf results are shown in blue; predictions of EpiSearch are indicated in green. Cyan indicates overlapping sites. Images were created using the software VMD 1.9.2.

Table 3.3: Epitope residues as predicted by EpiSearch and *PepSurf*

Mimotope	Residues predicted by EpiSearch	Residues predicted by *PepSurf*	Overlapping residues
Pt1-01	G54 T56 G61 T62 Y134 G143 G144 G146 M149 G209 M224 G225 E228	M104 I110 K109 E249 Y250 T107 G246 L247	
Pt1-02	Q32 F34 W35 K36 V38 T39 F42 F88 G93 H95 K114 V116 F117	F218 H230 W227 N226 M224 V142 S140 G61 K64	
Pt1-03	S55 T56 N58 W59 T62 P65 V68 D69 Y134 V136 P138 P139 S140 V141	N58 W59 G61 S140 V141 P138 P139 T137 Y134	N58 W59 P138 P139 S140 V141
Pt1-04	F34 W35 K36 V38 T39 F42 V85 F88 H90 S92 H95 K114 F117	Y134 V136 P138 T137 P139 V142 V141 S140	
Pt1-05	Q32 W35 K36 T39 L43 I91 G93 H95 I110 K114 I119 L124	W227 N229 A156 H158 T155 L154 Y207 G209 M149	
Pt1-07	T155 A156 G157 H158 I165 N229 H230 W231 W234 I238 I239	W234 W231 N229 A156 H158 G157 T155 V150 G152 L154	T155 A156 G157 H158 N229 W231
Pt1-08	Q32 A33 W35 S92 H95 M104 R108 K109 S111 A113 K114 A120	W231 H230 W227 N226 M224	
Pt1-10	F34 W35 V38 H95 V105 R108 K109 K114 V116 F117	V162 H158 A156 N229 E228 N226 W227 H230 F218 I127 G131	
Pt1-11	S55 N58 P65 L66 P67 V68 L72 P138 S140 V141	V251 P254 E249 L247 F168 Q169 T173 A176 R182 V185	
Pt1-12	V150 H151 G152 L154 G157 H158 L160 L161 V162 N229 H230 W231 V235	G157 L160 V162 H158 A156 N229 W227 G225 N226 E228	G157 H158 L160 V162 N229
Pt1-13	H151 L154 G157 H158 L160 L161 L164 F168 Q169 G200 H201 F203 G209 S211	G209 Y207 H151 V150 M149 N226 E228 H230 W234	H151 G209
Pt1-14	A176 S177 D179 S180 R182 D184 S188 I189 A192	F172 A176 D179 S180 R182 D184 T183 V185 S177 I174	A176 S177 D179 S180 R182 D184

Pt1-15	Q86 G89 G93 I174 S177 D179 S180 R182 G187 S188 I189 L191	V68 P67 L66 G60 K64 T62 G143 G144	
Pt1-18	A33 F34 W35 S92 H95 R108 S111 A113 F117 A120	H158 A156 N229 H230 F218	
Pt1-19	G143 G144 G146 V147 M149 V150 H151 G152 A156 Y207 G209 M224 W227 H230	W227 G225 M224 Y134 T137 P138 V141 W59 N58	M224 W227

3.5. Target specificity of single phage clones

In order to evaluate the target specificity of the single phage clones, ELISAs were conducted for every single phage stock with a correct insert. Each phage clone was tested for its binding affinity to NMO-IgG Pt1 constituting the actual target and to BSA (blocking reagent) and Subcuvia (polyclonal human IgG from healthy subjects) as controls.
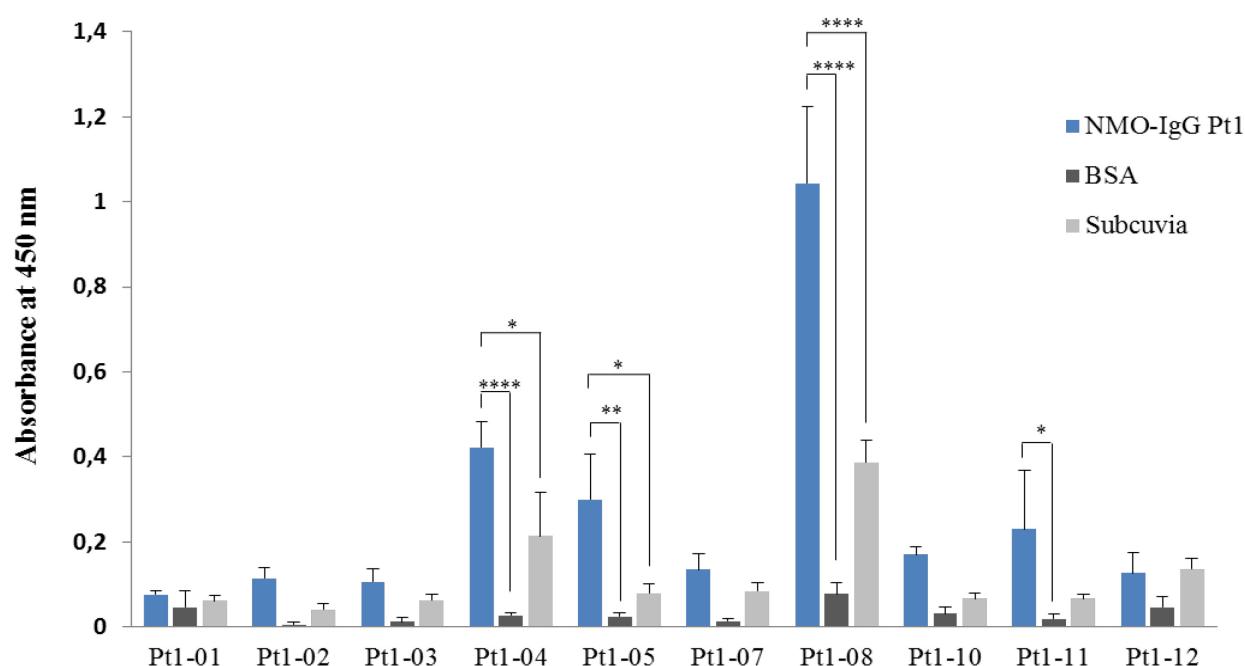
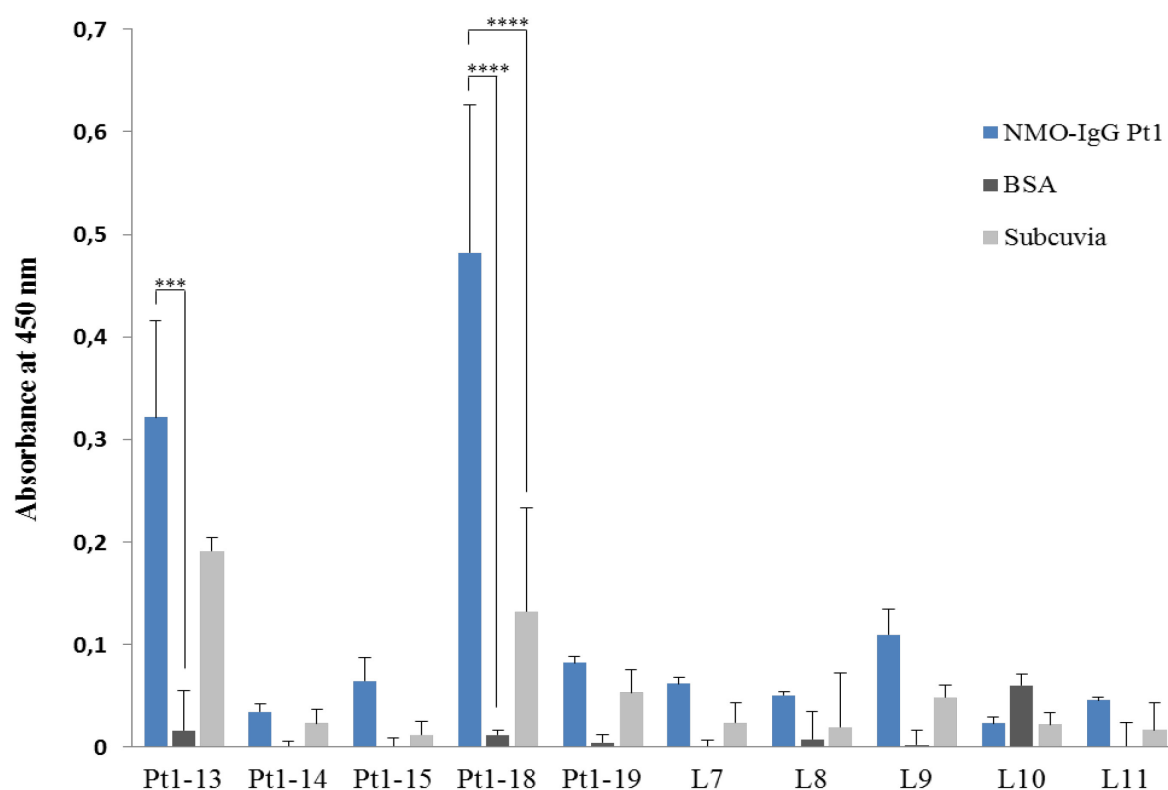**Figure 3.6: ELISA with single phage clones Pt1-01-12**

Reactivity of single phage clones with NMO-IgG Pt1, BSA and Subcuvia was measured. Pt1-04, Pt1-05 and Pt1-08 show decreased reactivity with BSA and Subcuvia in comparison to reactivity with NMO-IgG Pt1. Pt1-11 binds significantly better to NMO-IgG Pt1 than to BSA. The other samples do not vary significantly in their binding affinities to the three targets. Each sample contained 10^8 phages. Data represent three experiments (n=3) and are shown as mean + SEM (*p<0.05, **p<0.01, ****p<0.0001, detected with one-way ANOVA followed by Sidak's multiple comparisons test).

As shown in figure 3.6, the phage clones Pt1-01, Pt1-02, Pt1-03, Pt1-07, Pt1-10 and Pt1-12 do not differ significantly regarding their binding specificity to either NMO-IgG Pt1 or BSA or Subcuvia. However, the reactivity of Pt1-04 with NMO-IgG Pt1 is significantly increased as compared to its reactivity with both BSA and Subcuvia ($F_{(59, 120)}$ = 11,84, , p<0.0001, post-hoc:: Pt1-04/NMO-IgG Pt1 *vs*. Pt1-04/BSA: p<0.0001; Pt1-04/NMO-IgG Pt1 *vs*. Pt1-04/Subcuvia: p=0.0317). Also for Pt1-05, significant differences between their binding affinities to NMO-IgG Pt1 and BSA and Subcuvia, respectively, were observed ($F_{(59, 120)}$ = 11,84, , p<0.0001, post-hoc:: Pt1-05/NMO-IgG Pt1 *vs*. Pt1-05/BSA: p=0.0012; Pt1-05/NMO-IgG Pt1 *vs*. Pt1-05/Subcuvia: p=0.0206). Pt1-08 was shown to bind significantly better to NMO-IgG Pt1 than to BSA and to Subcuvia ($F_{(59, 120)}$ = 11,84, , p<0.0001, post-hoc:: Pt1-08/NMO-IgG Pt1 *vs*. Pt1-08/BSA: p<0.0001; Pt1-08/NMO-IgG Pt1 *vs*. Pt1-08/Subcuvia: p<0.0001). Testing Pt1-11 for its binding affinities, it turned out that it binds significantly better to NMO-IgG Pt1 in comparison to BSA but does not significantly differ in its reactivity to NMO-IgG Pt1 and to Subcuvia ($F_{(59, 120)}$ = 11,84, , p<0.0001, post-hoc:: Pt1-11/NMO-IgG Pt1 *vs*. Pt1-11/BSA: p=0.0309; Pt1-11/NMO-IgG Pt1 *vs*. Pt1-11/Subcuvia: p=0.1872) (figure 3.6).

ELISAs with the phage clone Pt1-13 revealed increased specificity for NMO-IgG Pt1 as compared to BSA but no significant difference in binding affinities to NMO-IgG Pt1 and Subcuvia ($F_{(59, 120)}$ = 11,84, , p<0.0001, post-hoc:: Pt1-13/NMO-IgG Pt1 *vs*. Pt1-13/BSA: p=0.0002; Pt1-13/NMO-IgG Pt1 *vs*. Pt1-13/Subcuvia: p=0.6669). Pt1-18 shows a significantly increased specificity to NMO-IgG Pt1 in comparison to both BSA and Subcuvia ($F_{(59, 120)}$ = 11,84, , p<0.0001, post-hoc:: Pt1-18/NMO-IgG Pt1 *vs*. Pt1-18/BSA: p=0.0002; Pt1-18/NMO-IgG Pt1 *vs*. Pt1-18/Subcuvia: p=0.6669). Pt1-14, Pt1-15 and Pt1-19 do not differ significantly in their binding affinities to either NMO-IgG Pt1 or BSA or Subcuvia and the same pattern could be observed for the random control phages L7-L11 (figure 3.7).

Figure 3.7: ELISA with single phage clones Pt1-13-19 and random phages L7-L11

Reactivity of single phage clones with NMO-IgG Pt1, BSA and Subcuvia was measured. Pt1-18 shows decreased reactivity with BSA and Subcuvia in comparison to reactivity with NMO-IgG Pt1. Pt1-13 binds significantly better to NMO-IgG Pt1 than to BSA. The other single phages as well as the control phages do not vary significantly in their binding affinities to the three targets. Each sample contained 10^8 phages. Data represent three experiments (n=3) and are shown as mean + SEM (*p<0.***p<0.001, ****p<0.0001, detected with one-way ANOVA followed by Sidak's multiple comparisons test).

3.6. Assessment of promising mimotopes

Based on the results of the ELISAs with the single phage clones and partly on the mapping results, potentially interesting mimotopes were chosen for further analysis. All phage clones that displayed significantly increased specificity for NMO-IgG Pt1 in the ELISA experiments were included in further analyses (Pt1-04, -05, -08, -11, -13 and -18). Furthermore, Pt1-07 and Pt1-19 were included based on coherent mapping results on the extracellular loops according to both mapping tools. Table 3.4 summarizes properties and results of the above mentioned experiments for the single phage clones.

Table 3.4: Mapping and ELISA results of all mimotopes

Promising candidates are highlighted in green

Mimotope	EpiSearch mapping	*PepSurf* mapping	Overlap EpiSearch/*PepSurf*	Sufficient target specificity in ELISA
Pt1-01	Loops A,C,E	intracellular	No	No
Pt1-02	intracellular	Loops A,C,E	No	No
Pt1-03	Loops A,C	Loops A,C	Yes	No
Pt1-04	intracellular	Loop C	No	Yes
Pt1-05	intracellular	Loops C, E	No	Yes
Pt1-07	Loops C,E	Loops C,E	Yes	No
Pt1-08	intracellular	Loop E	No	Yes
Pt1-10	intracellular	Loop C,E	No	No
Pt1-11	Loops A,C	intracellular	No	Yes
Pt1-12	Loops C,E	Loops C,E	Yes	No
Pt1-13	Loop C	Loops C,E	Yes	Yes
Pt1-14	intracellular	intracellular	Yes	No
Pt1-15	intracellular	Loops A,C	No	No
Pt1-18	intracellular	Loops C,E	No	Yes
Pt1-19	Loops C,E	Loops A,C,E	Yes	No

3.7. Confirmation of NMO-IgG Pt1 binding to human AQP4-M23-emGFP expressed by transfected HEK293A cells

In order to ensure that NMO-IgG Pt1 binds to AQP4-emGFP on transfected HEK293A cells, a staining was performed. Figure 3.8A depicts emGFP fused to AQP4 distributed in a speckled pattern across the cell indicating OAP formation. A very similar pattern can be observed in panel B showing Cy3 (indicating NMO-IgG Pt1) staining. Nuclei were stained with DAPI to prove cell identities. The merge in panel D revealed that NMO-IgG Pt1 (Cy3) and AQP4 (GFP) colocalize as indicated by yellow color arising from an overlap of emGFP and Cy3 (figure 3.8D). This staining provides evidence that NMO-IgG Pt1 is able to bind to human AQP4 on transfected HEK293A cells.
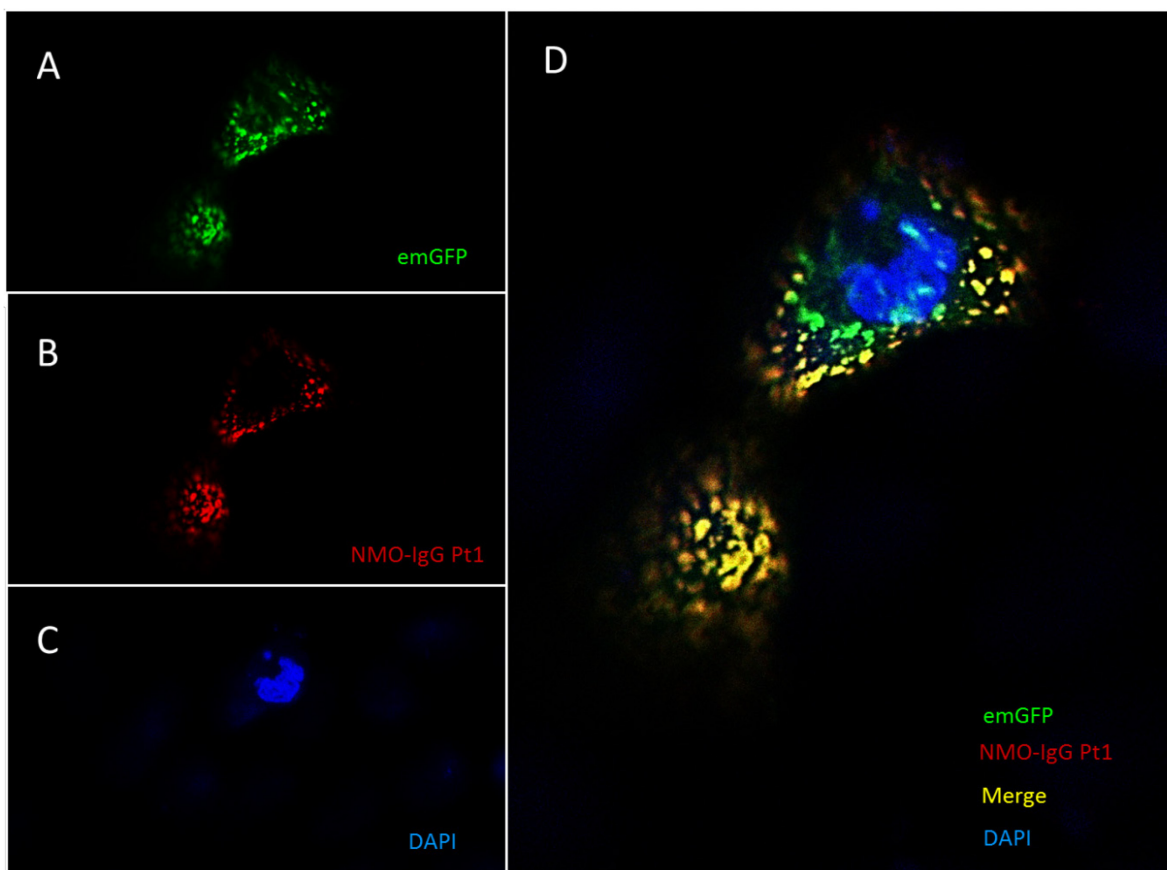
Figure 3.8: Staining of AQP4-M23-emGFP-transfected HEK293A cells with NMO-IgG Pt1

(A) shows the expression pattern of AQP4 as indicated by emGFP. Cells were further stained with NMO-IgG Pt1 (B) and DAPI (C) as a nuclear marker. The merge of all three channels (D) shows colocalization of AQP4 and NNO-IgG Pt1 as indicated by yellow color. Images were adjusted for brightness and contrast.

3.8. Four mimotopes are capable of decreasing NMO-IgG Pt1-binding to AQP4

The chosen mimotopes (compare chapter 3.6) were synthesized in order to test them for their ability to block the binding of NMO-IgG Pt1 to AQP4. This issue was addressed in an experiment where HEK293A cells were transfected with GFP-fused AQP4 and stained with NMO-IgG Pt1 and NMO-IgG Pt1 which was previously preincubated with the mimotopes, respectively. Using flow cytometry, the binding of NMO-IgG Pt1 and the mimotope-induced decrease of this binding capability has been evaluated as measured by the median fluorescence intensities of GFP (indicating AQP4) and Cy3 (indicating NMO-IgG Pt1).

The FACS measurements revealed four of the eight included peptides to be capable of reducing the reactivity of NMO-IgG Pt1 with its target, AQP4 (figure 3.9). Preincubating

NMO-IgG Pt1 with Pt1-04 reduced the ratio of the median fluorescence intensities of Cy3 and GFP by 22.9 % to 77.1 % (0.771 ± 0,065).
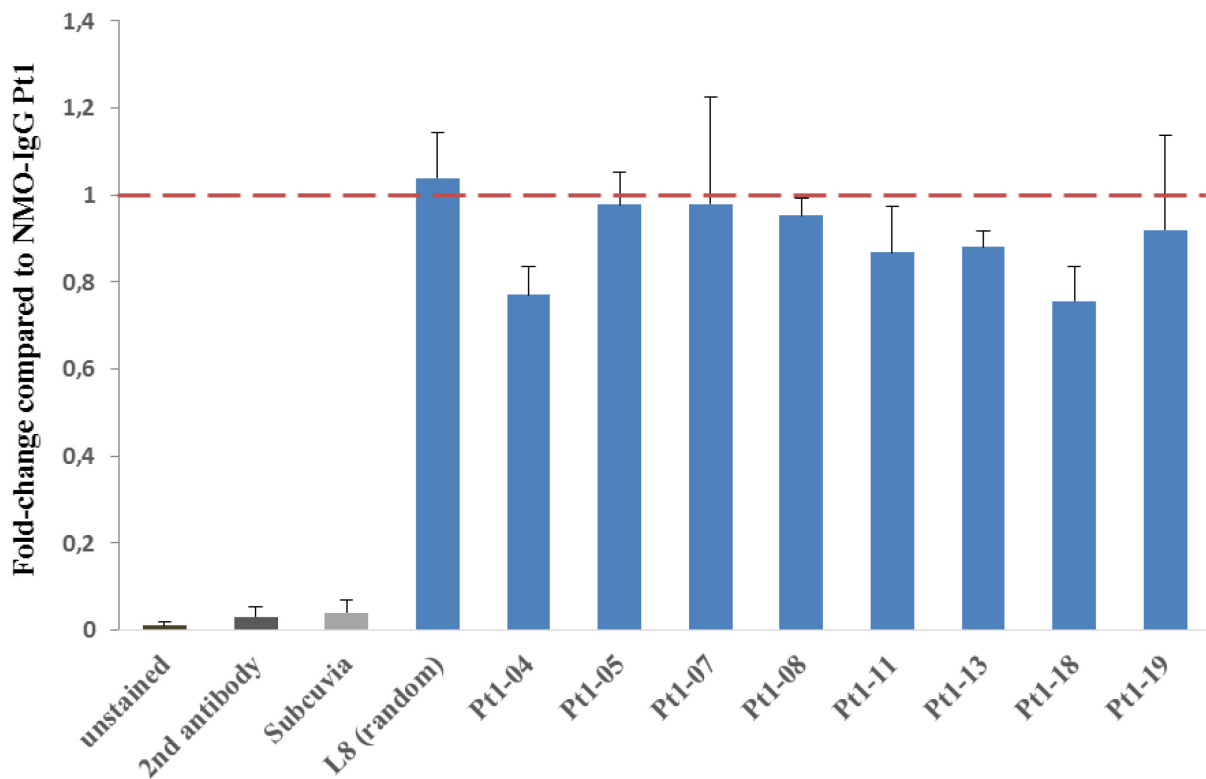
Figure 3.9: Peptide blocking assay

As measured via FACS, preincubation with Pt1-04, Pt1-11, Pt1-13 and Pt1-18 decreased the ratio of the median fluorescence intensities of Cy3 and GFP and hence the binding of NMO-IgG Pt1 to AQP4. Data represent three experiments (n=3), except for Pt1-05, -07 and -19, which were tested twice (n=2) and are shown as mean + SEM.

Preincubation with Pt1-11 results in a ratio of the median fluorescence intensities Cy3/GFP of 86.8 % as compared to the median fluorescence ratio from NMO-IgG Pt1 without peptide preincubation. Mimotope Pt1-13 reduced the ratio of the median fluorescence intensities to 88 % and thus showed the ability to block NMO-IgG Pt1-binding to AQP4-M23 by 12 % (0.88 ± 0.039). Binding of NMO-IgG Pt1 to AQP4 was reduced to 75.6 % by Pt1-18 (0.756 ± 0.079). Mimotopes Pt1-05, -07, -08 and -19 are not capable to induce a considerable reduction of NMO-IgG Pt1-binding to AQP4. The measurements of unstained HEK293A cells, as well as HEK293A cells which were solely incubated with the secondary antibody served as controls and show that there is negligible background staining as shown by the ratio of the median fluorescence intensities of GFP and Cy3 (unstained: 0.01 ± 0.007; secondary antibody: 0.03 ± 0.023). Staining with Subcuvia instead of NMO-IgG Pt1 as primary antibody served as control

to check for binding of a mixture of human IgG to HEK293A cells and revealed no considerable reactivity (0.04 ± 0.03).

3.9. Differential expression patterns of the two AQP4 isoforms in transfected HEK293A cells and resulting binding properties of NMO-IgG Pt1

In this study, HEK293A cells were transfected with two different constructs encoding the two isoforms of AQP4: M1 and M23 each C-terminally fused to emGFP. The M23 construct contains the AQP4 sequence beginning only from position 23 whereas the M1 construct provides the whole AQP4 sequence but still containing the methionine 23-encoding ATG triplet. As a consequence, the M1 construct eventually also permits translation of the M23 isoform by a leaky scanning mechanism (compare chapter *introduction*). Whether HEK293A cells transfected with AQP4-M1-emGFP actually also express the M23 isoform of AQP4 can be evaluated based on the presence of OAPs, since the isoform M1 is not capable of forming higher order structures without the coexistence of the M23 isoform (Crane and Verkman, 2009b).

To address this issue, a BN-PAGE was performed with HEK293A cells transfected with the M1 and M23 construct, respectively. Figure 3.10 shows several bands in the lane of the M23-transfected HEK293A cells of sizes exceeding the known size of AQP4 tetramers and thus indicating OAPs of different sizes. The M1 lane displays two bands, one indicating tetramers and one indicating also a small pool of OAPs. Thus, the M1 construct also allows expression of the M23 isoform, although in a smaller amount than M1.
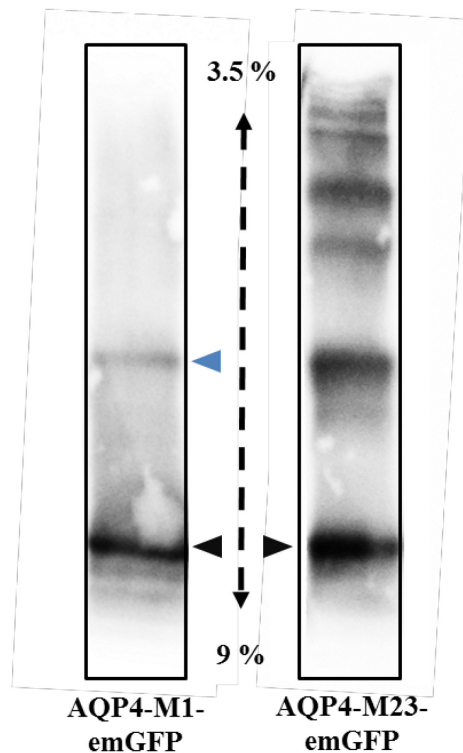
Figure 3.10: Analysis of OAPs in HEK293A cells expressing AQP4-M1 and AQP4-M23

OAPs were separated using BN-PAGE according to their size in a 3.5 to 9 % acrylamide gradient (large to small from top to bottom). The expression of AQP4-M23-emGFP results in six distinct OAP pools of different sizes. In AQP4-M1-emGFP-transfected cells, AQP4 is mostly present as tetramers (black arrow heads) whereby a small OAP pool is present as well (blue arrow head). The image was adjusted for brightness and contrast.

For further characterization of the M1 construct and to discover eventually differential binding properties of NMO-IgG Pt1 to the two isoforms, a staining of HEK293A cells transfected with the M1 construct using NMO-IgG Pt1 was performed. Figure 3.11D shows a colocalization of NMO-IgG Pt1 (Cy3) and AQP4 (emGFP), even though in a reduced amount as compared to the staining of HEK293A cells transfected with the M23 construct (compare figure 3.8). Moreover, the image provides evidence that NMO-IgG Pt1 only binds to AQP4 but not on any other surface molecules of HEK293A cells since the DAPI staining (figure 3.11C) also shows nuclei of untransfected cells and the merge of all channels (figure 3.11D) depicts no Cy3 signal (NMO-IgG Pt1) on these cells lacking AQP4 as indicated by the absence of emGFP signal (orange arrow-head in figure 3.11D).
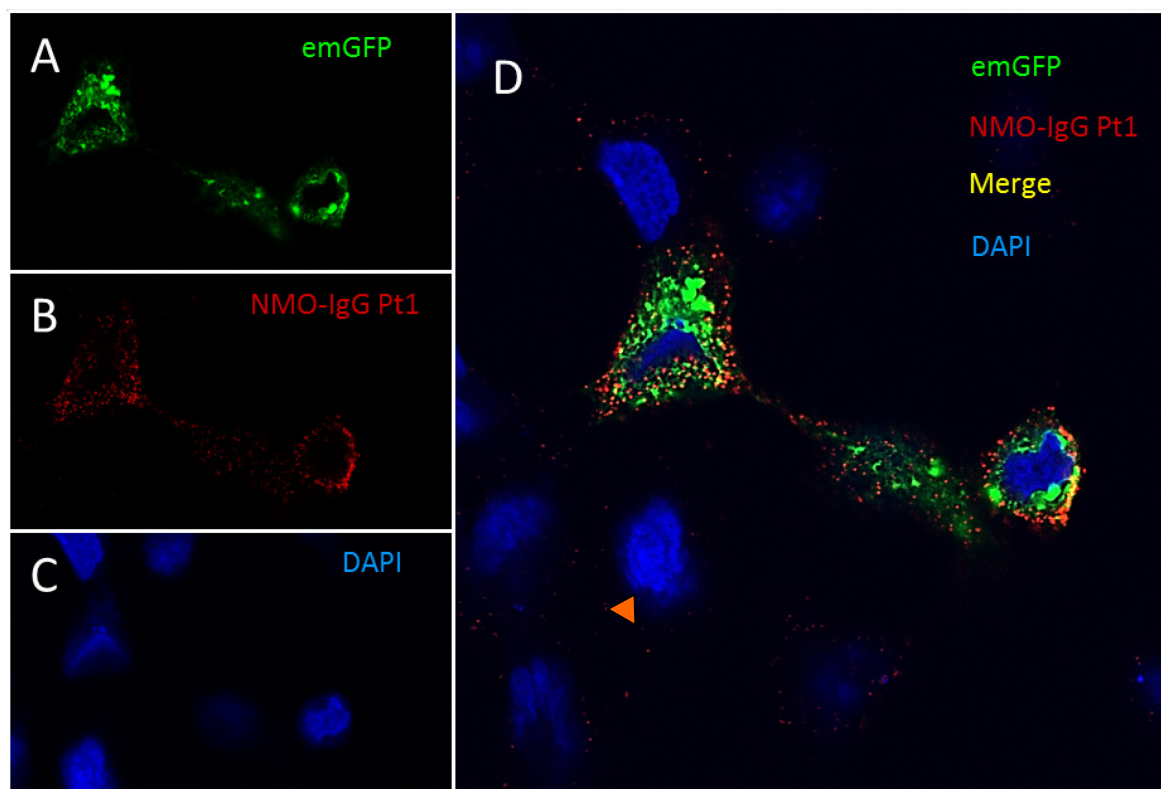
Figure 3.11: Staining of AQP4-M1-emGFP-transfected HEK293A cells with NMO-IgG Pt1

(A) shows the expression pattern of AQP4 as indicated by emGFP. Cells were further stained with NMO-IgG Pt1 (B) and DAPI (C) as a nuclear marker. The merge of all three channels (D) shows colocalization of AQP4 and NNO-IgG Pt1 as indicated by yellow color.
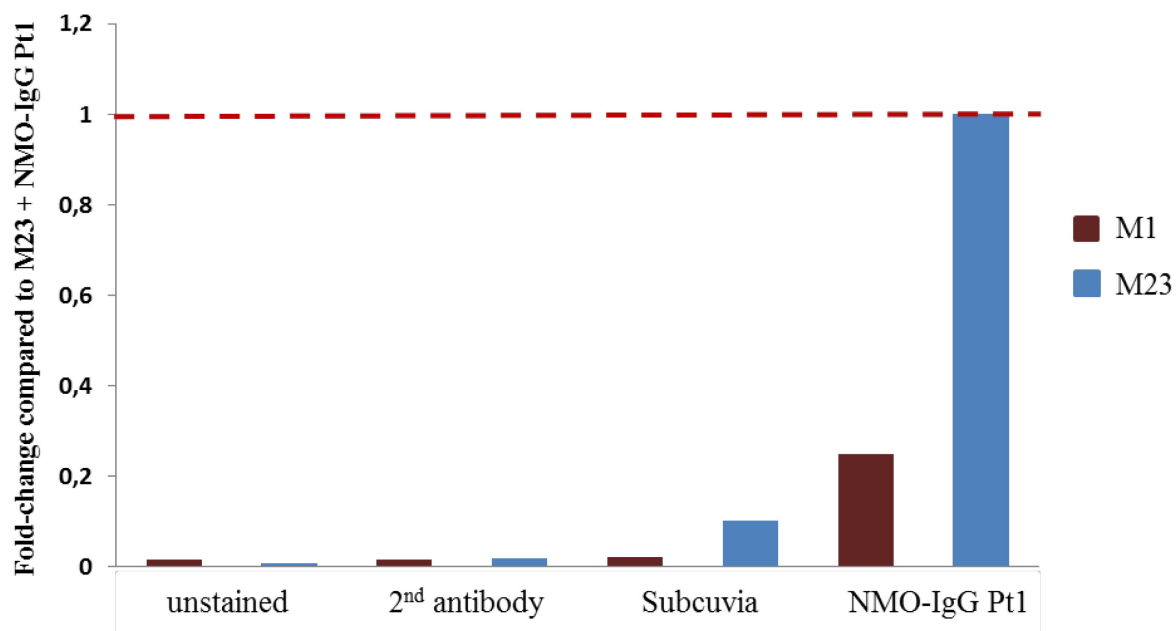
Figure 3.12: NMO-IgG Pt1 binding to AQP4-M1 as compared to AQP4-M23

As measured via FACS, M1-transfected HEK293A cells display a decreased ratio of the median fluorescence intensities of Cy3 and GFP and hence reduced binding of NMO-IgG Pt1 to AQP4.

The finding that NMO-IgG P1 binds less to AQP4-M1 than to AQP4-M23 is in line with the flow cytometric analysis of a staining of HEK293A cells expressing AQP4-M1-emGFP with NMO-IgG Pt1. As compared to the FACS results of a staining with HEK293A cells transfected with the M23 construct, the binding of NMO-IgG Pt1 to AQP4 is reduced by 75.3 % to 24.7 % (figure 3.12). Furthermore, several negative controls were included, such as unstained HEK293A cells expressing either M1 or M23, both isoforms stained solely with secondary antibody and with Subcuvia, respectively. All controls depict a negligible signal (figure 3.12).

4. Discussion

The present work addressed the identification of mimotopes for pathogenic NMO-IgG of an NMO patient via phage display. The prerequisite for the pathogenicity of these NMO-IgG is their binding to a conformational epitope formed by the three extracellular loops of AQP4. This reactivity has been confirmed for the utilized IgG, i.e. NMO-IgG Pt1, via immunofluorescence stainings of rat astrocytes and AQP4-transfected HEK293A cells.

For the mimotope discovery, a library of phages presenting random 12-mer peptides was used for biopanning with NMO-IgG Pt1 as a target. Three rounds of biopanning elicited a significant increase in target specificity, although with considerable background as measured by the phages' reactivity with the blocking agent BSA, which was supposed to prevent phages from binding to the plastic surface of the wells. However, this partial BSA-reactivity of the phages did not cause detrimental effects on the results: picking single phage clones and testing them for their binding characteristics via ELISA revealed that some of them indeed did not display enhanced specificity for the target, but bound as well to BSA. On the other hand, six of the 15 tested phage clones exhibited significant specificity for NMO-IgG Pt1, indicating that the biopanning process has been successful in elucidating peptides (as displayed by the phages) that bind specifically to NMO-IgG Pt1. Moreover, the five randomly picked phage clones serving as control confirm the success of the biopanning because none of them was specific for NMO-IgG Pt1 demonstrating that target specificity may not arise without previous contact to the target.

Sequencing data of the 15 phage clones were obtained and revealed the amino acid sequences of the peptides that were displayed by the phages. These so-called mimotopes were further characterized using mimotope-based prediction software tools, namely EpiSearch and *PepSurf*. These tools are able to predict epitopes on the crystal structure of human AQP4 based on the mimotopic amino acid sequence. However, these results have to be treated with caution since both software tools are only capable of mapping the peptides on monomers of AQP4. This restricts the ability of simulating realistic epitopes because it has been shown that NMO-IgG probably rather recognizes inter-tetrameric epitopes as found in OAPs (Nicchia et al., 2009). It can thus be concluded that both mapping programs

do not constitute optimal tools for the epitope prediction in this study. Moreover, EpiSearch and *PepSurf* revealed contradicting results for several mimotopes, where one predicted an intracellular and one an extracellular epitope, respectively. It is possible that the NMO-IgG preparation also contains antibodies against linear or non-extracellular AQP4 epitopes (Kampylafka et al., 2011), however, pathogenic NMO-IgG are supposed to target the extracellular portions of AQP4. Hence, this study focusses on the extracellular mapping results. However, there were some cases where both tools indicated corresponding epitope residues increasing the credibility of these epitope predictions.

The six candidates exhibiting target specificity in the ELISA experiments (Pt1-04, Pt1-05, Pt1-08, Pt1-11, Pt1-13 and Pt1-18) as well as two mimotopes that were mapped on the extracellular loops of AQP4 by both EpiSearch and *PepSurf* (Pt1-07, Pt1-19) were examined in terms of their ability to block the binding of NMO-IgG to AQP4 in a FACS-based analysis. Measurements confirmed four of them (Pt1-04, Pt1-11, Pt1-13 and Pt1-18) to be capable of reducing the binding of the antibody to its target. Pt1-04 and Pt1-18 were able to decrease binding of NMO-IgG by 22.9 % and 24.4 %, respectively, constituting the greatest effect among all tested mimotopes. Both of them were among the most specific in binding to NMO-IgG in the ELISA experiments indicating that they indeed mimic a part of the NMO-IgG epitope. Pt1-11 and Pt1-13 were able to decrease binding of NMO-IgG to AQP4 by 13 % and 12 %, respectively, depicting a smaller success in blocking antibody-binding as compared to Pt1-04 and Pt1-18. These findings of Pt1-11 and Pt1-13 being – less but still - specific for NMO-IgG Pt1 is also mirrored in the ELISA results. This correlation between the blocking ability of the peptides and the target specificity of the phages displaying these peptides is not self-evident: since NMO-IgG binds to a conformational epitope, the requirement for epitope mimics is not their linear sequence but their structural features, and these may differ when being part of the phage and when being presented as 12-mer peptide, respectively. Furthermore, there is evidence that the polyclonal NMO-IgG Pt1 comprises different subpopulations of NMO-IgG harboring different paratopes and hence binding different epitopes (Bennett et al., 2009). Thus, one peptide may not be capable to prevent all subpopulations of NMO-IgG from binding to their target and hence a reduction in NMO-IgG Pt1-binding by more than 20 % already constitutes a remarkable potential.

In the blocking experiments, AQP4-transfected HEK293A cells were trypsinized prior to staining with NMO-IgG Pt1. It should be considered that trypsin may induce cleavage sites to extracellularly exposed parts of AQP4. The ExPASy peptide cutter (available online at http://web.expasy.org/peptide_cutter/), an enzymatic cleavage site prediction tool, was used to identify eventual disruptions by trypsin. The online program revealed two extracellularly located possible cleavage sites, one at residue 64 in the A loop with a cleavage probability of 26.4 % and one in the E loop at residue 216 which is cleaved with a probability of 100 %. Residue 216 belongs to an α-helical part of loop E which is extended into the plasma membrane. Hence, the membrane probably shields this site from being cleaved by trypsin. However, one should bear in mind that trypsin may induce changes to the cell surface and the extracellular parts of AQP4 which might alter the properties and interfere with the binding characteristics of NMO-IgG Pt1 and its antigen and thus, the blocking ability of the mimotopes might be underrepresented. These induced disruptions might be prevented by using a suspension-adapted HEK293A cell line sparing the need to be detached from surfaces via trypsin.

Recently, Owens and colleagues used mutagenesis of AQP4 to identify residues within the extracellular domains of AQP4 which are crucial for binding of NMO-IgG. They examined the epitope specificities of patient-derived recombinant monoclonal antibodies regarding their epitope specificities by applying them to AQP4 with induced serial and point mutations in the extracellular loops (Owens et al., 2015). The study revealed that all antibodies required the conserved amino acid V150 on loop C as well as H230 and W231 on loop E for binding. Furthermore, two broad patterns of NMO-IgG epitope recognition depending on their sensitivity to loop A were identified. The binding of a subtype of NMO-IgG insensitive to mutagenesis in loop A was strongly influenced by the presence of loop C residues M149, H151 and L154 as well as N226 and N228 on the E loop. Loop A dependent NMO-IgG needed the presence of E63, K64, P65 as well as C loop V141, H151 and L154. Figure 4.1 gives an overview of the critical residues.
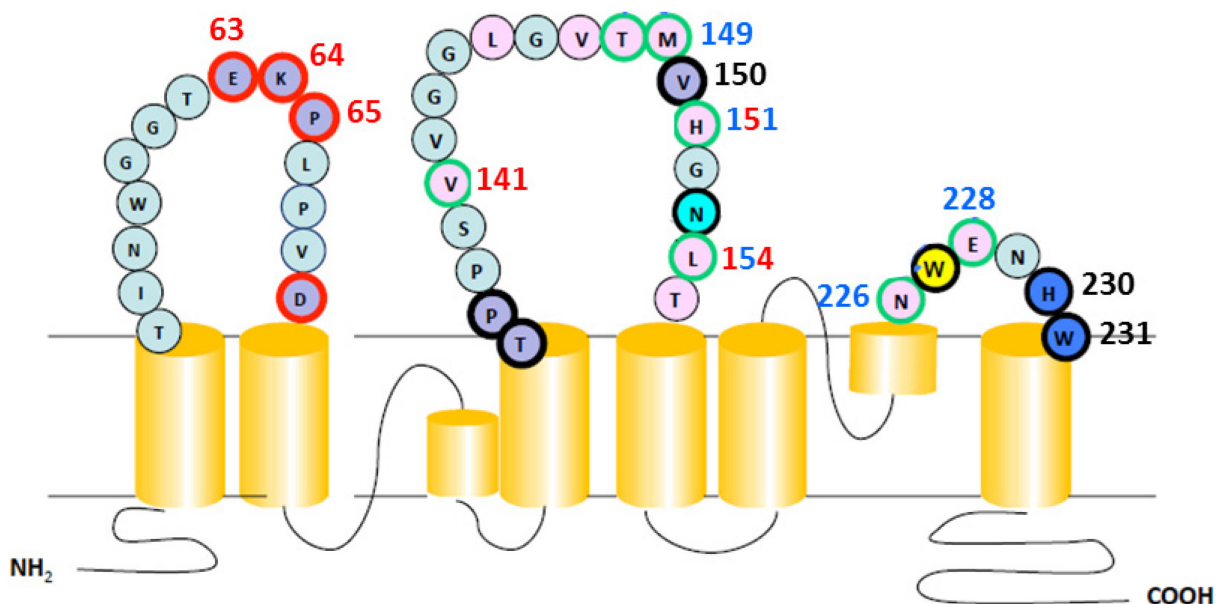
Figure 4.1: Critical residues and binding pattern of different NMO-IgG clones on AQP4

Black numbers indicate residues necessary for binding of all NMO-IgG, red numbers point out residues that are required by the loop A-dependent subtype, blue numbers account for residues which are necessary for the loop A-insensitive subtype and numbers in red and blue indicate that these residues need to be present for both subtypes. Figure adapted and modified from Owens et al., 2015

The four promising mimotopes (Pt1-04, Pt1-11, Pt1-13, Pt1-18) were all mapped on the extracellular loops of AQP4 by at least one mapping tool and the predicted residues coincide at least partially with the critical residues identified by Owens and colleagues. Pt1-04 was located to the extracellular C loop by *PepSurf* predicting it to comprise the residue V141, indicating the loop A dependent subtype. Pt1-11 was mapped on the extracellular loops A and C containing the residues P65 and V141 when employing EpiSearch. For mimotope Pt1-13, both mapping tools agreed on an extracellular location: EpiSearch indicates loop C with residues 151 and 154, whereby one cannot distinguish between the loop A dependent and loop A independent subgroup. *PepSurf* locates Pt1-13 to loops C and E whereby residues that coincide with the critical residues defined by Owens and colleagues are M149, V150, H151, N226, E228 and H230. This suggests that mimotope Pt1-13 belongs to the loop A insensitive subtype. According to *PepSurf*, Pt1-18 locates to loops C and E comprising the residue H230 which does not indicate whether Pt1-18 mimics an epitope for loop A dependent or independent antibodies.

These findings corroborate the suitability of the four peptides Pt1-04, Pt1-11, Pt1-13 and Pt1-18 to mimic epitopes for NMO-IgG Pt1.

Furthermore, this study provides evidence that NMO-IgG Pt1 preferentially binds to AQP4 when organized in OAPs as compared to tetrameric AQP4 as indicated by the FACS measurements of NMO-IgG Pt1 binding to HEK293A cells transfected with the two different AQP4 isoforms M1 and M23. As confirmed via BN-PAGE, M23 forms large OAPs of different sizes, whereas the M1 isoform mostly assembles as tetramers and only a small portion as OAPs. The FACS-based analysis revealed that NMO-IgG Pt1 binds with much higher affinity to AQP4-M23; the binding of NMO-IgG Pt1 to AQP4 is reduced by 75.3 % to 24.7 % when the M1 construct was employed. These findings are in line with several previous studies (Nicchia et al., 2009; Pisani et al., 2011) and contribute to the elucidation of the epitope(s) of NMO-IgG. However, to finally determine whether NMO-IgG Pt1 also binds to intra-tetrameric epitopes, an AQP4-M1 construct that prevents translation of the M23 form would be useful. Since the M1-construct, which was used for this study, also allows translation of the OAP-forming M23 isoform via the leaky scanning mechanism (Rossi et al., 2010), one cannot determine whether the NMO-IgG Pt1 portion that is binding to AQP4-M1-transfected HEK293A cells targets tetramers or OAPs. To avoid translation of M23 from the M1 construct, the Met-23 could be substituted by isoleucine via mutagenesis. Upon elimination of the start codon in position 23, translation could solely start at Met-1 and thus, no other isoform could be expressed (Rossi et al., 2010).

The major obstacle of the experimental work was the polyclonal nature of NMO-IgG Pt1 since phage display is known to be a suitable technique for obtaining mimotopes from monoclonal but not from polyclonal antibody pools (Willats et al, 2002). However, this study provides evidence that the phage display technique may also be applicable for the identification of mimotopes when engaging polyclonal antibodies – probably due to the fact that the antigen surface is relatively small, i.e. there are limited alternative locations for epitopes. Another reason that acts in favor is the high titer of NMO-IgG in the used plasmapheresis product allowing to neglect the presence of smaller IgG pools and thus minimizing the probability to identify mimotopes for IgG that are not targeting AQP4. Moreover, this polyclonal origin of NMO-IgG does not allow for the identification of one distinct epitope as indicated by several mimotopes but may give rise to several mimotope subpopulations that mimic different epitopes. This study revealed peptides that mimic two different epitopes when employing the classification of Owens and coworkers (Owens et al.,

2015). Pt1-04 and Pt1-11 are likely to mimic an epitope for loop A dependent NMO IgG, whereas Pt1-13 may represent an epitope for loop A independent antibodies.

5. Conclusion

Taken together, the present study provides evidence that the phage display technique may also be suitable for the identification of mimotopes when engaging polyclonal antibodies. Using this method, we successfully identified four mimotopes for NMO-IgG Pt1 with blocking potential. However, further investigation is needed to completely validate these mimotopes and to better characterize the epitopes they mimic. In further peptide blocking experiments, the peptide concentration should be varied to elucidate eventual effects of the antibody-peptide ratio on the blocking potential of the mimotopes. An improvement of the experimental setup might be achieved upon avoiding the application of trypsin by using suspension-adapted HEK cells. It would be particularly intriguing whether these adaptations still reproduce the same results or whether they would highlight the peptides' mimicking potential even more. Additionally, the use of monoclonal NMO-IgG in a blocking experiment with the four promising candidates might help to further evaluate their epitope mimicking potential.

With the identification of the four mimotopes Pt1-04, Pt1-11, Pt1-13 and Pt1-18 we made a step towards achieving our goal to characterize the epitopes of NMO-IgG. After complete validation, the mimotopes might be used to generate valid animal models for NMO via active immunization and to evaluate the effect of different antibody subpopulations. Moreover, these mimotopes, together with further identified mimotopes, might in the long term help to classify NMO IgG pools of NMO patients upon identifying different subpopulations of antibodies. This classification of patients according to their antibody composition might be used to predict eventual differences in the disease course or severity and thus help to select suitable therapies.

Huge efforts are made by scientists to capture the broad variety of aspects contributing to the etiology and pathogenesis of NMO, whereby a lot remains to be elucidated. This study forms part of these efforts and contributes with the identification of four mimotopes that form a solid basis for further investigation.

6. Acknowledgements

7. List of figures

8. List of tables

9. References

Abboud, H., Petrak, A., Mealy, M., Sasidharan, S., Siddique, L., and Levy, M. (2015). Treatment of acute relapses in neuromyelitis optica: Steroids alone versus steroids plus plasma exchange. Multiple sclerosis (Houndmills, Basingstoke, England).

Arabshahi, B., Pollock, A.N., Sherry, D.D., Albert, D.A., Kreiger, P.A., and Pessler, F. (2006). Devic disease in a child with primary Sjogren syndrome. Journal of child neurology *21*, 285-286.

Barbieri, F., and Buscaino, G.A. (1989). Neuromyelitis optica in the elderly. Acta neurologica *11*, 247-251.

Barnes, P.J. (2006). Corticosteroids: the drugs to beat. European journal of pharmacology *533*, 2-14.

Bennett, J.L., Lam, C., Kalluri, S.R., Saikali, P., Bautista, K., Dupree, C., Glogowska, M., Case, D., Antel, J.P., Owens, G.P.*, et al.* (2009). Intrathecal Pathogenic Anti-Aquaporin-4 Antibodies in Early Neuromyelitis Optica. Annals of neurology *66*, 617-629.

Bichuetti, D.B., Oliveira, E.M.L.d., Souza, N.A.d., Tintoré, M., and Gabbai, A.A. (2013). Patients with neuromyelitis optica have a more severe disease than patients with relapsingremitting multiple sclerosis, including higher risk of dying of a demyelinating disease. Arquivos de Neuro-Psiquiatria *71*, 275-279.

Bonnan, M., Valentino, R., Olindo, S., Mehdaoui, H., Smadja, D., and Cabre, P. (2009). Plasma exchange in severe spinal attacks associated with neuromyelitis optica spectrum disorder. Multiple sclerosis (Houndmills, Basingstoke, England) *15*, 487-492.

Bradl, M., Misu, T., Takahashi, T., Watanabe, M., Mader, S., Reindl, M., Adzemovic, M., Bauer, J., Berger, T., Fujihara, K.*, et al.* (2009). Neuromyelitis optica: pathogenicity of patient immunoglobulin in vivo. Ann Neurol *66*, 630-643.

Braley, T., and Mikol, D.D. (2007). Neuromyelitis optica in a mother and daughter. Archives of neurology *64*, 1189-1192.

Brunner, C., Lassmann, H., Waehneldt, T.V., Matthieu, J.M., and Linington, C. (1989). Differential ultrastructural localization of myelin basic protein, myelin/oligodendroglial glycoprotein, and 2',3'-cyclic nucleotide 3'-phosphodiesterase in the CNS of adult rats. Journal of neurochemistry *52*, 296-304.

Ceppellini, R., Polli, E., and Celada, F. (1957). A DNA-reacting factor in serum of a patient with lupus erythematosus diffusus. Proceedings of the Society for Experimental Biology and Medicine Society for Experimental Biology and Medicine (New York, NY) *96*, 572-574.

Collongues, N., Brassat, D., Maillart, E., Labauge, P., Ouallet, J.C., Carra-Dalliere, C., Moreau, T., Bourre, B., Papeix, C., Brochet, B.*, et al.* (2015). Efficacy of rituximab in refractory neuromyelitis optica. Multiple sclerosis (Houndmills, Basingstoke, England).

Crane, J.M., Bennett, J.L., and Verkman, A.S. (2009). Live cell analysis of aquaporin-4 m1/m23 interactions and regulated orthogonal array assembly in glial cells. The Journal of biological chemistry *284*, 35850-35860.

Crane, J.M., Lam, C., Rossi, A., Gupta, T., Bennett, J.L., and Verkman, A.S. (2011). Binding affinity and specificity of neuromyelitis optica autoantibodies to aquaporin-4 M1/M23 isoforms and orthogonal arrays. The Journal of biological chemistry *286*, 16516-16524.

Crane, J.M., and Verkman, A.S. (2009a). Determinants of aquaporin-4 assembly in orthogonal arrays revealed by live-cell single-molecule fluorescence imaging. J Cell Sci *122*, 813-821.

Crane, J.M., and Verkman, A.S. (2009b). Determinants of aquaporin-4 assembly in orthogonal arrays revealed by live-cell single-molecule fluorescence imaging. Journal of Cell Science *122*, 813-821.

de Seze, J., Lebrun, C., Stojkovic, T., Ferriby, D., Chatel, M., and Vermersch, P. (2003). Is Devic's neuromyelitis optica a separate disease? A comparative study with multiple sclerosis. Multiple sclerosis (Houndmills, Basingstoke, England) *9*, 521-525.

Devic, E. (1894). Myelite subaiguë compliquée de névrite optique. Le Bulletin Médicale, 8, 1033–34 *8*, 1033–1034.

Fujiyoshi, Y., Mitsuoka, K., de Groot, B.L., Philippsen, A., Grubmuller, H., Agre, P., and Engel, A. (2002). Structure and function of water channels. Current opinion in structural biology *12*, 509-515.

Furman, C.S., Gorelick-Feldman, D.A., Davidson, K.G., Yasumura, T., Neely, J.D., Agre, P., and Rash, J.E. (2003). Aquaporin-4 square array assembly: opposing actions of M1 and M23 isoforms. Proceedings of the National Academy of Sciences of the United States of America *100*, 13609-13614.

Gault, F. (1894). De la neuromyélite optique aiguë. . Thése: Faculté de Médecine et de Pharmacie.

Geysen, H.M., Rodda, S.J., and Mason, T.J. (1986). A priori delineation of a peptide which mimics a discontinuous antigenic determinant. Molecular immunology *23*, 709-715.

Ghezzi, A., Bergamaschi, R., Martinelli, V., Trojano, M., Tola, M.R., Merelli, E., Mancardi, L., Gallo, P., Filippi, M., Zaffaroni, M.*, et al.* (2004). Clinical characteristics, course and prognosis of relapsing Devic's Neuromyelitis Optica. Journal of neurology *251*, 47-52.

Hardy, B., and Raiter, A. (2005). A mimotope peptide-based anti-cancer vaccine selected by BAT monoclonal antibody. Vaccine *23*, 4283-4291.

Hinson, S.R., Pittock, S.J., Lucchinetti, C.F., Roemer, S.F., Fryer, J.P., Kryzer, T.J., and Lennon, V.A. (2007). Pathogenic potential of IgG binding to water channel extracellular domain in neuromyelitis optica. Neurology *69*, 2221-2231.

Hinson, S.R., Romero, M.F., Popescu, B.F., Lucchinetti, C.F., Fryer, J.P., Wolburg, H., Fallier-Becker, P., Noell, S., and Lennon, V.A. (2012). Molecular outcomes of neuromyelitis optica (NMO)-IgG binding to aquaporin-4 in astrocytes. Proceedings of the National Academy of Sciences of the United States of America *109*, 1245-1250.

Huang, J., Gutteridge, A., Honda, W., and Kanehisa, M. (2006). MIMOX: a web tool for phage display based epitope mapping. BMC Bioinformatics *7*, 451.

Huang, J., Ru, B., Li, S., Lin, H., and Guo, F.-B. (2010). SAROTUP: scanner and reporter of target-unrelated peptides. BioMed Research International *2010*.

Humphrey, W., Dalke, A., and Schulten, K. (1996). VMD: visual molecular dynamics. Journal of molecular graphics *14*, 33-38, 27-38.

Ishibashi, K., Sasaki, S., Fushimi, K., Uchida, S., Kuwahara, M., Saito, H., Furukawa, T., Nakajima, K., Yamaguchi, Y., and Gojobori, T. (1994). Molecular cloning and expression of a member of the aquaporin family with permeability to glycerol and urea in addition to water expressed at the basolateral membrane of kidney collecting duct cells. Proceedings of the National Academy of Sciences *91*, 6269-6273.

Kampylafka, E.I., Routsias, J.G., Alexopoulos, H., Dalakas, M.C., Moutsopoulos, H.M., and Tzioufas, A.G. (2011). Fine specificity of antibodies against AQP4: epitope mapping reveals intracellular epitopes. Journal of autoimmunity *36*, 221-227.

Kantarci, O.H., and Weinshenker, B.G. (2005). Natural history of multiple sclerosis. Neurologic clinics *23*, 17-38, v.

Ketelslegers, I.A., Modderman, P.W., Vennegoor, A., Killestein, J., Hamann, D., and Hintzen, R.Q. (2011). Antibodies against aquaporin-4 in neuromyelitis optica: distinction between recurrent and monophasic patients. Multiple Sclerosis Journal *17*, 1527-1530.

Khalili-Araghi, F., Gumbart, J., Wen, P.C., Sotomayor, M., Tajkhorshid, E., and Schulten, K. (2009). Molecular dynamics simulations of membrane channels and transporters. Current opinion in structural biology *19*, 128-137.

Kitchen, P., Day, R.E., Salman, M.M., Conner, M.T., Bill, R.M., and Conner, A.C. (2015). Beyond water homeostasis: Diverse functional roles of mammalian aquaporins. Biochimica et Biophysica Acta (BBA) - General Subjects.

Knittelfelder, R., Riemer, A.B., and Jensen-Jarolim, E. (2009). Mimotope vaccination--from allergy to cancer. Expert opinion on biological therapy *9*, 493-506.

Kozak, M. (1987). An analysis of 5'-noncoding sequences from 699 vertebrate messenger RNAs. Nucleic acids research *15*, 8125-8148.

Kozak, M. (1999). Initiation of translation in prokaryotes and eukaryotes. Gene *234*, 187-208.

Leite, M.I., Coutinho, E., Lana-Peixoto, M., Apostolos, S., Waters, P., Sato, D., Melamud, L., Marta, M., Graham, A., Spillane, J.*, et al.* (2012). Myasthenia gravis and neuromyelitis optica spectrum disorder: a multicenter study of 16 patients. Neurology *78*, 1601-1607.

Lennon, V.A., Kryzer, T.J., Pittock, S.J., Verkman, A.S., and Hinson, S.R. (2005). IgG marker of optic-spinal multiple sclerosis binds to the aquaporin-4 water channel. The Journal of Experimental Medicine *202*, 473-477.

Lennon, V.A., Wingerchuk, D.M., Kryzer, T.J., Pittock, S.J., Lucchinetti, C.F., Fujihara, K., Nakashima, I., and Weinshenker, B.G. (2004). A serum autoantibody marker of neuromyelitis optica: distinction from multiple sclerosis. The Lancet *364*, 2106-2112.

Li, M., Yan, Z., Han, W., and Zhang, Y. (2006). Mimotope vaccination for epitope-specific induction of anti-CD20 antibodies. Cellular Immunology *239*, 136-143.

Lu, M., Lee, M.D., Smith, B.L., Jung, J.S., Agre, P., Verdijk, M.A., Merkx, G., Rijss, J.P., and Deen, P.M. (1996). The human AQP4 gene: definition of the locus encoding two water channel polypeptides in brain. Proceedings of the National Academy of Sciences of the United States of America *93*, 10908-10912.

Lucchinetti, C.F., Guo, Y., Popescu, B.F.G., Fujihara, K., Itoyama, Y., and Misu, T. (2014). The Pathology of an Autoimmune Astrocytopathy: Lessons Learned from Neuromyelitis Optica. Brain pathology (Zurich, Switzerland) *24*, 83-97.

Lucchinetti, C.F., Mandler, R.N., McGavern, D., Bruck, W., Gleich, G., Ransohoff, R.M., Trebst, C., Weinshenker, B., Wingerchuk, D., Parisi, J.E*., et al.* (2002). A role for humoral mechanisms in the pathogenesis of Devic's neuromyelitis optica, Vol 125.

Mader, S., Gredler, V., Schanda, K., Rostassy, K., Dujmovic, I., Pfaller, K., Lutterotti, A., Jarius, S., Di Pauli, F., Kuenz, B*., et al.* (2011). Complement activating antibodies to myelin oligodendrocyte glycoprotein in neuromyelitis optica and related disorders. Journal of Neuroinflammation *8*.

Manley, G.T., Fujimura, M., Ma, T., Noshita, N., Filiz, F., Bollen, A.W., Chan, P., and Verkman, A.S. (2000). Aquaporin-4 deletion in mice reduces brain edema after acute water intoxication and ischemic stroke. Nat Med *6*, 159-163.

Matiello, M., Kim, H.J., Kim, W., Brum, D.G., Barreira, A.A., Kingsbury, D.J., Plant, G.T., Adoni, T., and Weinshenker, B.G. (2010). Familial neuromyelitis optica. Neurology *75*, 310-315.

Matiello, M., Lennon, V.A., Jacob, A., Pittock, S.J., Lucchinetti, C.F., Wingerchuk, D.M., and Weinshenker, B.G. (2008). NMO-IgG predicts the outcome of recurrent optic neuritis. Neurology *70*, 2197-2200.

Mayrose, I., Shlomi, T., Rubinstein, N.D., Gershoni, J.M., Ruppin, E., Sharan, R., and Pupko, T. (2007). Epitope mapping using combinatorial phage-display libraries: a graph-based algorithm. Nucleic acids research *35*, 69-78.

McKeon, A., and Pittock, S.J. (2009). Neuromyelitis optica and the evolving spectrum of water channel autoimmunity: a new direction. European journal of neurology : the official journal of the European Federation of Neurological Societies *16*, 433-435.

Misu, T., Fujihara, K., Nakashima, I., Sato, S., and Itoyama, Y. (2005). Intractable hiccup and nausea with periaqueductal lesions in neuromyelitis optica. Neurology *65*, 1479-1482.

Miyamoto, K., and Kusunoki, S. (2009). Intermittent plasmapheresis prevents recurrence in neuromyelitis optica. Therapeutic apheresis and dialysis : official peer-reviewed journal of the International Society for Apheresis, the Japanese Society for Apheresis, the Japanese Society for Dialysis Therapy *13*, 505-508.

Moreau, V., Granier, C., Villard, S., Laune, D., and Molina, F. (2006). Discontinuous epitope prediction based on mimotope analysis. Bioinformatics *22*, 1088-1095.

Musa-Aziz, R., Chen, L.M., Pelletier, M.F., and Boron, W.F. (2009). Relative CO_2/NH_3 selectivities of AQP1, AQP4, AQP5, AmtB, and RhAG. Proceedings of the National Academy of Sciences of the United States of America *106*, 5406-5411.

Neely, J.D., Christensen, B.M., Nielsen, S., and Agre, P. (1999). Heterotetrameric composition of aquaporin-4 water channels. Biochemistry *38*, 11156-11163.

Negi, S.S., and Braun, W. (2009). Automated Detection of Conformational Epitopes Using Phage Display Peptide Sequences. Bioinformatics and Biology Insights *3*, 71-81.

Nicchia, G.P., Mastrototaro, M., Rossi, A., Pisani, F., Tortorella, C., Ruggieri, M., Lia, A., Trojano, M., Frigeri, A., and Svelto, M. (2009). Aquaporin-4 orthogonal arrays of particles are the target for neuromyelitis optica autoantibodies. Glia *57*, 1363-1373.

Nicchia, G.P., Rossi, A., Mola, M.G., Pisani, F., Stigliano, C., Basco, D., Mastrototaro, M., Svelto, M., and Frigeri, A. (2010). Higher order structure of aquaporin-4. Neuroscience *168*, 903-914.

Nielsen, S., Nagelhus, E.A., Amiry-Moghaddam, M., Bourque, C., Agre, P., and Ottersen, O.P. (1997). Specialized membrane domains for water transport in glial cells: high-resolution immunogold cytochemistry of aquaporin-4 in rat brain. The Journal of neuroscience : the official journal of the Society for Neuroscience *17*, 171-180.

Nishiyama, S., Ito, T., Misu, T., Takahashi, T., Kikuchi, A., Suzuki, N., Jin, K., Aoki, M., Fujihara, K., and Itoyama, Y. (2009). A case of NMO seropositive for aquaporin-4 antibody more than 10 years before onset. Neurology *72*, 1960-1961.

Owens, G.P., Ritchie, A., Rossi, A., Schaller, K., Wemlinger, S., Schumann, H., Shearer, A., Verkman, A.S., and Bennett, J.L. (2015). Mutagenesis of the Aquaporin 4 Extracellular Domains Defines Restricted Binding Patterns of Pathogenic Neuromyelitis Optica IgG. Journal of Biological Chemistry.

Papadopoulos, M.C., Bennett, J.L., and Verkman, A.S. (2014). Treatment of neuromyelitis optica: state-of-the-art and emerging therapies. Nature reviews Neurology *10*, 493-506.

Papais-Alvarenga, R.M., Carellos, S.C., Alvarenga, M.P., Holander, C., Bichara, R.P., and Thuler, L.C. (2008). Clinical course of optic neuritis in patients with relapsing neuromyelitis optica. Archives of ophthalmology (Chicago, Ill : 1960) *126*, 12-16.

Phuan, P.W., Ratelade, J., Rossi, A., Tradtrantip, L., and Verkman, A.S. (2012). Complement-dependent cytotoxicity in neuromyelitis optica requires aquaporin-4 protein assembly in orthogonal arrays. The Journal of biological chemistry *287*, 13829-13839.

Pisani, F., Mastrototaro, M., Rossi, A., Nicchia, G.P., Tortorella, C., Ruggieri, M., Trojano, M., Frigeri, A., and Svelto, M. (2011). Identification of two major conformational aquaporin-4 epitopes for neuromyelitis optica autoantibody binding. The Journal of biological chemistry *286*, 9216-9224.

Pisani, F., Mola, M.G., Simone, L., Rosito, S., Alberga, D., Mangiatordi, G.F., Lattanzi, G., Nicolotti, O., Frigeri, A., Svelto, M.*, et al.* (2014). Identification of a Point Mutation Impairing the Binding between Aquaporin-4 and Neuromyelitis Optica Autoantibodies. Journal of Biological Chemistry *289*, 30578-30589.

Pittock, S.J., Lennon, V.A., McKeon, A., Mandrekar, J., Weinshenker, B.G., Lucchinetti, C.F., O'Toole, O., and Wingerchuk, D.M. (2013). Eculizumab in AQP4-IgG-positive relapsing neuromyelitis optica spectrum disorders: an open-label pilot study. The Lancet Neurology *12*, 554-562.

Pittock, S.J., Weinshenker, B.G., Lucchinetti, C.F., Wingerchuk, D.M., Corboy, J.R., and Lennon, V.A. (2006). Neuromyelitis optica brain lesions localized at sites of high aquaporin 4 expression. Archives of neurology *63*, 964-968.

Radaelli, M., Moiola, L., Sangalli, F., Esposito, F., Barcella, V., Ferre, L., Rodegher, M., Colombo, B., Fazio, R., Martinelli, V.*, et al.* (2015). Neuromyelitis optica spectrum disorders:

long-term safety and efficacy of rituximab in Caucasian patients. Multiple sclerosis (Houndmills, Basingstoke, England).

Ramanathan, S., Reddel, S.W., Henderson, A., Parratt, J.D.E., Barnett, M., Gatt, P.N., Merheb, V., Kumaran, R.-Y.A., Pathmanandavel, K., Sinmaz, N*., et al.* (2014). Antibodies to myelin oligodendrocyte glycoprotein in bilateral and recurrent optic neuritis. Neurology - Neuroimmunology Neuroinflammation *1*.

Rash, J.E., Yasumura, T., Hudson, C.S., Agre, P., and Nielsen, S. (1998). Direct immunogold labeling of aquaporin-4 in square arrays of astrocyte and ependymocyte plasma membranes in rat brain and spinal cord. Proceedings of the National Academy of Sciences of the United States of America *95*, 11981-11986.

Rodi, D.J., and Makowski, L. (1999). Phage-display technology – finding a needle in a vast molecular haystack. Current Opinion in Biotechnology *10*, 87-93.

Rossi, A., Pisani, F., Nicchia, G.P., Svelto, M., and Frigeri, A. (2010). Evidences for a Leaky Scanning Mechanism for the Synthesis of the Shorter M23 Protein Isoform of Aquaporin-4: IMPLICATION IN ORTHOGONAL ARRAY FORMATION AND NEUROMYELITIS OPTICA ANTIBODY INTERACTION. Journal of Biological Chemistry *285*, 4562-4569.

Rossi, A., Ratelade, J., Papadopoulos, M.C., Bennett, J.L., and Verkman, A.S. (2012). Neuromyelitis optica IgG does not alter aquaporin-4 water permeability, plasma membrane M1/M23 isoform content, or supramolecular assembly. Glia *60*, 2027-2039.

Schneider, C.A., Rasband, W.S., and Eliceiri, K.W. (2012). NIH Image to ImageJ: 25 years of image analysis. Nat Meth *9*, 671-675.

Smith, G.P. (1985). Filamentous fusion phage: novel expression vectors that display cloned antigens on the virion surface. Science (New York, NY) *228*, 1315-1317.

Smith, G.P., and Petrenko, V.A. (1997). Phage Display. Chemical reviews *97*, 391-410.

Takahashi, T., Fujihara, K., Nakashima, I., Misu, T., Miyazawa, I., Nakamura, M., Watanabe, S., Shiga, Y., Kanaoka, C., Fujimori, J*., et al.* (2007). Anti-aquaporin-4 antibody is involved in the pathogenesis of NMO: a study on antibody titre. Brain *130*, 1235-1243.

Umenishi, F., and Verkman, A.S. (1998). Isolation and functional analysis of alternative promoters in the human aquaporin-4 water channel gene. Genomics *50*, 373-377.

Verkman, A.S. (2008). Dissecting the roles of aquaporins in renal pathophysiology using transgenic mice. Seminars in nephrology *28*, 217-226.

Verkman, A.S. (2012). Aquaporins in clinical medicine. Annual review of medicine *63*, 303-316.

Verkman, A.S., Anderson, M.O., and Papadopoulos, M.C. (2014). Aquaporins: important but elusive drug targets. Nature reviews Drug discovery *13*, 259-277.

Verkman, A.S., Phuan, P.W., Asavapanumas, N., and Tradtrantip, L. (2013). Biology of AQP4 and anti-AQP4 antibody: therapeutic implications for NMO. Brain Pathol *23*, 684-695.

Walz, T., Fujiyoshi, Y., and Engel, A. (2009). The AQP structure and functional implications. Handbook of experimental pharmacology, 31-56.

Watanabe, S., Nakashima, I., Misu, T., Miyazawa, I., Shiga, Y., Fujihara, K., and Itoyama, Y. (2007). Therapeutic efficacy of plasma exchange in NMO-IgG-positive patients with neuromyelitis optica. Multiple sclerosis (Houndmills, Basingstoke, England) *13*, 128-132.

Waters, P., Jarius, S., Littleton, E., and et al. (2008). AQuaporin-4 antibodies in neuromyelitis optica and longitudinally extensive transverse myelitis. Archives of neurology *65*, 913-919.

Weinshenker, B.G., O'Brien, P.C., Petterson, T.M., Noseworthy, J.H., Lucchinetti, C.F., Dodick, D.W., Pineda, A.A., Stevens, L.N., and Rodriguez, M. (1999). A randomized trial of plasma exchange in acute central nervous system inflammatory demyelinating disease. Annals of Neurology *46*, 878-886.

Weinshenker, B.G., Wingerchuk, D.M., Pittock, S.J., Lucchinetti, C.F., and Lennon, V.A. (2006a). NMO-IgG: A Specific Biomarker for Neuromyelitis Optica. Disease Markers *22*, 197-206.

Weinshenker, B.G., Wingerchuk, D.M., Vukusic, S., Linbo, L., Pittock, S.J., Lucchinetti, C.F., and Lennon, V.A. (2006b). Neuromyelitis optica IgG predicts relapse after longitudinally extensive transverse myelitis. Ann Neurol *59*, 566-569.

Willats, W.T. (2002). Phage display: practicalities and prospects. Plant Mol Biol *50*, 837-854.

Wingerchuk, D.M. (2006). Neuromyelitis optica. International MS journal / MS Forum *13*, 42-50.

Wingerchuk, D.M., Hogancamp, W.F., O'Brien, P.C., and Weinshenker, B.G. (1999). The clinical course of neuromyelitis optica (Devic's syndrome). Neurology *53*, 1107-1114.

Wingerchuk, D.M., Lennon, V.A., Lucchinetti, C.F., Pittock, S.J., and Weinshenker, B.G. (2007). The spectrum of neuromyelitis optica. The Lancet Neurology *6*, 805-815.

Wingerchuk, D.M., Lennon, V.A., Pittock, S.J., Lucchinetti, C.F., and Weinshenker, B.G. (2006). Revised diagnostic criteria for neuromyelitis optica. Neurology *66*, 1485-1489.

Wingerchuk, D.M., and Weinshenker, B.G. (2003). Neuromyelitis optica: clinical predictors of a relapsing course and survival. Neurology *60*, 848-853.

Wittig, I., Braun, H.P., and Schagger, H. (2006). Blue native PAGE. Nature protocols *1*, 418-428.

Zekeridou, A., and Lennon, V.A. (2015). Aquaporin-4 autoimmunity. Neurology(R) neuroimmunology & neuroinflammation *2*, e110.

Zephir, H., Bernard-Valnet, R., Lebrun, C., Outteryck, O., Audoin, B., Bourre, B., Pittion, S., Wiertlewski, S., Ouallet, J.C., Neau, J.P.*, et al.* (2015). Rituximab as first-line therapy in neuromyelitis optica: efficiency and tolerability. Journal of neurology.
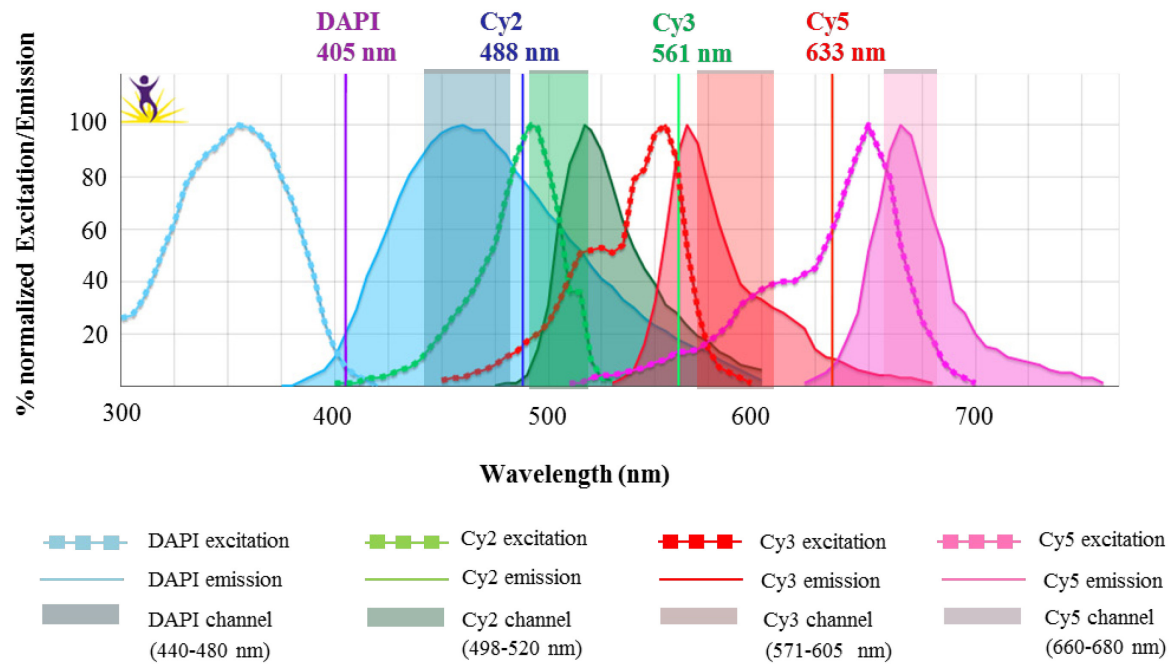
10. Supplement

Figure S 1: Spectral properties of the fluorophores used for the staining of rat astrocytes. Laser excitation wavelengths are given above the graph and the detector bandwidths for each channel are shown as colored columns. The image was generated using Fluorescence Spectra Analyzer (available online at www.biolegend.com/spectraanalyzer).

Table S1: Amino acid sequences of the peptides obtained in the biopanning control experiment with Streptavidin as target. The peptides CTRL-03-05 contain the HPQ-motif.

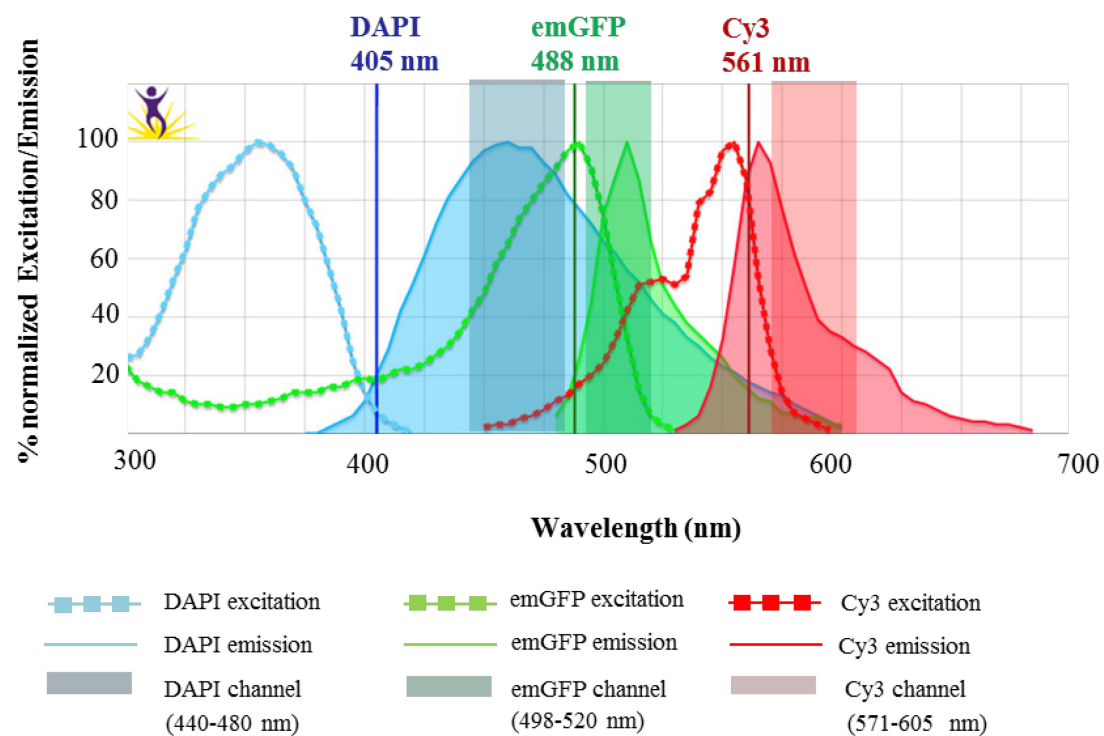| ID	Peptide sequence
CTRL-01	invalid
CTRL-02	HTSSLWHLFRST-GGGS
CTRL-03	GPASWLAM**HPQ**R-GGGS
CTRL-04	LFANWLAPS**HPQ**-GGGS
CTRL-05	LFANWLAPS**HPQ**-GGGS
CTRL-06	invalid
CTRL-07	invalid
CTRL-08	invalid
CTRL-09	invalid
CTRL-10	invalid

Figure S 2: Spectral properties of the fluorophores used for the staining of HEK293A-M1/M23-emGFP cells. Laser excitation wavelengths are given above the graph and the detector bandwidths for each channel are shown as colored columns. The image was generated using Fluorescence Spectra Analyzer (available online at www.biolegend.com/spectraanalyzer).
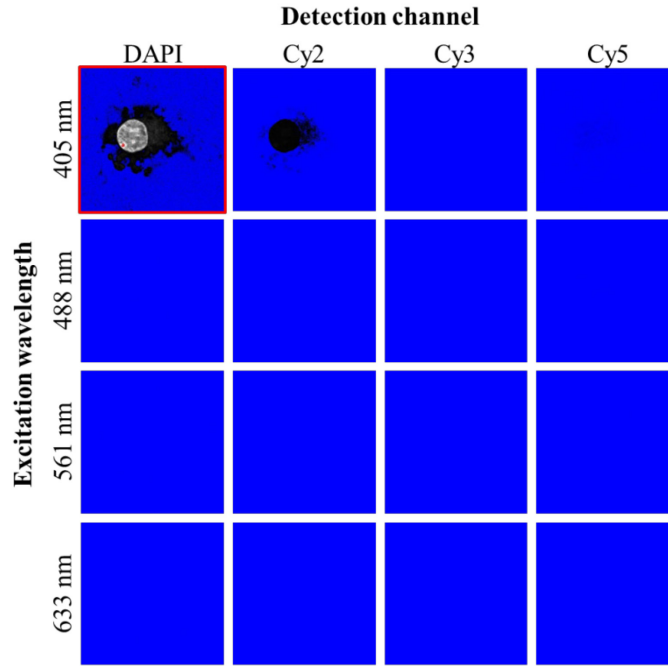
Figure S 3: DAPI single staining control with rat astrocytes. The signal captured with the actual excitation wavelength (405 nm) and the detection channel for DAPI is shown in the panel which is marked by a red rectangle. Excitation at 405 nm produces also a signal in the Cy2 channel and yields autofluorescence which are detected in both the DAPI and the Cy2 channel. Blue areas indicate a pixel value of 0 and red areas indicate pixel values of 255. Dark to light grey indicate increasing saturation from 1 to 245. Gain and offset were kept constant for acquisition of all images.
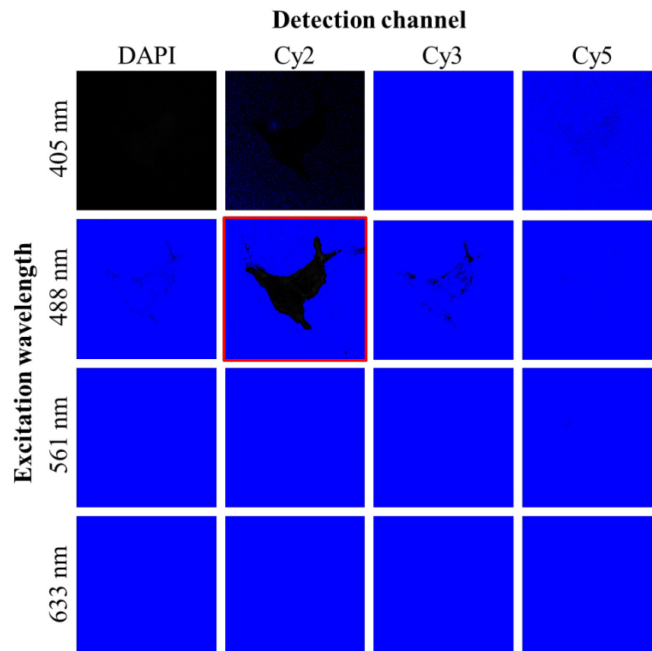

Figure S 4: Cy2 single staining control with rat astrocytes. The signal captured with the actual excitation wavelength (488 nm) and the detection channel for Cy2 is shown in the panel which is marked by a red rectangle. Excitation at 488 nm produces bleed-through into the Cy3 channel. Blue areas indicate a pixel value of 0 and red areas indicate pixel values of 255. Dark to light grey indicate increasing saturation from 1 to 245. Gain and offset were optimized for the Cy2 signal and kept constant for acquisition of all images explaining the background in the first two images.
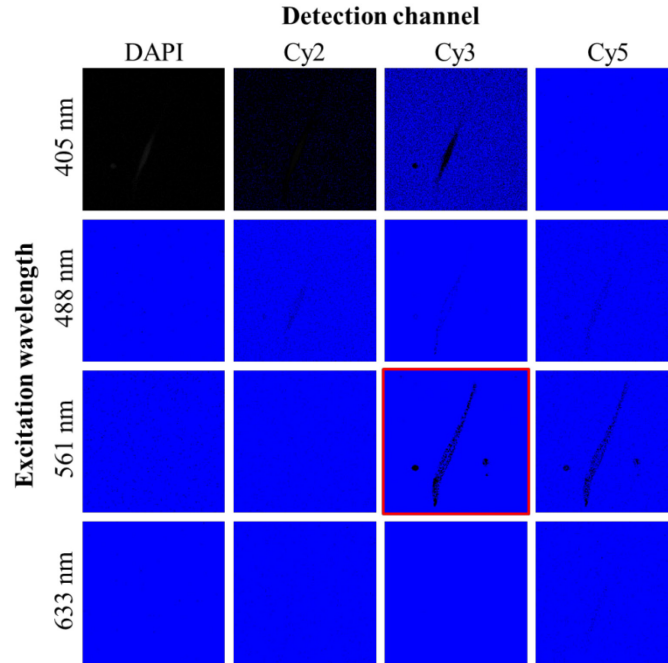
Figure S 5: Cy3 single staining control with rat astrocytes. The signal captured with the actual excitation wavelength (561 nm) and the detection channel for Cy3 is shown in the panel which is marked by a red rectangle. Excitation at 561 nm produces bleed-through into the Cy5 channel. Blue areas indicate a pixel value of 0 and red areas indicate pixel values of 255. Dark to light grey indicate increasing saturation from 1 to 245. Gain and offset were optimized for the Cy3 signal and kept constant for acquisition of all images explaining the background in the first two images.
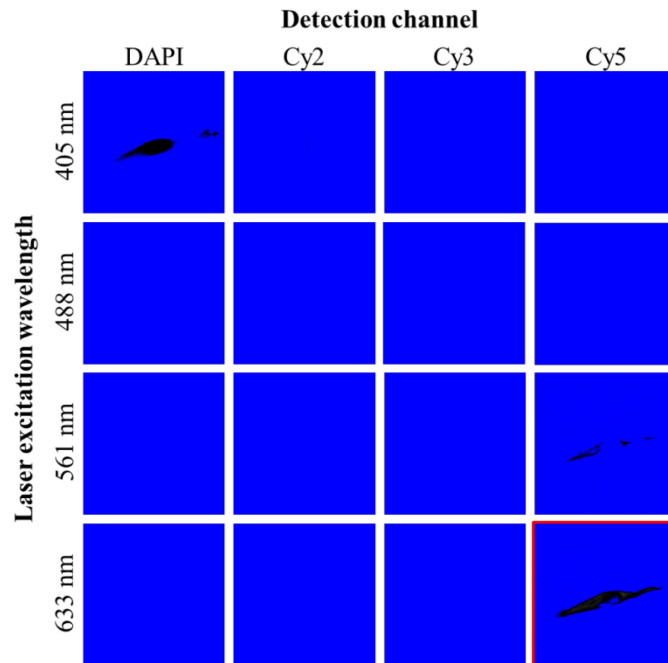

Figure S 6: Cy5 single staining control with rat astrocytes. The signal captured with the actual excitation wavelength (633 nm) and the detection channel for Cy5 is shown in the panel which is marked by a red rectangle. When exciting with 561 nm, Cy5 also produces a signal. Autofluorescence is yielded in the DAPI channel when excited with 405 nm. Blue areas indicate a pixel value of 0 and red areas indicate pixel values of 255. Dark to light grey indicate increasing saturation from 1 to 245. Gain and offset were optimized for the Cy5 signal and kept constant for acquisition of all images.
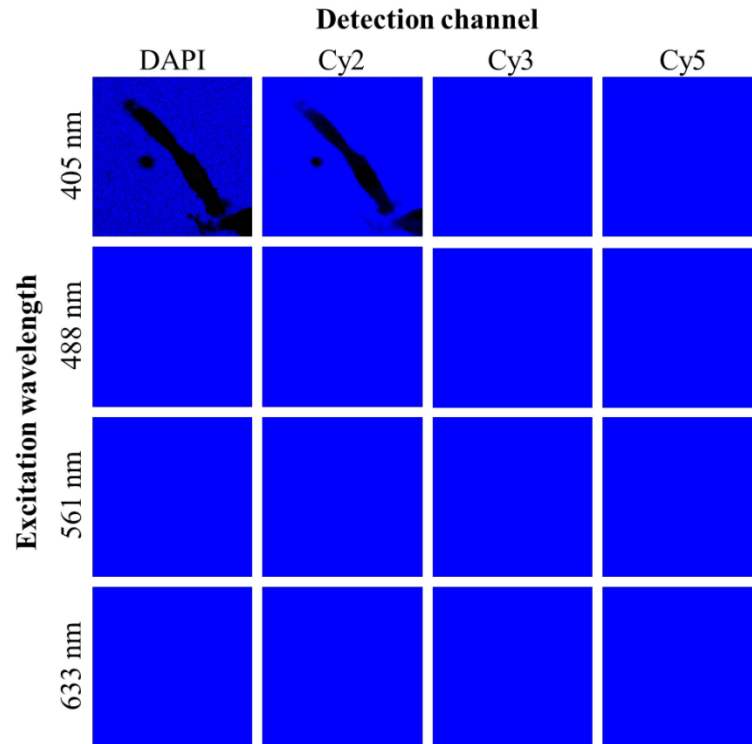
Figure S 7: Unstained control with rat astrocytes. Autofluorescence can be captured with 405 nm in both the DAPI and the Cy2 channel. Blue areas indicate a pixel value of 0 and red areas indicate pixel values of 255. Dark to light grey indicate increasing saturation from 1 to 245. Gain and offset were optimized for the Cy2 signal excited with 405 nm and kept constant for acquisition of all images.

Pt1-01 QMMKASSEYTGF

Pt1-02 GPFHWHQKVTGK

Pt1-03 NSPWAHDVPPTYK

Pt1-04 WRYHVHPTPFKS

Pt1-05 WHRTHILQYGKP

Pt1-07 WPWHAHGNTRGI

Pt1-08 WHWKPYMSSRAQ

Pt1-10 VHKDHHRWHFLK

Pt1-11 VPSNSLLQSSRV

Figure S 8: EpiSearch mapping results of mimotopes Pt1-1 to Pt1-11 on human AQP4. Brown dots indicate the location of the predicted epitopes**.**

93

Pt1-12

GLVHHKHWRGNQ

Pt1-13

GPFHFLHHHWSQ

Pt1-14

YRNDSRDAINMM

Pt1-15

IPLGRDGGSYQR
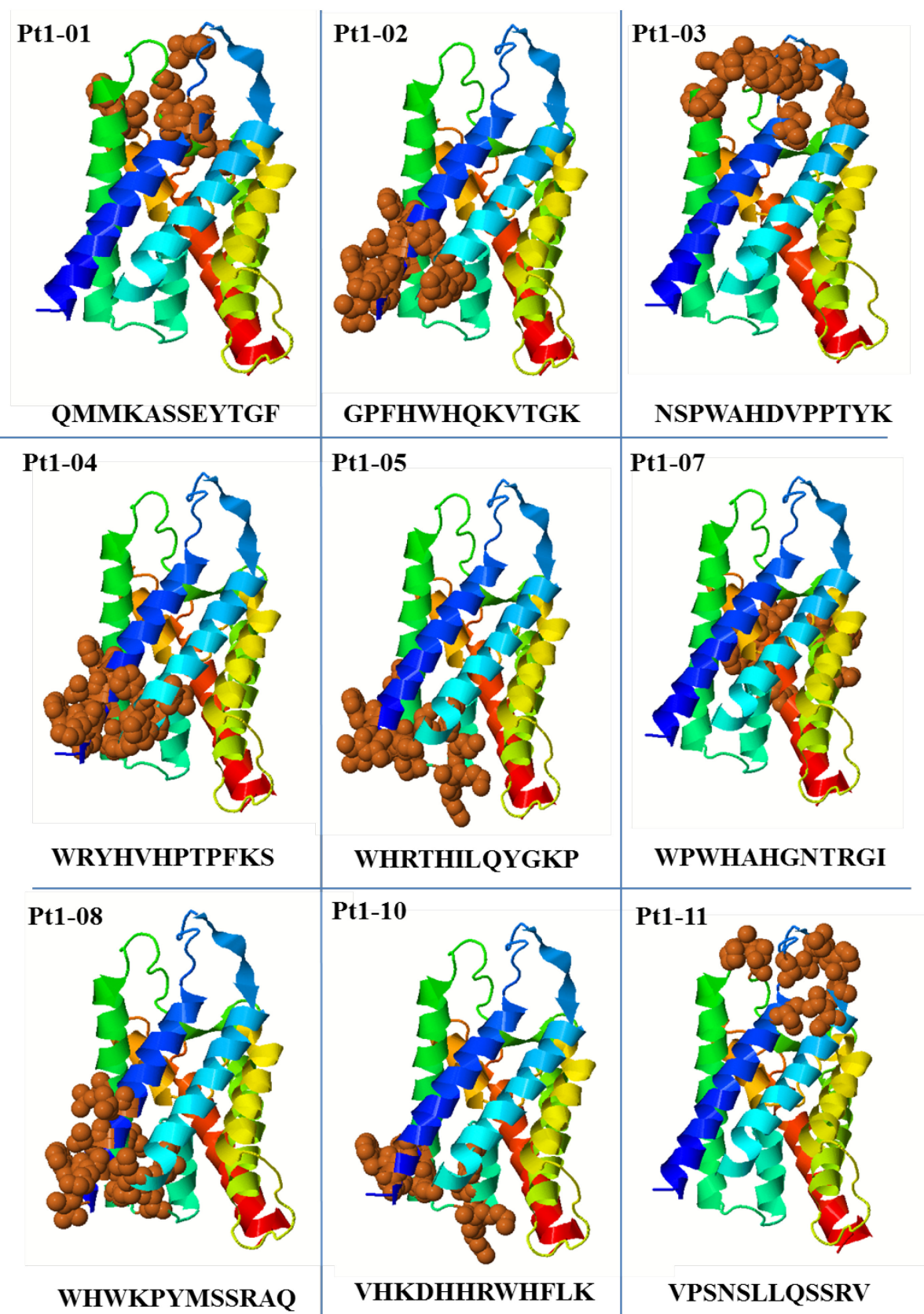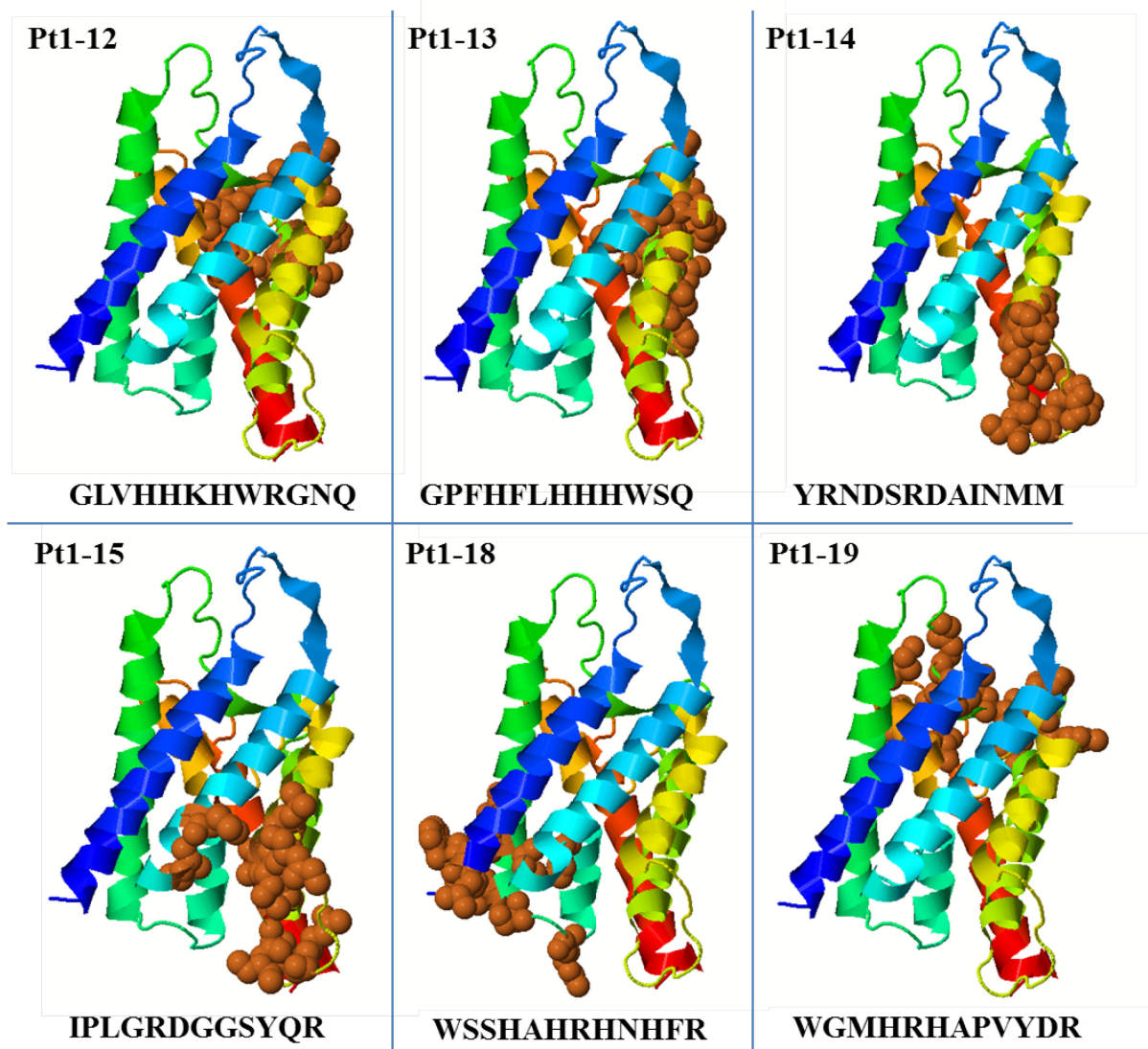
Pt1-18

WSSHAHRHNHFR

Pt1-19

WGMHRHAPVYDR

Figure S 9: EpiSearch mapping results of mimotopes Pt1-12 to Pt1-19 on human AQP4. Brown dots indicate the location of the predicted epitopes**.**

Pt1-01
QMMKASSEYTGF

Pt1-02
GPFHWHQKVTGK

Pt1-03
NSPWAHDVPPTYK

Pt1-04
WRYHVHPTPFKS

Pt1-05
WHRTHILQYGKP

Pt1-07
WPWHAHGNTRGI

Pt1-08
WHWKPYMSSRAQ
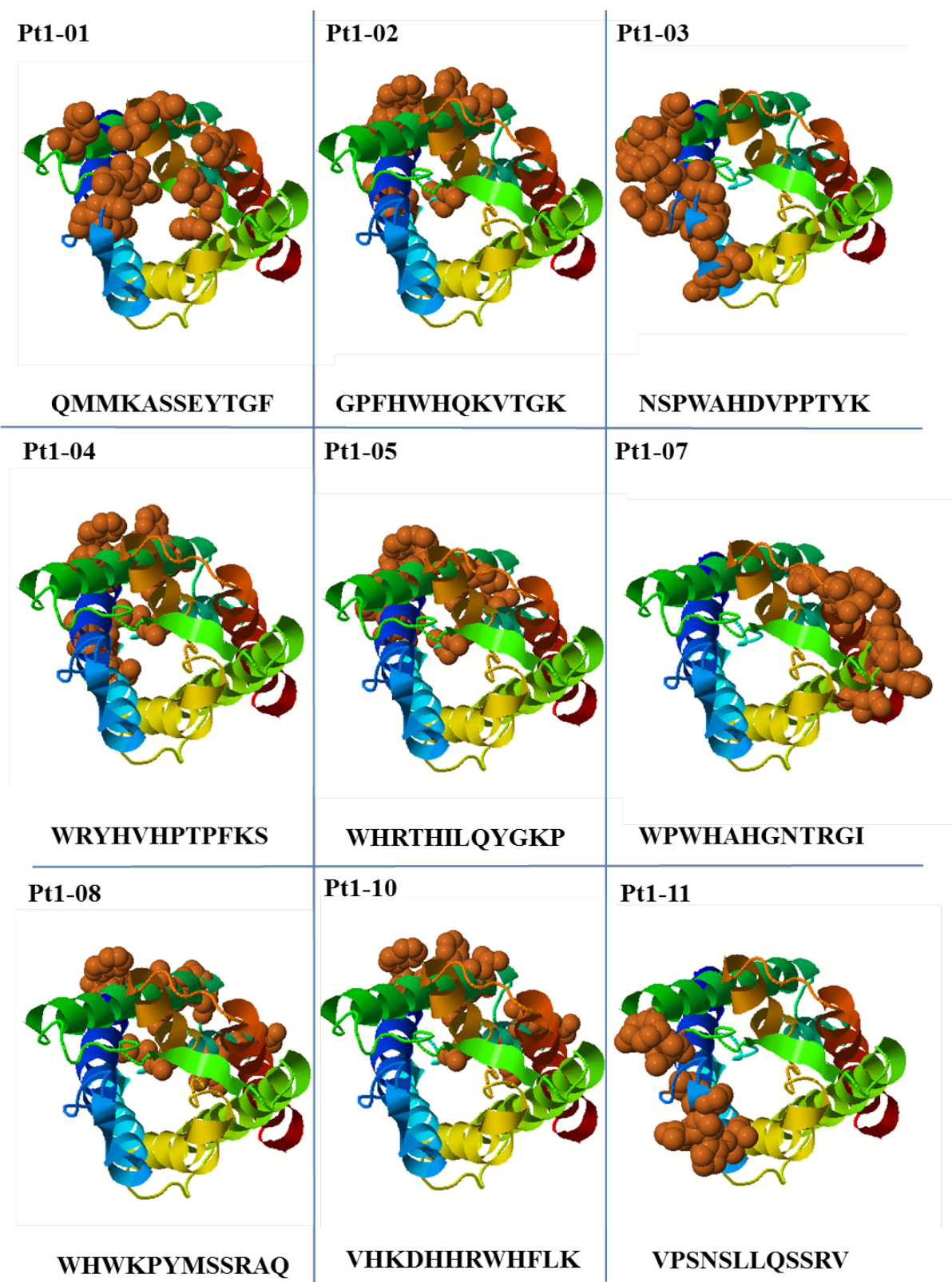
Pt1-10
VHKDHHRWHFLK

Pt1-11
VPSNSLLQSSRV

Figure S 10: Top View of EpiSearch mapping results of mimotopes Pt1-1 to Pt1-11 on human AQP4. Brown dots indicate the location of the predicted epitopes**.**

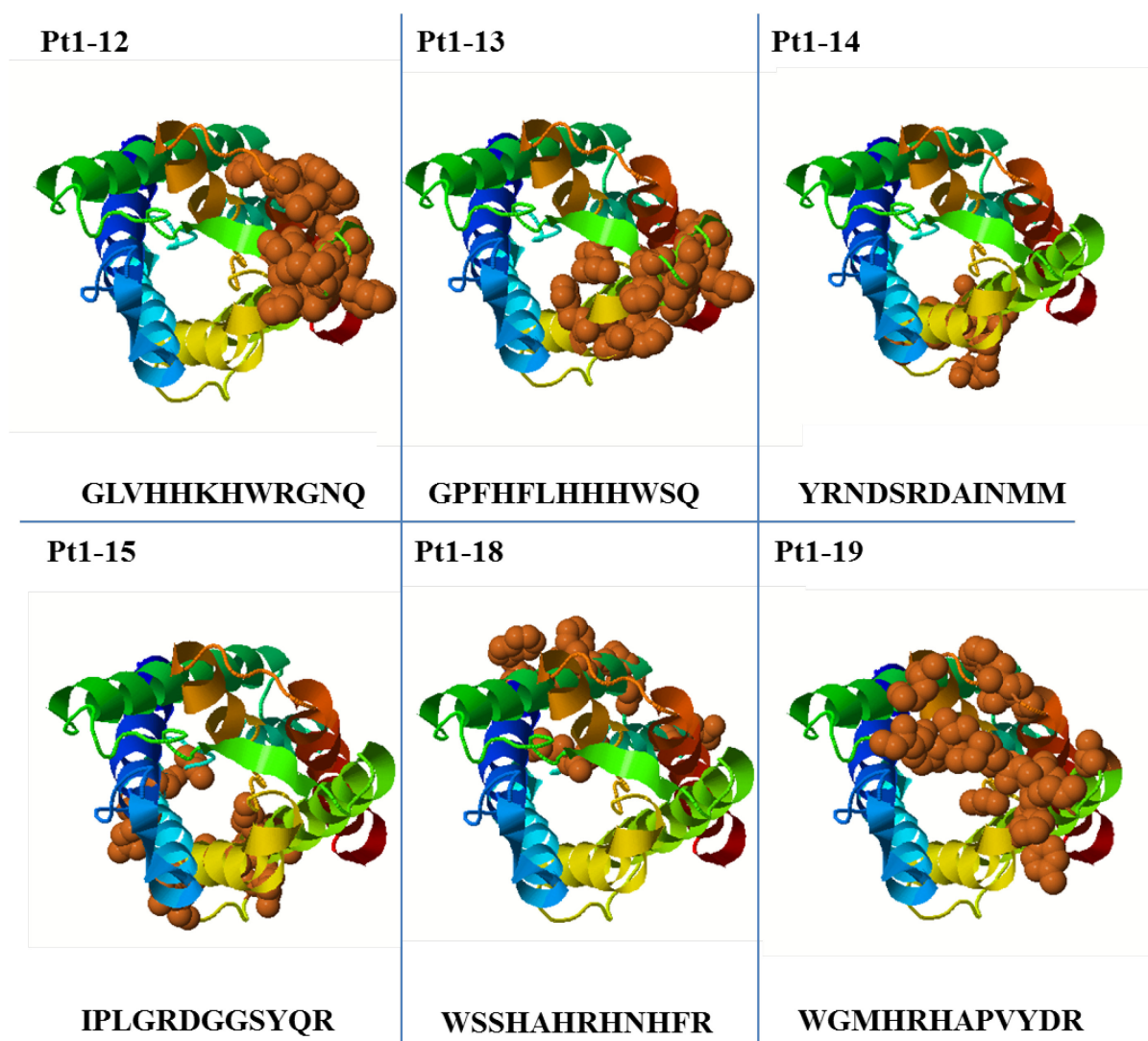| Pt1-12	Pt1-13	Pt1-14
GLVHHKHWRGNQ	**GPFHFLHHHWSQ**	**YRNDSRDAINMM**
Pt1-15	Pt1-18	Pt1-19
IPLGRDGGSYQR	**WSSHAHRHNHFR**	**WGMHRHAPVYDR**

Figure S 11: Top View of EpiSearch mapping results of mimotopes Pt1-12 to Pt1-19 on human AQP4. Brown dots indicate the location of the predicted epitopes.
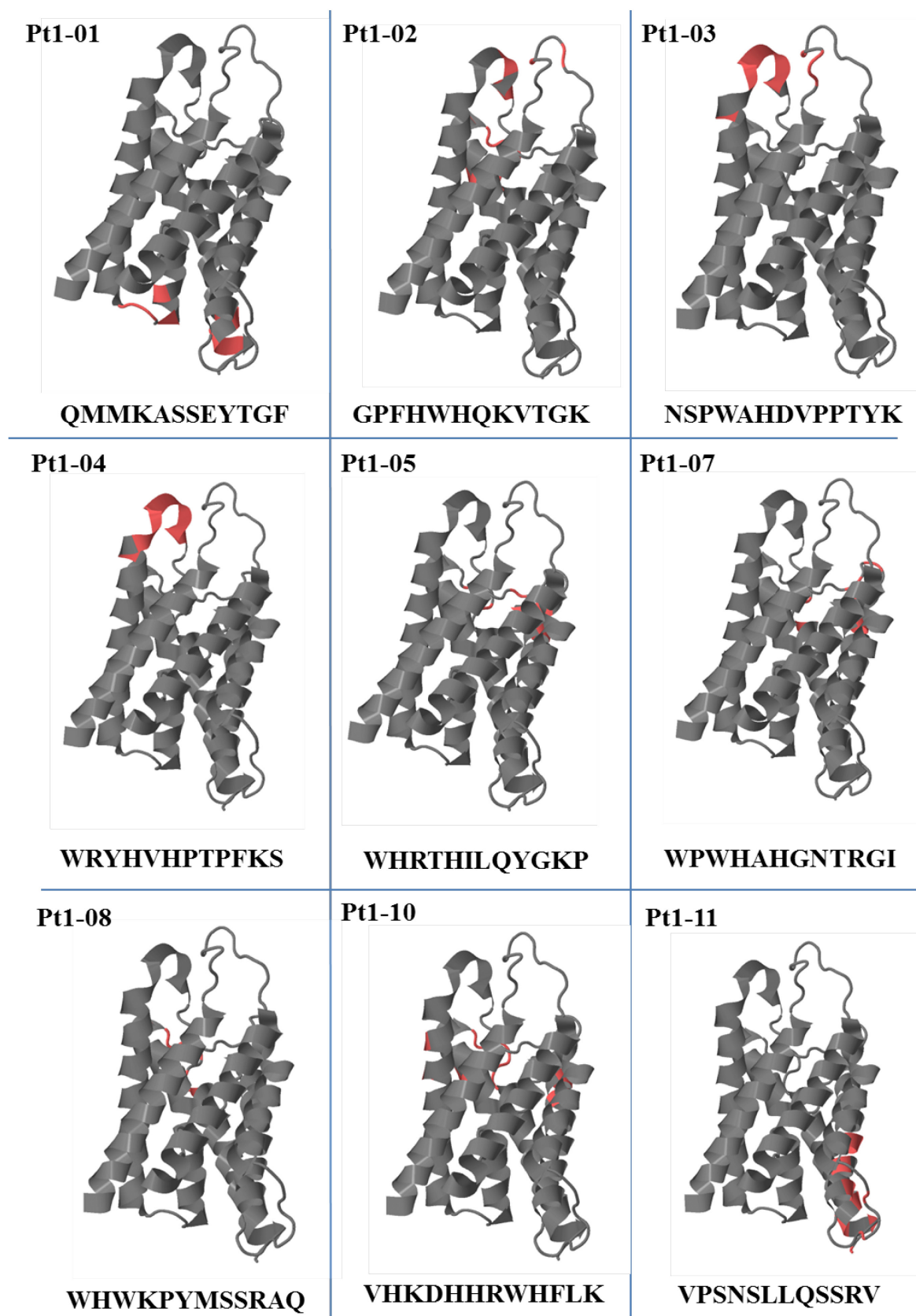
Figure S 12: Epitope prediction of *PepSurf* of mimotopes Pt1-1 to Pt1-11 on human AQP4. Red color indicates the epitope position.

Pt1-12

GLVHHKHWRGNQ

Pt1-13

GPFHFLHHHWSQ

Pt1-14

YRNDSRDAINMM

Pt1-15

IPLGRDGGSYQR

Pt1-18

WSSHAHRHNHFR

Pt1-19

WGMHRHAPVYDR

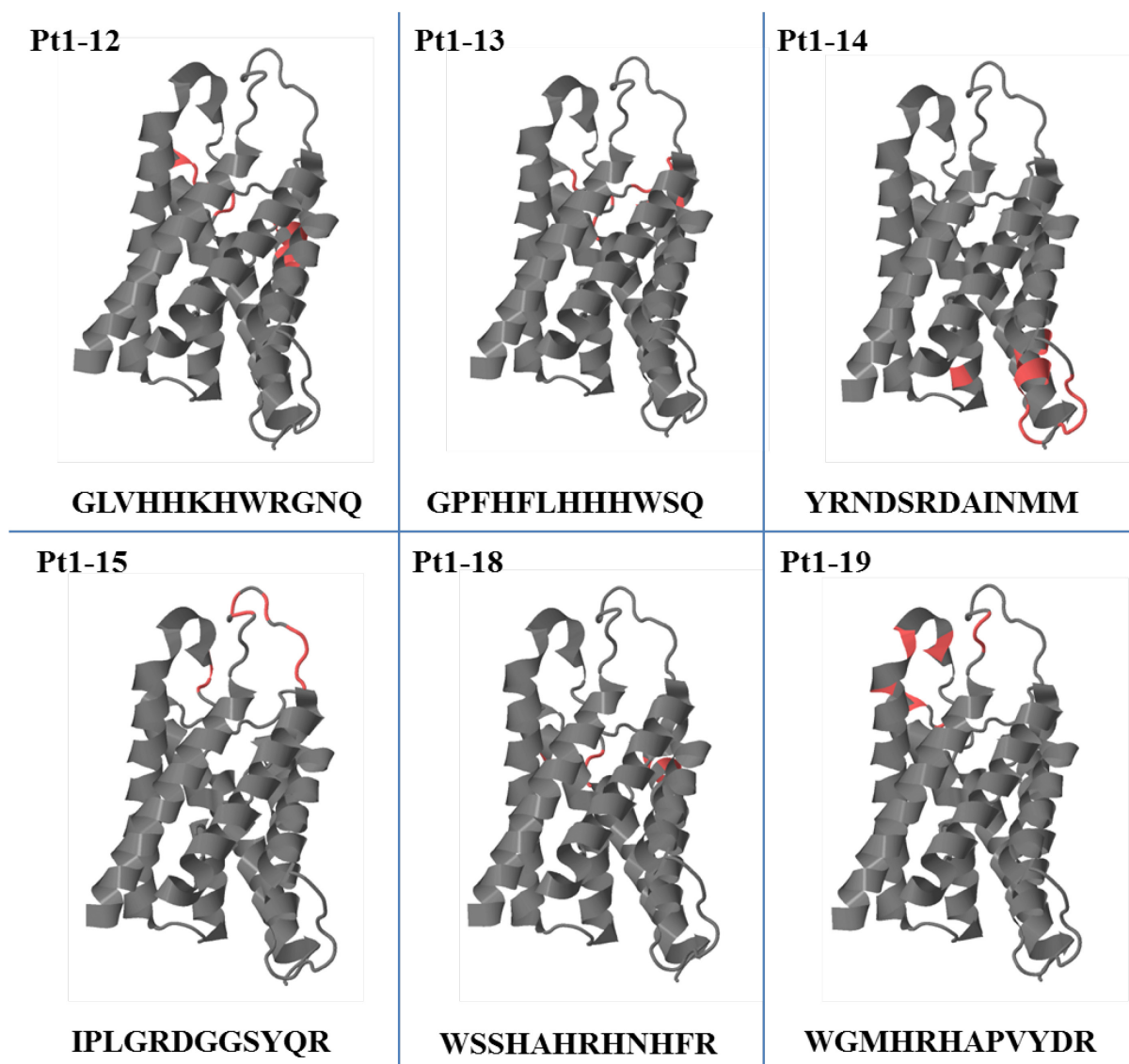**Figure S 13: Epitope prediction of *PepSurf* of mimotopes Pt1-12 to Pt1-19 on human AQP4.** Red color indicates the epitope position.

Pt1-01

QMMKASSEYTGF

Pt1-02

GPFHWHQKVTGK

Pt1-03

NSPWAHDVPPTYK

Pt1-04

WRYHVHPTPFKS

Pt1-05

WHRTHILQYGKP

Pt1-07

WPWHAHGNTRGI

Pt1-08

WHWKPYMSSRAQ
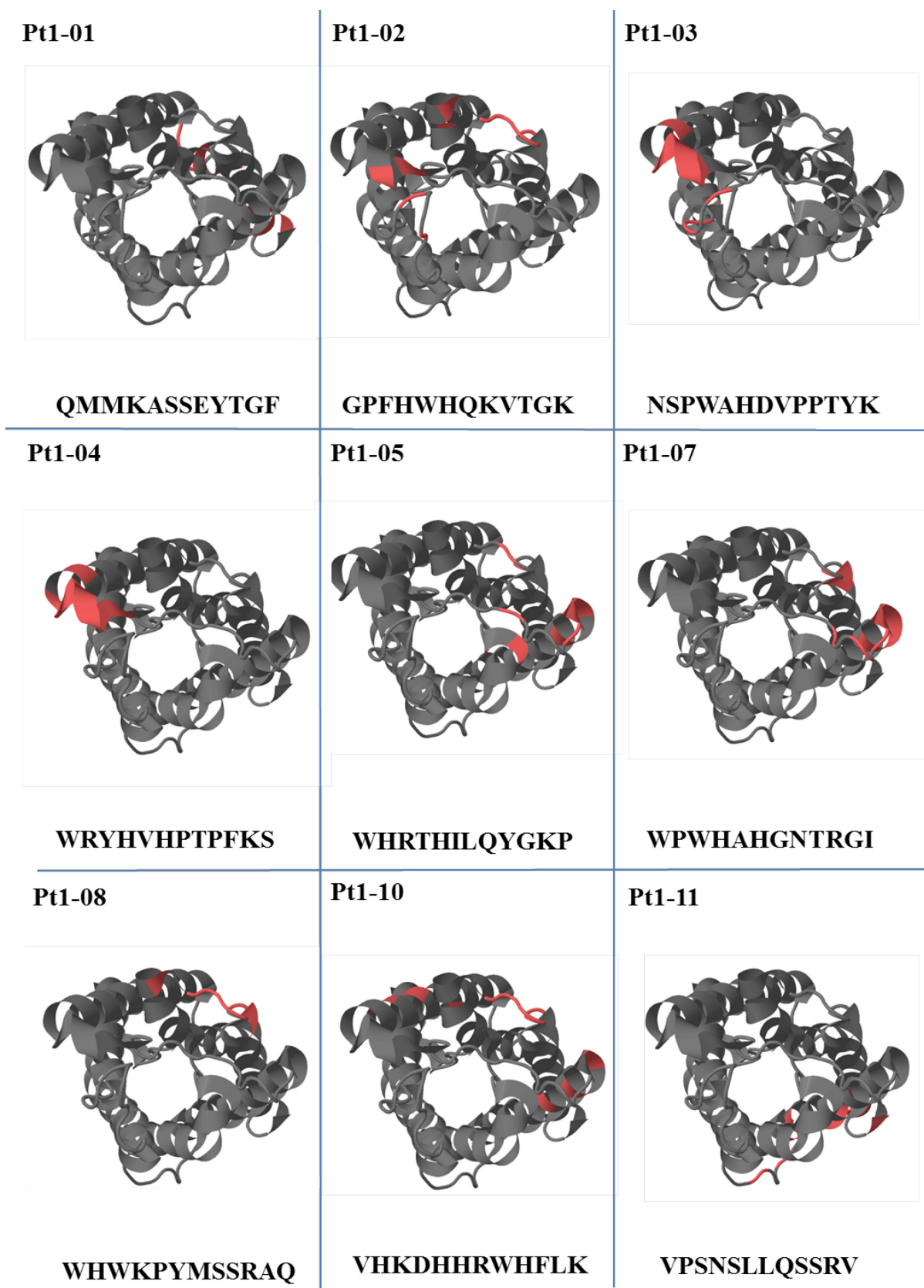
Pt1-10

VHKDHHRWHFLK

Pt1-11

VPSNSLLQSSRV

Figure S 14: Top view of the *PepSurf* epitope prediction of mimotopes Pt1-1 to Pt1-11 on human AQP4. Red color indicates the epitope position.

Pt1-12

GLVHHKHWRGNQ

Pt1-13

GPFHFLHHHWSQ

Pt1-14

YRNDSRDAINMM

Pt1-15

IPLGRDGGSYQR

Pt1-18

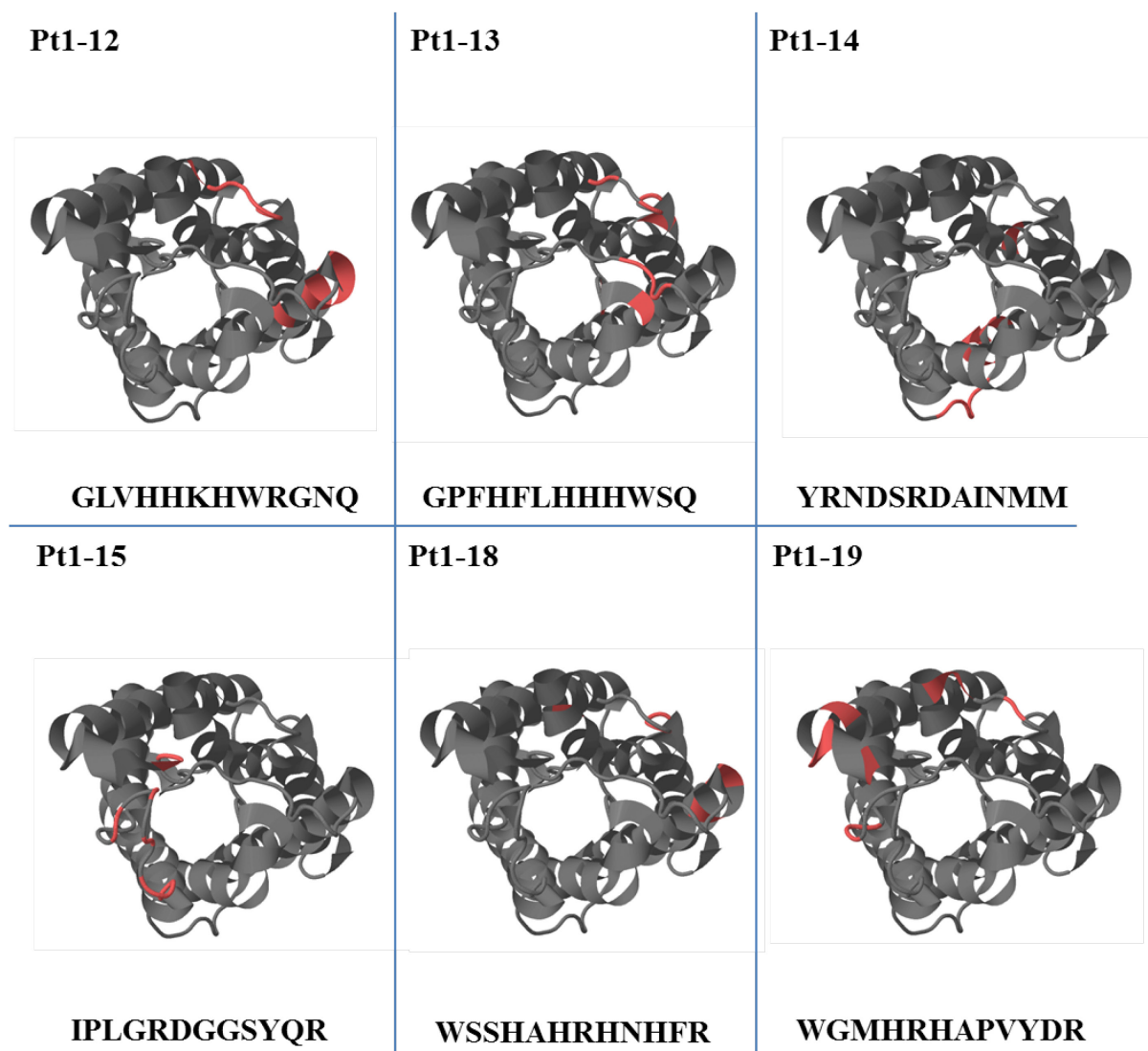
WSSHAHRHNHFR

Pt1-19

WGMHRHAPVYDR

Figure S 15: Top view of the *PepSurf* epitope prediction of mimotopes Pt1-12 to Pt1-19 on human AQP4. Red color indicates the epitope position.
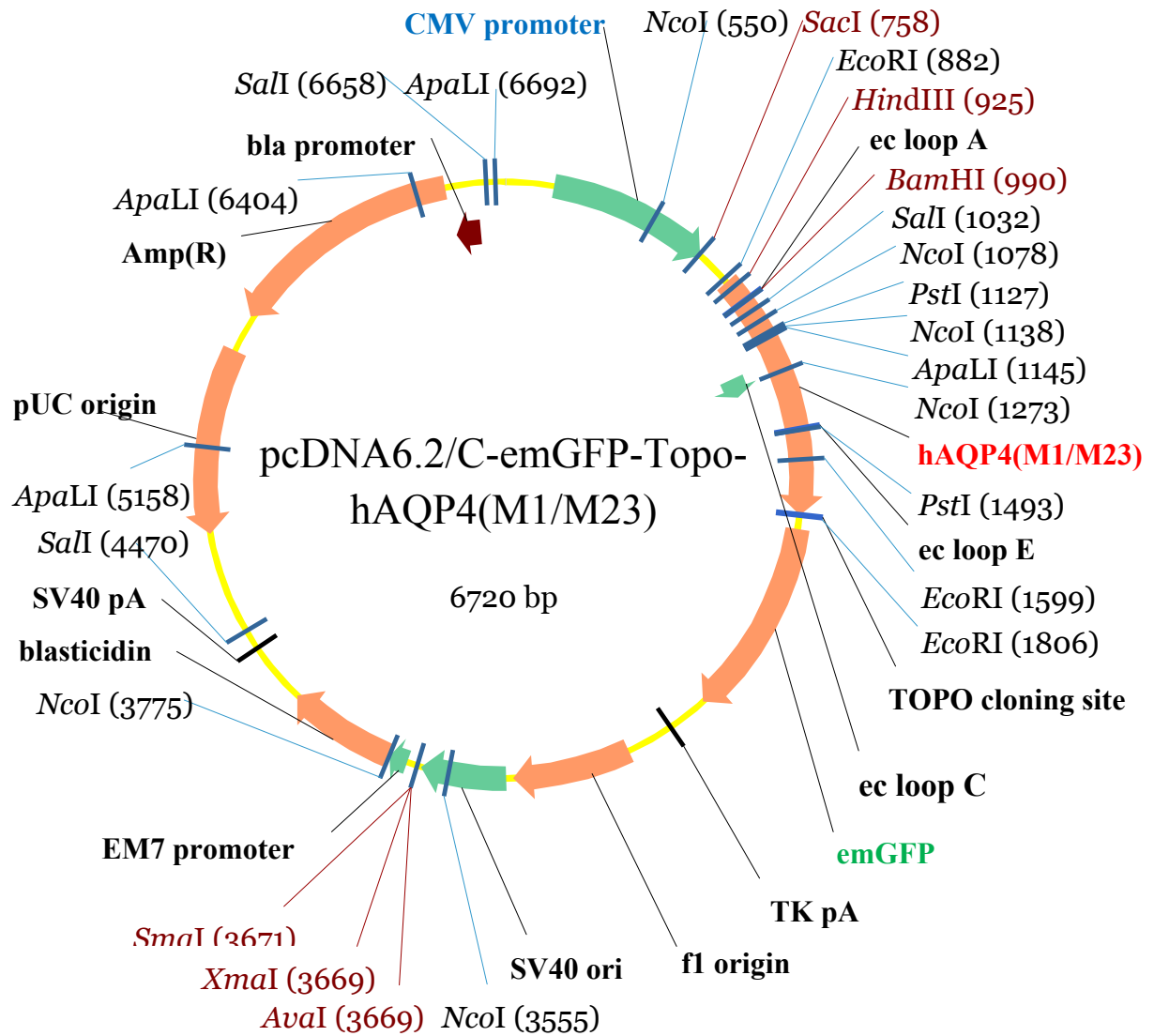
Figure S 16: plasmid map of the AQP4-encoding constructs. Both constructs contain the sequence of a C-terminal AQP4-emGFP fusion protein which is transcriptionally controlled by the human cytomegalovirus (CMV) promoter. One construct contains the human sequence for the AQP4-M1 isoform whereas the other one encodes the AQP4-M23 isoform.

11. Curriculum Vitae

Personal information

Name	Isabel Julia Bauer
Date of Birth	25.10.1990
Place of Birth	Ebersberg, Bavaria, Germany
Nationality	German
Marital status	Single
Address	Linke Bahngasse 3/11
	1030 Vienna, Austria
Phone	+43 660 3965185
E-Mail	bella.bauer@web.de

Education

10/ 2013 – present	Faculty of Life Sciences, **University of Vienna**, Austria *Master of Science (MSc) Behavior, Neurobiology and Cognition;*
10/2010 – 07/2013	Faculty of Biology, **Ludwig Maximilian University of Munich**, Germany *Bachelor of Science (BSc) Biology*
09/2001 – 06/2010	Humboldt-Gymnasium Vaterstetten, Bavaria, Germany *A Levels*

Work Experience

March 2015 – present	Department of Neuroimmunology, **Center for Brain Research**, Medical University of Vienna; Spitalgasse 4; 1090 Vienna, Austria Master student Project title: "Epitope mimics for pathogenic anti-aquaporin 4 autoantibodies in Neuromyelitis optica" Supervisor: Assoc. Prof. Dr. Monika Bradl
July/August 2014	AG Simon Rumpel, **Institute of Molecular Pathology**; Dr.-Bohr-Gasse 7, 1030 Vienna, Austria Intern Project title: "Analysis of *in vivo* Calcium Imaging Data during Sound Processing in the Auditory Cortex" Supervisor: Prof. Dr. Simon Rumpel

March – June 2013	Behavioral Neuroendocrinology, **Max Planck Institute of Psychiatry**, Kraepelinstr. 2-10, 80804 Munich, Germany
	Bachelor student
	Project title: "Expression of *Crhr1* in the prefrontal cortex and the hippocampus of high anxiety-related behavior mice"
	Supervisor: Prof. Dr. Rainer Landgraf

Scholarships

Performance scholarship of the University of Vienna, total amount € 770 for the academic year 2013 – 2014.

Additional skills

Languages	German (mother tongue), English (very good command) French (basic communication skills), Italian (basic communication skills)
Computer skills	MS Office package, Windows OS (Win XP, Win 7, Win 8)